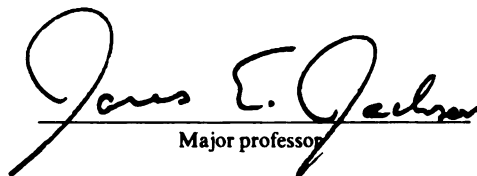This is to certify that the

dissertation entitled

DESIGN, SYNTHESIS, AND PROPERTIES
OF A NEW CLASS OF BUILDING BLOCKS
FOR ASSEMBLY OF MOLECULE-BASED MAGNETS

presented by

ANDRZEJ WLADYSLAW MISIOLEK

has been accepted towards fulfillment
of the requirements for

___PH.D.___ degree in __CHEMISTRY__

_____
Major professor

Date__June 27, 2000__

O-12771

PLACE IN RETURN BOX to remove this checkout from your record.
TO AVOID FINES return on or before date due.
MAY BE RECALLED with earlier due date if requested.

DATE DUE	DATE DUE	DATE DUE

DESIGN, SYNTHESIS, AND PROPERTIES OF A NEW CLASS OF BUILDING

BLOCKS FOR ASSEMBLY OF MOLECULE-BASED MAGNETS

By

Andrzej Władysław Misiołek

A DISSERTATION

Submitted to
Michigan State University
in partial fulfillment of the requirements
for the degree of

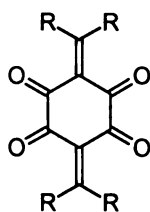DOCTOR OF PHILOSOPHY

Department of Chemistry

2000

ABSTRACT

DESIGN, SYNTHESIS, AND PROPERTIES OF A NEW CLASS OF BUILDING BLOCKS FOR ASSEMBLY OF MOLECULE-BASED MAGNETS
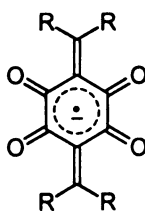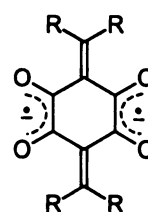
By

Andrzej Władysław Misiołek

In this work, mono and dianions of the tetrone **1** were proposed as discrete building blocks for assembly of molecular magnets.


These anionic subunits are designed to form extended multidimensional structures upon complexation with metal cations. This particular framework also was chosen so that dianion 1^{2-} (or its derivatives) would possess a paramagnetic triplet as a ground state.

High quality *ab-initio* CASSCF(14, 12)/6-31+G* calculations showed that indeed the singlet-triplet gap of metal complexes of 1^{2-} is small and its sign and magnitude tongly depends on structural modifications. For example a 17.3 kcal/mol preference for a

singlet is predicted for isolated 1^{2-} while the triplet state is preferred by 4.3 kcal/mol for the symmetrically coordinated complex $1(AlF_2)_2$.
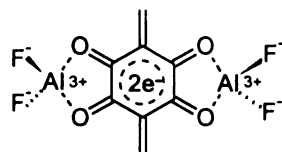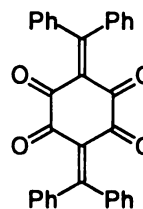
$$1(AlF_2)_2 \qquad\qquad\qquad 2$$

Synthetic procedures leading to a family of neutral aryl substituted tetrones (2) has been developed and electrochemical studies have shown that they may be reversibly reduced in two successive one-electron processes to mono- and dianions.

These mono- and dianions have been generated on a preparative scale by reduction of the parent tetrones with alkali metals under anaerobic conditions. Solutions of anions were characterized by Vis-NIR, NMR and EPR spectroscopy. EPR of the anion radicals 2^- reveals the high symmetry of the spin delocalisation. Spectroscopic studies of dianions were hampered by low solubility and aggregation phenomena and no definite answer concerning their ground spin states could be obtained.

Several attempts were made to grow single crystals of 2^- and 2^{2-} in order to probe the self-assembling properties of those species and to obtain definite answers concerning the ground state of the dianion. These attempts turned out to be successful only for alkali metal salts of the monoanion $(t\text{-Bu})_8(MeO)_4 2^-$. Its K^+ salt crystallized as 1-D chains with the expected bridging and chelating mode of coordination. The closely related Na^+ salt, recently crystallized by Robert Gentner, shows a similar 1-D chain structure.

ACKNOWLEDGMENTS

TABLE OF CONTENTS

LIST OF TABLES

LIST OF FIGURES

FIGURE

LIST OF ABBREVIATIONS

AcOH-   Acetic Acid (CH_3COOH)

c(2.2.2)-   4,13,16,21,24,-hexaoxa-1,10-diazabicyclo-[8.8.8]hexacosane

CAN-   Ceric Ammonium Nitrate (($NH_4)_2Ce(NO_3)_6$)

CASSCF (CAS)-   Complete Active Space Self-Consistent Field

DDQ-   2,3-Dichoro-5,6-dicyano-1,4-benzoquinone

DDQH$_2$-   2,3-Dichoro-5,6-dicyano-1,4-catechole

DHQ-   2,5-Dihydroxy-1,4-benzoquinone

DMF-   N,N-Dimethylformamide ($HCOON(CH_3)_2$)

ENDOR-   Electron-Nuclear Double Resonance

Et$_2$O-   Diethyl ether (($C_2H_5)_2O$)

EtOH-   Ethanol (C_2H_5OH)

MeCN-   Acetonitryle (CH_3CN)

MeOH-   Methanol (CH_3OH)

ROHF-   Restricted Open-Shell Hartree-Fock

TCSCF-   Two-Configuration Self-Consisted Field

THF-   Tetrahydrofuran (C_4H_8O)

INTRODUCTION

In this work mono and dianions of tetrone **1** are proposed as new building blocks

for assembly of molecular magnets.

$$1 \qquad 1^{-\bullet} \qquad 1^{2-\bullet\bullet}$$
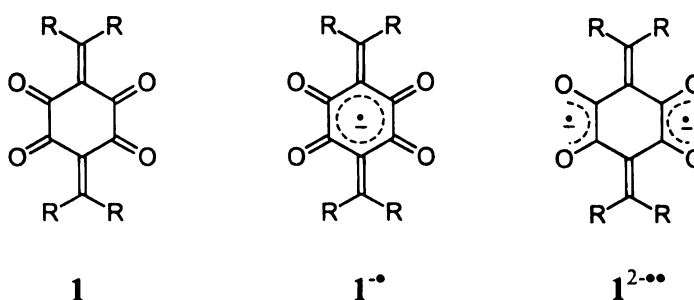
Molecular magnets are materials where the magnetically active elements are

organic molecules instead or in addition to traditional inorganic components like

transition metal or lanthanide ions and atoms.[1] Since synthetic chemists have much better

control over organic than inorganic molecules, the main advantage of such materials

would be the feasibility of their rational design and 'fine tuning' of their properties.

Properties unknown for traditional magnets such as optical transparency, chirality,

solubility in organic solvents, etc. may also lead to new applications in future

technologies.

A purely organic and hybrid inorganic-organic (preferred in our group) approach

is used to synthesize these materials. In the first one, only organic molecules (mainly

stable organic radicals) are assembled into the magnet. In the hybrid approach the organic

components are used together with metal cations. The cations aid their organization into

desired extended magnetic solid state structures and additionally play the role of robust

spin carriers or relays. So far, neither of these approaches have produced any molecular magnet promising practical application. Among the reasons for this failure are the shortcomings of the organic components available to date. The design and synthesis of **1** is an attempt to change that situation and the following discussion will rationalize that choice.

Organic molecules used as building blocks for assembly of molecular magnetic materials must meet a few crucial conditions. First of all two basic requirements concerning their abilities to form solid state magnetic networks must be met:

- <u>They should possess strong and predictable spin communicating abilities.</u> Magnetism is a cooperative phenomenon and organic spacers must possess ability to strongly 'couple' separate paramagnetic centers of the magnetic solid (usually unpaired electrons of the metal cations or of the other spacers). A high magnitude of coupling is required in order to obtain 'room temperature' magnets

- <u>They should have high probability of self-assembly into extended structures in which magnetic interactions can be propagated along multidimensional extended networks.</u> Two coupled paramagnetic centers do not make a magnet. In order to produce a domain of magnetic material <u>extended</u> cooperative magnetic interactions among thousands of paramagnetic components in the solid state is required. But even an infinite chain of high-spin coupled paramagnetic centers is not enough. Multidimensional interactions (2D sheets or better 3D nets) are required in order to observe a ferromagnetic phase transition.

The first requirement should be easily met by 1^- (or 1^{2-}). Due to its chelating and bidentate structure, paramagnetic anions of **1** should have high chance to bind two metallic centers at the same time. The unpaired electron of such a spacing ligand 1^- would have close contact with the unpaired electrons concentrated on the metal cations or their coordination sphere. Such a close contact should assure particularly strong spin-spin interactions and coupling of considerable strength.

Fulfillment of the second requirement, so far, is the most difficult for all compounds investigated as a discrete elements of Molecular Magnets. Although some paramagnetic spacers with relatively good coupling abilities has been prepared, their self-organizing properties were left too much to chance. Consequently solids obtained from them do not form robust magnetic materials because the structures obtained do not possess required multidimensional topology of intermolecular magnetic interactions. We believe that contrary to most other such molecules, anions of 1 have a high probability of forming extended magnetic networks with metal cations. Some evidence for this assumption will be presented in Chapter 1.

In addition to the above two pivotal 'magnetic' requirements, anions of **1** have other interesting properties, which should increase the chances of their successful self-assembly into molecular magnets.

- **1 may be paramagnetic on multiple stages of reduction.** As a result of careful design 1^{2-} has a high chance of having paramagnetic triplet as its ground state (see Chapter 2). This dianion diradical could be thus used as a paramagnetic coupler in

combination with or in place of the monoanion monoradical. This notion offers flexibility in terms of charge balancing with counteranions and consequently, increases the chance of achieving the desired structures. A higher spin density diradical could be favorable for forming magnets based on a fully ferromagnetic coupling network while the monoradical might be preferred for construction of ferrimagnets. Fine tuning of the triplet-singlet gap of **1** on the molecular level should also enable control over material properties and lead to magnets with 'custom designed' properties.

- Both 1^- and 1^{2-} are anionic. In many of the reported solids discrete organic paramagnetic components are neutral and solid state intermolecular interactions between them rely on relatively weak Van der Waals or second order electrostatic forces. The opposite charges of the anions of **1** and the metal cations should strengthen intermolecular interactions, bringing them closer together and facilitate their magnetic communication. It would also allow synthesis of a hybrid organic-inorganic material without disruption of the magnetic networks by insulating diamagnetic counterions.

- Electronic and packing properties of **1** should be easy to modify by different substituents **R.** Since one of the most desirable properties of molecular magnets is the possibility of fine-tuning of their properties on the molecular level, the electronic properties of the basic unit should be easily modifiable. Direct conjugation of **R** with the π system should provide that possibility for the electronic properties of **1**.

The later parts of this thesis will provide some background information concerning the possibility of the triplet ground state for 1^{2-} and the chances of 1^{-} and 1^{2-} to self-assemble into hoped for magnetic structures, followed by presentation and discussion of results obtained during the course of the study.

BIBLIOGRAPHY

(1)   (a) Caneschi, A.; Gatteschi, D.; Sessoli, R.; Rey, P. *Accounts Chem. Res.* **1989**, *22*, 392. (b) Gatteschi, D.; Kahn, O.; Miller, J. S.; Palacio, F. *Adv. Mater.* **1991**, *3*, 161. (c) Gatteschi, D.; Sessoli, R. *J. Magn. Magn. Mater.* **1992**, *104*, 2092. (d) Gatteschi, D. *Adv. Mater.* **1994**, *6*, 635. (e) Kollmar, C.; Kahn, O. *Accounts Chem. Res.* **1993**, *26*, 259. (f) Kahn, O. *Nature* **1995**, *378*, 667. (g) Miller, J. S.; Epstein, A. J. *Angew. Chem.-Int. Edit. Engl.* **1994**, *33*, 385. (h) Miller, J. S.; Epstein, A. J. In *Materials Chemistry*, 1995; Vol. 245; pp 161-188. (i) Iwamura, H. *Pure Appl. Chem.* **1987**, *59*, 1595. (j) Rajca, A. *Chem. Rev.* **1994**, *94*, 871.

Chapter 1

BACKGROUND

1.1 Dianion 1^{2-} *vs.* π conjugated diradicals

The possibility that derivatives of dianion 1^{2-} may have triplet ground states is intriguing both from theoretical and practical points of view. Triplet ground state organic molecules are very uncommon and despite great theoretical and experimental effort invested into the study of such compounds there are only a few classes of them known to date. Triplet state derivatives of 1^{2-} would not only be interesting examples of a novel class of such molecules, but thanks to their potential for self-assembly via interaction with metal cations, they would be of special interest for material science. The reason for the rarity of triplets is not only their diradical character and consequent high reactivity. The frontier orbitals of such molecules must also fulfill some specific conditions. Only when their HOMO-LUMO gap is small or zero and the two orbitals overlap significantly in space may a triplet ground state be expected. Fulfillment of these conditions leads to Hunds rule for atoms and ions or some simple molecules (e.g. O_2) which are probably the best known examples of high-spin species.

Dianion 1^{2-} could be classified as an organic diradical with both unpaired electrons belonging to a single planar π conjugated system. Other rare examples of similar high-spin organic molecules are Non-Kekule hydrocarbons where HOMO-LUMO degeneracy is based on their topology and $4n\pi$ electron annulenes where it is based on the symmetry of the molecule. Both groups of diradicals will be briefly presented and

their relation to 1^{2-} will be used to rationalize the hope for triplet as a ground state of that molecule.

Non-Kekule hydrocarbons. In 1858 Friedrich August Kekulé put forward the idea that carbon atoms are quadrivalent and link together to form 'backbones' of organic compounds.[1] The proposed rules were so successful in assigning structures of the already known and newly discovered compounds that with time it became unimaginable that substances that violate Kekule's principles might exist. However Gomberg's discovery of triphenylmethyl, a free radical with trivalent carbon, proved such violations to be possible.[2] 15 years later, an even more fascinating molecule was prepared. Following the methodology used by Gomberg, Schlenk and Brauns[3] allowed a solution of dichloroxylene **2** to react with powdered copper under a CO_2 atmosphere (figure 1.1). Abstraction of chlorine atom from **2** generated a yellow monoradical **3•** that reacted further with another equivalent of copper forming a blue colored product **4••**. Remarkably, **4••** retained the radical character of **3•** despite the fact that both of its radical centers belonged to a single conjugated system. Although such results might be intuitively explained considering the fact that no Kekule structure with all valences paired could be drawn for **4••**, no rigorous explanation based on fundamental physical principles could be supplied at that time. Better insight into the character of this and similar hydrocarbons had to wait for refinement of the theoretical methods of quantum chemistry.
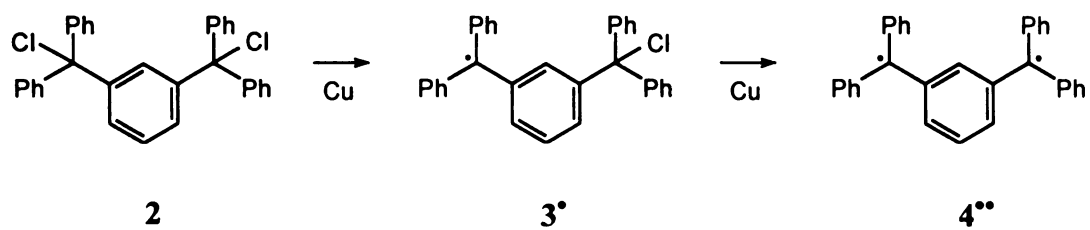
Figure 1.1. Generation of α,α,α',α'-tetraphenyl-m-benzoquinonodimethane

MBQDM   **TMM**   **TME**   **TMB**
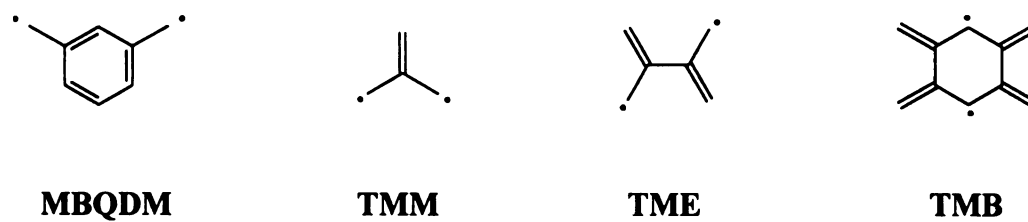
Figure 1.2. Some non-Kekiile hydrocarbons

In 1950 Longuet-Higgins proved that, in the non-Kekule hydrocarbons (as he called hydrocarbons for which no closed shell structure could be drawn despite the fact that they possessed even number of free valences) that do not contain 4n-membered rings, the number of atoms that cannot be assigned to π bonds is equal to both the number of π nonbonding degenerate molecular orbitals (NBDMO's) and the number of electrons that must to be accommodated in them.[4] Some simple examples of such hydrocarbons are m-benzoquinodimethane (**MBQDM**), trimethylenemethane (**TMM**), tetramethyleneethane (**TME**), and 1,2,4,5-tetramethylene-benzene (**TMB**). Thus each of the molecules on figure 1.2 has two π NBDMO, which contain a total of two electrons. In order to avoid coulombic repulsion, each of those electrons tends to occupy a different NBDMO, which explains the diradical character of the molecule.

A full description of the electronic states of such diradicals requires specification of their spin states. It is possible for the spins of the frontier electrons to be parallel or anti parallel to each other producing a molecule with spin number S=0 (singlet) or S=1 (triplet) (figure 1.3). Longuet-Higgins came up with the idea that Hund's rule, which so successfully explained the spin states of atoms and atomic ions could be straightforwardly extended to molecules, so that each of the diradicals in figure 1.2 should have a triplet as their ground state.

The introduction of Electron Paramagnetic Resonance Spectroscopy (EPR) and matrix isolation techniques offered experimental verification of those speculations, generally supporting Longuet-Higgins' hypothesis. In 1966 Dowd generated the simplest non-Kekule hydrocarbon, **TMM**, by photolysis of pyrazoline **5** in a frozen glass of perfluorinated solvents (Figure 1.4).[5] The presence of **TMM** in its triplet state was

confirmed by ESR spectroscopy. The broad spectrum obtained, a general feature of triplet

diradicals, could be fitted to a Hamiltonian with zero field splitting parameters[*] being in a

fair agreement with those predicted for **TMM** by MO calculations. Using a similar

technique, in 1970, Dowd prepared and recorded the triplet spectrum of **TME** (Figure

1.5)[6,7] while in 1983 the spectrum of unsubstituted **MBQDM** (generated from the

dicarbene) was reported by Platz's group (Figure 1.6).[8] The intensity of the EPR triplet

signals vs. temperature of all those diradicals obeyed the Curie law which meant that they

had either a strong preference for the triplet state or energetic near degeneracy of triplet

and singlet states (within ca. 10 cal/mol) with the second possibility being obviously

much less likely. Such ideal Curie behavior of obtained diradicals seemed to verify the

applicability of Hund's rule for all non-Kekule hydrocarbons.

---

[*]Zero field parameter D relates to the average distance between unpaired electrons while E relates to

deviation from the two fold symmetry of the molecule (see Chapter 4.1).
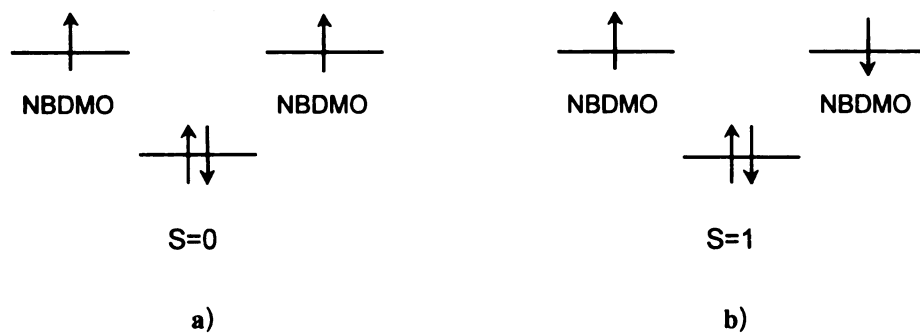
Figure 1.3. Possible spin states of a biradical (**a**) Triplet (**b**) Singlet
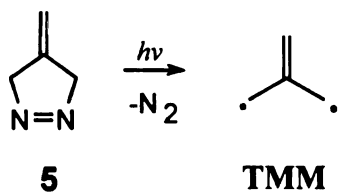
Figure 1.4. Generation of **TMM** by photolysis of pyrazoline **5**.
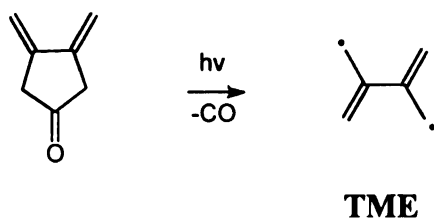
Figure 1.5. Generation of **TME** by photolysis of dimethylenecyclopentanone
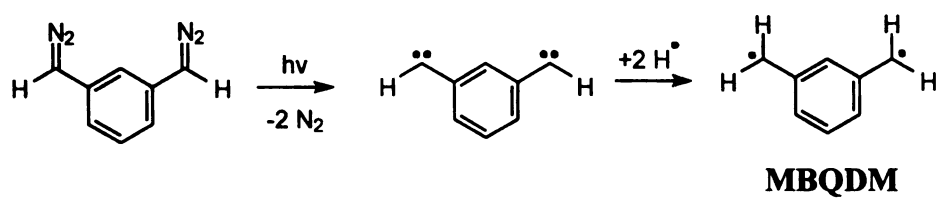
Figure 1.6. Generation of **MBQDM** from dicarbene.

This conclusion however was challenged by W. T. Borden. Inspired by his own failure to observe the triplet of D_{8h} cyclooctatetraene (**COT**), Borden realized the necessity of considering the effects of electron-electron repulsion more carefully. He classified non-Kekule hydrocarbons into two groups: with disjoint (like **TME, TMB**) and non-disjoint NBDMOs (like **MBQDM, TMM**).[9,10] The physical basis for Hund's rule is that, when two electrons have the same spin, the Pauli exclusion principle does not allow the electrons to occupy the same regions of space simultaneously, even if they are in different molecular orbitals. Since electrons of opposite spins are not prevented by the Pauli principle from appearing in the same regions of space, they usually have a much higher mutual Coulombic repulsion energy than two electrons of the same spin.

TME

TMM

(a)

(b)
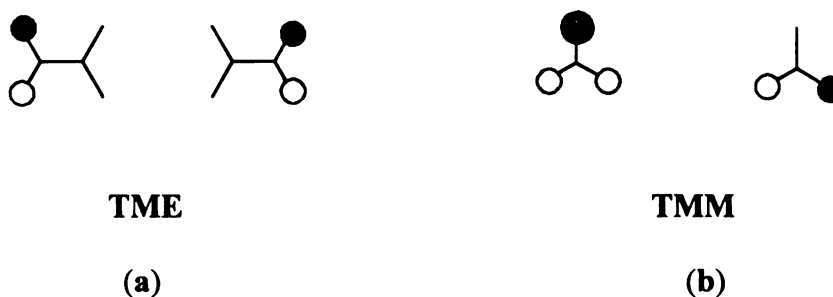
Figure 1.7. An example of non-Kekule hydrocarbons with (a) disjont and (b) non-disjoint NBDMOs

However, as can be shown on the example of **TME** (figure 1.7), the two singly occupied molecular orbitals can be chosen so that they are disjoint, i.e., have no atoms in common. In both the lowest singlet and the lowest triplet states then, one electron occupies each one of those NBDMOs. Because these MOs are disjoint, regardless of whether the electrons in them have the same or opposite spin, there is no probability that both electrons will simultaneously occupy the same AOs. Thus to a first approximation,

the lowest singlet and the lowest triplet state of **TME** have exactly the same energy.

Moreover electron correlation between the electrons in the NBMOs and those that remain

in the bonding MOs of the molecular fragment usually drops the energy of the singlet

well below that of the triplet. Although the diradical character of such hydrocarbons is

retained, there is little to favor the triplet anymore, and indeed, a modest singlet

preference is expected. Later high quality *ab-initio* calculations[11,12] along with gas phase

photoelectron spectroscopy[13,14] confirmed the strong triplet preference of both **TMM**

(~15kcal/mol) and **MBQDM** (~10 kcal/mol), while CISD(Q) calculations on planar

TME gave 1.6 kcal/mol preference for singlet.[15] The preference for the singlet ground

state was also established by photoelectron spectroscopy.[16]

6
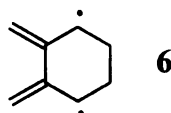
These results for **TME** seemed to be in disagreement with the previously observed Curie

behavior of the intensity of its EPR signal. This paradox prompted Matsuda and Iwamura

to reinvestigate the magnetic behavior of this system with the use of a SQUID

magnetometer, a much more precise instument than the EPR spectrometer. Indeed, study

of the magnetization of conformationally fixed **6** indicated a miniscule singlet rather than

a strong triplet preference.[17]

To distinguish quickly between disjoint and non-disjoint non-Kekule

hydrocarbons the concept of odd and even alternate hydrocarbons may be applied. Each

of the carbon atoms from the extended π system of non-Kekule hydrocarbons may be

marked (starred) or remain unmarked (unstarred) (figure 1.8) such that starred carbons

15

adjoin only with unstarred and vice-versa. It has been proven[18] that when the number of

starred (N*) and unstarred (N) carbons are equal (N*-N=0), each of the two NBMOs of

the hydrocarbon can be localized on a separate set of carbons so they can remain disjoint.

However, if there is an excess of one type of carbons over another, all NBMOs are

nondisjoint. As a consequence, such an entity follows Hund's rule and the spin number of

the molecule is equal to (N*-N)/2.
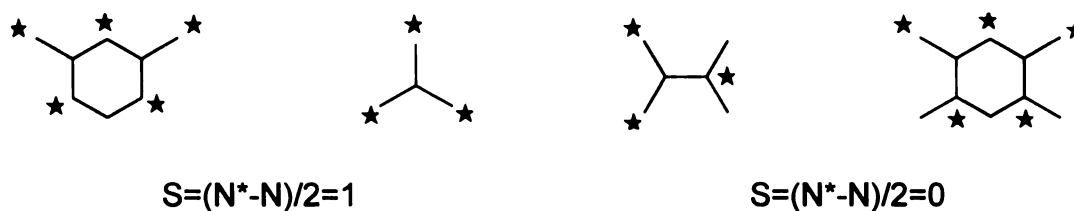
Figure 1.8. Examples of odd and even alternant non-Kekule hydrocarbons.

Determination of the singlet as a ground state of the another even alternant non-

Kekule hydrocarbon **TMB** (figure 1.2) seems to confirm the viability of Borden's

hypothesis.[19-21]

4nπ electron ('antiaromatic') annulenes. Besides the non-Kekule systems, another

group of fully conjugated hydrocarbons possessing degenerate HOMO and LUMO are

annulenes with 4nπ electrons. Such hydrocarbons are particulary unstable, in contrast to

the highly stabilized aromatic 4n+2 systems, and are called 'antiaromatic'. As explained

earlier degeneracy of frontier orbitals does not always lead to a triplet as a ground state.

CB   COT
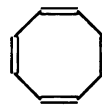
Neutral 4nπ annulenes square cyclobutadiene (**CB**) and planar 1,3,5,7-cyclooctatetraene

(**COT**) are not subject to Hund's rule because of the disjoint character of their half-

occupied orbitals.[10] The 4nπ rule of degeneracy can be extended, however to charged

conjugated cyclic systems (figure 1.9). For example, besides cyclobutadiene other

systems with 4 electrons which could potentially have a triplet ground state are the anion

of cyclopropene (**a**), the cation of cyclopentadiene (**b**) and the dication of benzene (**c**).

Frontier orbitals of charged 4nπ annulenes are unable to localize their unpaired electrons

on separate sets of carbon atoms to become disjoint so their ground states are thus

expected to be triplets, barring significant molecular distortion. Such charged

antiaromatic systems have attracted interest of chemists for a long time and experiments

probing their electronic structure date back to the early sixties.
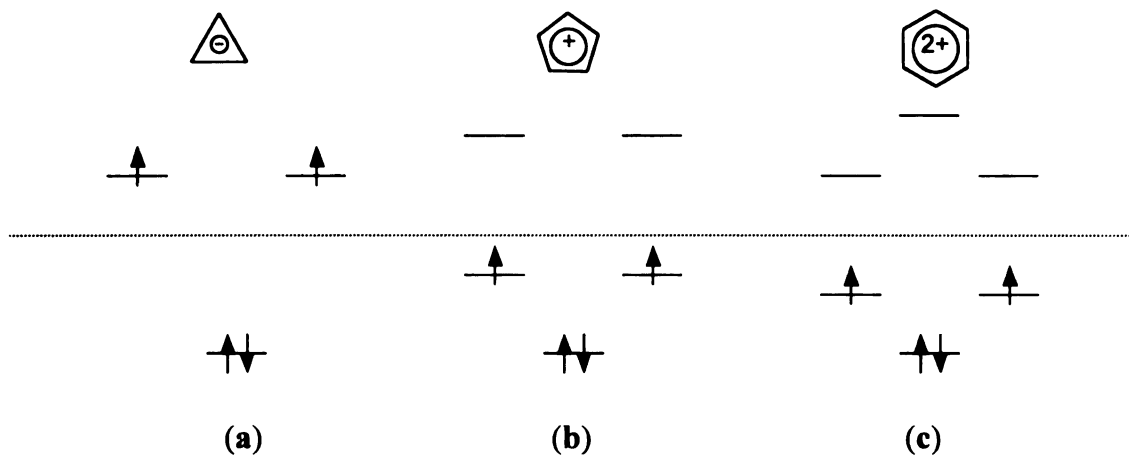
Figure 1.9. Molecular orbital diagram for π orbitals of 4e antiaromatic ions

(a) cyclopropene anion (b) cyclopentadiene cation and (c) benzene dication.
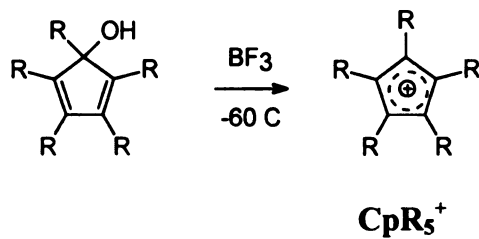
Figure 1.10. Generation of the cations of cyclopentadienes.
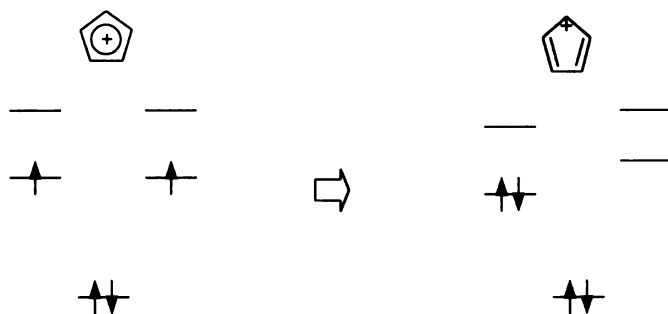
Figure 1.11. Perturbation of the molecular degeneracy caused by Jahn-Teller distortion

on the example of the cyclopentadiene cation.
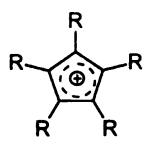
R	D (cm^{-1})	$E_{(T-S)}$ (kcal/mol)
H	0.1865	~0
Cl	0.1495	~0
Ph	0.1050	0.35-1.15
p-MeO-Ph	Not rep	0.05

Table 1.1 Values of zero field splitting parameter D and S-T gaps for some

cyclopentadiene cations.

The simplest member of this group, the cyclopropenyl anion, is known only as a transient reactive intermediate and has not been experimentally investigated in detail.

Study of the cyclopentadienyl cation system turned out to be more successful. Its derivatives were prepared by reaction of cyclopentadienols or cyclopentadienyl halides with Lewis acids below –60°C (Figure 1.10).[22] The cations so prepared are extremely reactive and decompose when their solutions are warmed up. EPR spectroscopy of frozen solutions detected triplet diradical signals for some of them, but only a couple of them had linear Curie plots that could indicate triplet ground states. Evidently their preference for the Triplet State is intrinsically low. D values and relative energies of the triplet and singlet states for some investigated cations are presented in table 1.1. As can be expected with higher delocalization of the frontier orbitals, spin-spin interactions of the frontier electrons become weaker (as indicated by decreasing D values). Higher delocalization of interacting electrons also leads to smaller preferences for the triplet state, as expected considering the Columbic basis of Hund's rule.

A very important factor determining the magnitude of the S-T gap is the symmetry of the molecule. Not all systems with $4n\pi$ electrons have the potential to have triplet ground states. Only if they have C_3 or greater symmetry does one expect degeneracies in some orbitals with half occupancy of a degenerate orbital pair. However even a molecule which could have this symmetry, need not adopt it if distortions are readily available. Instead the possible degeneracy of the orbitals can be lifted by Jahn-Teller distortion, which stabilizes the singlet state relative to the triplet since the paired electrons of the singlet state can both go into the orbital whose energy has been lowered by distortion (Figure 1.11).[23]

20

The freedom of rotation of phenyl rings makes molecules such as **Cp(*p*-MeO-Ph)$_5$$^+$** especially prone to this type of behavior and may be another reason besides delocalization for the failure to observe triplet signal in some cases. Due to the highly reactive nature of cyclopentadiene cations, efforts to use them for synthesis of molecular magnets has been essentially futile, and no direct information about the structures of **CpR$_5$$^+$** is available.

Derivatives of benzene dications displayed sufficient thermal stability that crystals of their charge transfer complexes could be grown. Although addition of a second positive charge might be expected to make the molecule more reactive, this drawback is offset by the synthetic accessibility of systems with more electron donating substituents than are possible for cyclopentadienyl system. The ground state of 7^{2+} in the solid state is a singlet by ~4.8 kcal/mol.[24] Examination of the crystal structures reveals that this dication undergoes Jahn-Teller distortion to adopt D_{2h} rather than higher D_6 symmetry optimal for the triplet. Bond lengths of 7^{2+} suggest a description of its structure as a union of two cyanine dye fragments. EPR signals of 7^{2+} in solution and solid state vary, in solution the exited triplet state molecule is able to minimize its energy by coming back to its high symmetry state with an E value equal to 0. Such interconversion is impossible in the crystalline solid, where molecule is immobilized in the lattice and the resulting EPR spectrum is that of a D_{2h} species. This phenomenon indicates that the thermal equilibria between both spin states observed in solution is complicated by equilibria between many possible conformers of the molecules.

7^{2+}

8

9

10

11

12

13

14
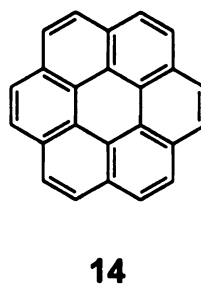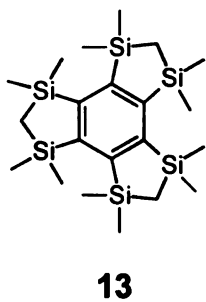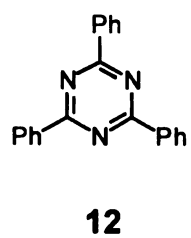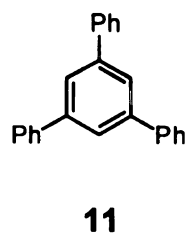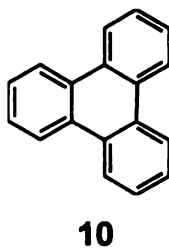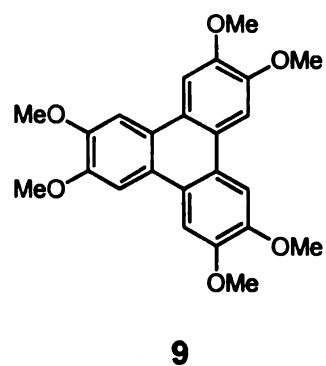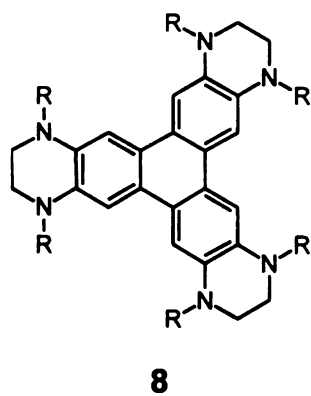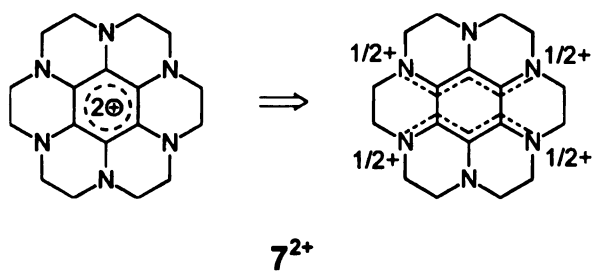
Dication 8^{2+} has a much more delocalized π system than 7^{2+}. EPR studies in this system established the linearity of the Curie plot (meaning either near degeneracy of singlet and triplet or strong preference for the triplet state). The less flexible framework presumably helps to prevent distortion.[23] A definite answer, however, will be difficult to reach until a crystal structure of a salt of dication 8^{2+} can be determined. Unfortunately, this goal remains elusive due to the low stability of 8^{2+}. Similar EPR behavior was displayed by the even less stable (although easier to prepare) dication 9^{2+}.

Besides being oxidized to 4π electrons, benzene derivatives may be also reduced to 8π electron systems. Several series of such dianion-diradicals were studied in the sixties and some of them (10^{2-}, 11^{2-}, 12^{2-}) produced triplet signals.[25-27] Values of the observed zero-field splitting parameters were solvent and counter anion dependent pointing to the great importance of ion pairing phenomena. The most informative studies have been done recently on the silyl stabilized dianion 13^{2-}.[28] Crystals of its lithium salt suitable for x-ray diffraction could be grown and their structure determined. Like 7^{2+}, 13^{2-} undergoes Jahn-Teller distortion leading to D_{2h} symmetry in the dianion despite the C_3 mode of substitution. An especially interesting case is coronene 14 for which the triplet states of both dianion 14^{2-} and dication 14^{2+} have been observed. [29,30]

Classification of 1^{2-}. The dianion 1^{2-} can be simply classified neither as non-Kekule hydrocarbon nor as antiaromatic annulene. In a rather straightforward way, however, it can be related to both groups of diradicals. Dianion 1^{2-} can be looked at as a formal derivative of the well-characterized non-Kekule diradical, dimethylene-cyclobutane-1,3-diyl (DMCD) 15.[7,31,32]

23

DMCB

$C_2O_2^{-\bullet}$

1^{2-}

a $(1b_{3g})$ **b** $(2b_{1u})$

A $(2b_{2g})$ **B** $(3b_{1u})$
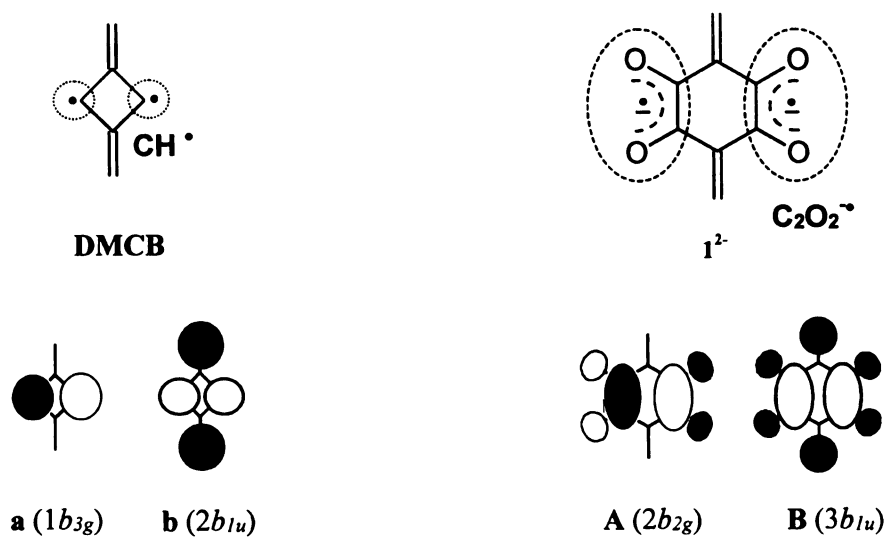
Figure 1.12. Dianion 1^{2-} as a derivative of **DMCB** (15).

Exchange of methine carbon atoms with semidione radical anion (Figure 1.12) produces 1^{2-} with a pair of frontier orbitals **A** ($2b_{2g}$) and **B** ($3b_{1u}$) related to the frontier orbitals of **15** (**a** ($1b_{3g}$) and **b** ($2b_{1u}$)). Preliminary semiempirical calculations have shown that this exchange should not excessively perturb the degeneracy of the frontier orbitals. It can be rationalized by the relative closeness of the SOMO energies of the exchanged fragments (methine carbons and semidione units). Since the new orbitals should retain degenerate and non-disjoint character of **a** and **b**, 1^{2-} (if stable) can have a triplet as ground state. In a more systematic manner the π orbitals of 1^{2-} can be derived from those of benzene. In order to do this, it is convenient to consider also the orbitals of the related dianion of rhodizonic acid (16^{2-}). Figure 1.13 presents energies of molecular orbitals calculated for benzene, 16^{2-} and 1^{2-} calculated with use of the Hückel method. Each of the π orbitals of the benzene can be assigned to two orbitals of 16^{2-}. Both of them will have the same nodal planes as the parent benzene orbital and one of them in addition includes a radial node going around the molecule in-between the carbon and oxygen atoms rings. It can be considered as an effect of constructive and destructive interactions of the p AO of internal carbon and external oxygen rings. Since the lowest orbital with a radial node has higher energy then the highest one without it, two distinct, six orbital subsets are formed, preserving the orbital pattern of benzene. Out of the two degenerate SOMOs of 1^{2-}, the one not having coefficients over external carbon atoms (**A**) remains relatively unperturbed compared to the related orbital in 16^{2-}, while the energy of the delocalized over carbon atoms **B** gets higher. The Magnitude of that shift has value close to the HOMO/LUMO gap in 16^{2-} and **A** and **B** orbitals in 1^{2-} are almost degenerate.
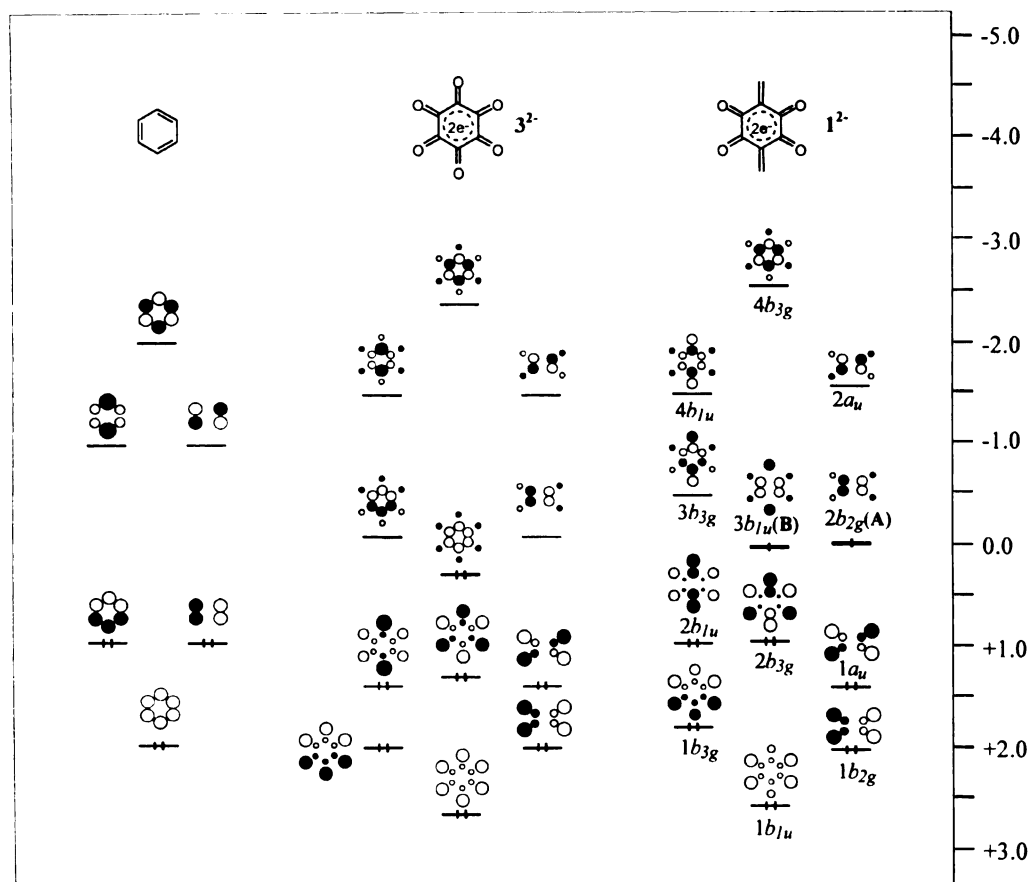
Figure 1.13. Molecular orbital diagram for benzene, rhodazonoic acid dianion (16^{2-}) and 1^{2-}.

These interesting preliminary results encouraged us to pursue a more detailed theoretical study which will be described in chapter 2.

1.2. Self-assembly of 1^- and 1^{2-} into magnetic structures

Proposed anions 1^{1-} and 1^{2-} are structurally akin to 17^{2-} and the abilities of such derivatives of dihydroxyquinone dianion and metal cations to self-assemble into extended networks is well documented.
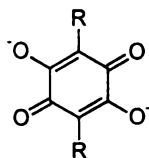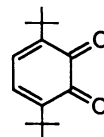
17^{2-} **18**

Structures with various dimensionalities, including infinite chains,[33-41] honeycomb layers[42] or even diamond-like 3D nets[43] have been reported for salts of 17^{2-} or its derivatives. Replacing 17^{2-} with paramagnetic structural equivalents should not destroy its self-organizing properties and would hopefully replicate such motifs. In addition to ensuring the required multidimensional extended topology of interactions, the expected honeycomb motifs like **X** (figure 1.14) should posses high symmetry of the coordination sphere (a_X) of the metal cation. This fact gives hope that predictable intermolecular coupling in such networks can also be fulfilled. Strong evidence supporting that hope is the fact that radical anions **18** coordinated around cations of some main group metals (Ga^{3+}, Al^{3+}) form complexes a'_X with almost identical to a_X symmetry and are high-spin coupled (figure 1.14). The J coupling between paramagnetic ligands equal to 6.2 cm^{-1} (17.7 cal/mol) and 8.6 cm^{-1} (24.6 cal/mol) for Ga^{3+}, Al^{3+}respectively.[44] In, related to **X**, $Al_{2n}1_{3n}$ or $Ga_{2n}1_{3n}$ honeycomb structures all unpaired spins would be supplied by organic anions with diamagnetic cations playing inert, structural role.

28
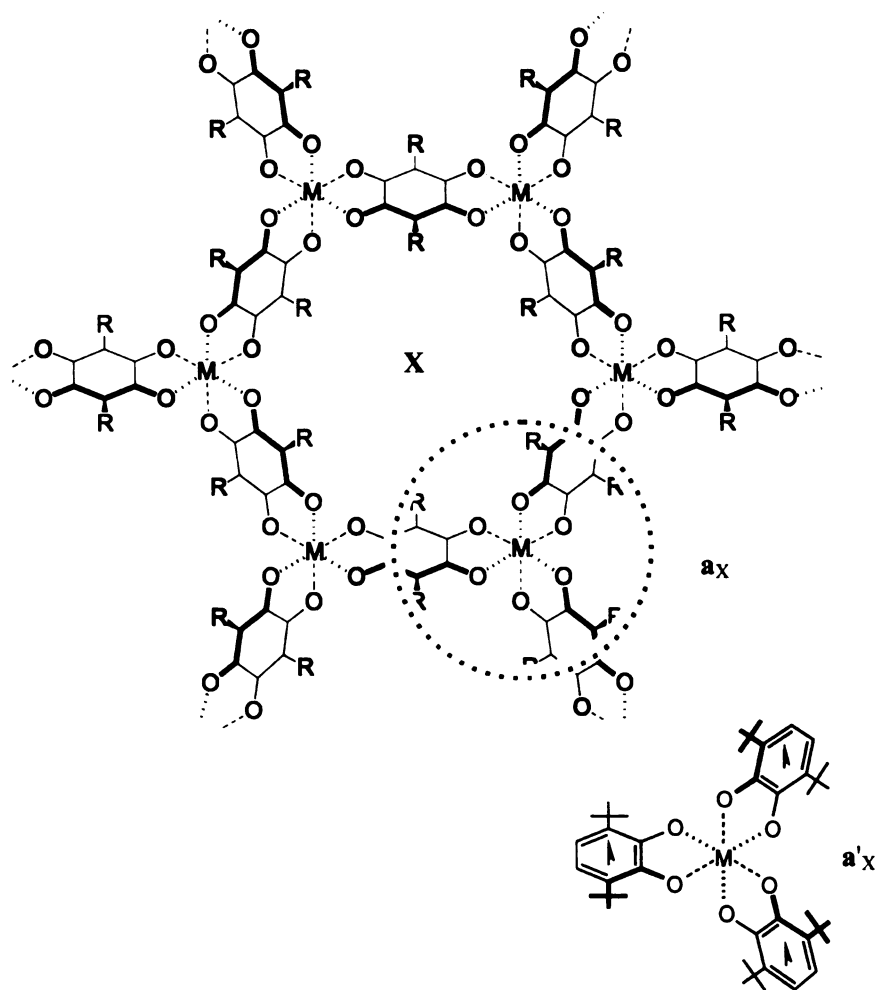
Figure 1.14. Hypothetical 2-D honeycomb magnetic structures formed from anions of **1**

and metal cations (**X**) with spin relay centers (**a**$_X$) symmetry related to high-

spin semiquinone complexes (**a'**$_X$).
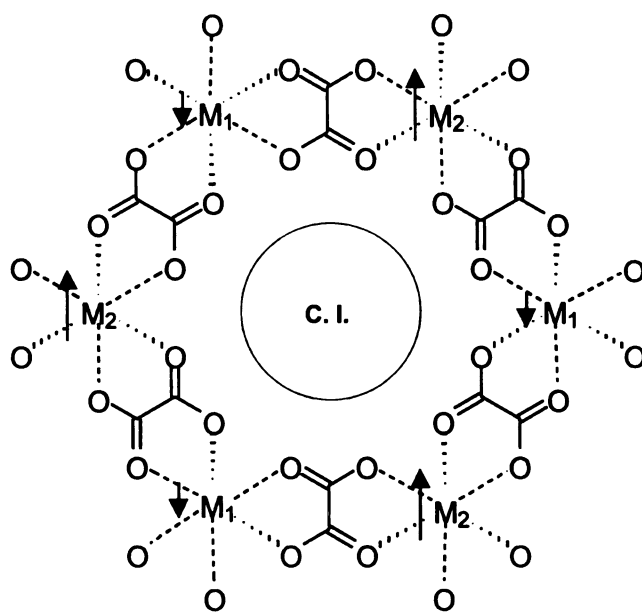
Figure 1.15. Oxalate bridged ferromagnetic honeycomb structures with bulky counterions filling void space.

The strength of the ferromagnetic interactions in such networks may be at best moderate and in order to increase the couplings paramagnetic cations may be used in place of the above diamagnetic main group cations.

A strong magnetic couplings between transition metal cations and various semiquinone ligands coordinated to them has been reported.[45,46] Strong interactions of both high- and low-spin nature are possible, depending on the type of metal cation and geometry of the coordination. As expected antiferromagnetic interactions are generally more common then the more desired ferromagnetic ones. The former type of interactions may still be utilized however for construction of magnets based on the ferrimagnetic principle. Many ferrimagnets with honeycomb magnetic structures have been indeed prepared. A net magnetic moment in those structures is achieved by uneven canceling of different low-spin coupled transition metal cations linked trough oxalate anions (figure 1.15).[47-50] Void space of such structures is filled by bulky counterions which also help to balance the charge of the solid. Although the highest phase transition temperatures of those solids were only in the range of 40K, use of paramagnetic (like **1**⁻) instead of diamagnetic linkers offers the possibility of significantly strenghtening the coupling and hence the ferrimagnetic transition temperatures.

BIBLIOGRAPHY

(1)   Kekule, A. *Annalen* **1858**, *106*, 129.

(2)   Gomberg, M. *Ber. Deutsch. Chem. Ges.* **1900**, *33*, 3150.

(3)   Schlenck, W.; Brauns, M. *Ber. Deutsch. Chem. Ges.* **1915**, *48*, 661.

(4)   Longuet-Higgins, H. C. *J. Chem. Phys.* **1950**, *18*, 265; 275; 283.

(5)   Dowd, P. *J. Am. Chem. Soc.* **1966**, *88*, 2587.

(6)   Dowd, P. *J. Am. Chem. Soc.* **1970**, *92*, 1066.

(7)   Dowd, P.; Chang, W.; Paik, Y. H. *J. Am. Chem. Soc.* **1986**, *108*, 7416.

(8)   Wright, B. B.; Platz, M. S. *J. Am. Chem. Soc.* **1983**, *105*, 628.

(9)   Borden, W. T.; Davidson, E. R. *J. Am. Chem. Soc.* **1977**, *99*, 4587.

(10)   Borden, W. T.; Iwamura, H.; Berson, J. A. *Accounts Chem. Res.* **1994**, *27*, 109.

(11)   Cramer, C. J.; Smith, B. A. *J. Phys. Chem.* **1996**, *100*, 9664.

(12)   Fort, R. C.; Getty, S. J.; Hrovat, D. A.; Lahti, P. M.; Borden, W. T. *J. Am. Chem. Soc.* **1992**, *114*, 7549.

(13)   Wenthold, P. G.; Hu, J.; Squires, R. R. *J. Am. Chem. Soc.* **1994**, *116*, 6961.

(14)   Wenthold, P. G.; Kim, J. B.; Lineberger, W. C. *J. Am. Chem. Soc.* **1997**, *119*, 1354.

(15)   Nachtigall, P.; Jordan, K. D. *J. Am. Chem. Soc.* **1992**, *114*, 4743.

(16)   Clifford, E. P.; Wenthold, P. G.; Lineberger, W. C.; Ellison, G. B.; Wang, C. X.; Grabowski, J. J.; Vila, F.; Jordan, K. D. *J. Chem. Soc.-Perkin Trans. 2* **1998**, 1015.

(17)   Matsuda, K.; Iwamura, H. *J. Am. Chem. Soc.* **1997**, *119*, 7412.

(18)   Ovchinnikov, A. A. *Theor. Chim. Acta* **1978**, *47*, 297.

(19)   Reynolds, J. H.; Berson, J. A.; Scaiano, J. C.; Berinstain, A. B. *J. Am. Chem. Soc.* **1992**, *114*, 5866.

(20)   Reynolds, J. H.; Berson, J. A.; Kumashiro, K. K.; Duchamp, J. C.; Zilm, K. W.; Rubello, A.; Vogel, P. *J. Am. Chem. Soc.* **1992**, *114*, 763.

(21)   Reynolds, J. H.; Berson, J. A.; Kumashiro, K. K.; Duchamp, J. C.; Zilm, K. W.; Scaiano, J. C.; Berinstain, A. B.; Rubello, A.; Vogel, P. *J. Am. Chem. Soc.* **1993**, *115*, 8073.

(22)   Breslow, R.; Chang, H. W.; Hill, R.; Wasserman, E. *J. Am. Chem. Soc.* **1967**, *89*, 1112.

(23)   Breslow, R. *Pure Appl. Chem.* **1982**, *54*, 927.

(24)   Miller, J. S.; Dixon, D. A.; Calabrese, J. C.; Vazquez, C.; Krusic, P. J.; Ward, M. D.; Wasserman, E.; Harlow, R. L. *J. Am. Chem. Soc.* **1990**, *112*, 381.

(25)   van Willigen, H.; van Broekhoven, J. A. M.; de Boer, E. *Mol. Phys.* **1967**, *12*, 533.

(26)   van Broekhoven, J. A. M.; van Willigen, H.; de Boer, E. *Mol. Phys.* **1968**, *15*, 101.

(27)   Broekhoven, J. A. M.; van Willigen, H.; de Boer, E. *Mol. Phys.* **1971**, *20*, 993-997.

(28)   Ebata, K.; Setaka, W.; Inoue, T.; Kabuto, C.; Kira, M.; Sakurai, H. *J. Am. Chem. Soc.* **1998**, *120*, 1335.

(29)   Glasbeek, M.; van Voorst, J. D. W.; Hoijtink, G. J. *J. Chem. Phys.* **1966**, *45*, 1852.

(30)   Krusic, P. J.; Wasserman, E. *J. Am. Chem. Soc.* **1991**, *113*, 2322.

(31)   Snyder, G. J.; Dougherty, D. A. *J. Am. Chem. Soc.* **1989**, *111*, 3927.

(32)   Du, P.; Hrovat, D. A.; Borden, W. T. *J. Am. Chem. Soc.* **1989**, *111*, 3773.

(33)   Kawata, S.; Kitagawa, S.; Kondo, M.; Katada, M. *Synth. Met.* **1995**, *71*, 1917.

(34)   Kawata, S.; Kitagawa, S.; Kumagai, H.; Kudo, C.; Kamesaki, H.; Ishiyama, T.; Suzuki, R.; Kondo, M.; Katada, M. *Inorg. Chem.* **1996**, *35*, 4449.

(35)   Robl, C.; Weiss, A. *Z.Naturforsch. (B)* **1986**, *41*, 1337.

(36)   Robl, C. *Mater. Res. Bull.* **1987**, *22*, 1483.

(37)   Robl, C. *Z.Naturforsch. (B)* **1987**, *42*, 972.

(38)   Robl, C.; Weiss, A. *Mater. Res. Bull.* **1987**, *22*, 497.

(39)   Robl, C.; Kuhs, W. F. *J. Solid State Chem.* **1989**, *79*, 46.

(40)   Cueto, S.; Straumann, H. P.; Rys, P.; Petter, W.; Gramlich, V.; Rys, F. S. *Acta Crystallogr. Sect. C-Cryst. Struct. Commun.* **1992**, *48*, 458.

(41) Decurtins, S.; Schmalle, H. W.; Zheng, L. M.; Ensling, J. *Inorg. Chim. Acta* **1996**, *244*, 165.

(42) Weiss, A.; Riegler, E.; Robl, C. *Z.Naturforsch.(B)* **1986**, *41*, 1501.

(43) Abrahams, B. F.; Coleiro, J.; Hoskins, B. F.; Robson, R. *Chem. Commun.* **1996**, 603.

(44) Lange, C. W.; Conklin, B. J.; Pierpont, C. G. *Inorg. Chem.* **1994**, *33*, 1276.

(45) Pierpont, C. G.; Lange, C. W. In *Progress in Inorganic Chemistry*, 1994; Vol. 41; pp 331-442.

(46) Dei, A.; Gatteschi, D. *Inorg. Chim. Acta* **1992**, *200*, 813.

(47) Tamaki, H.; Zhong, Z. J.; Matsumoto, N.; Kida, S.; Koikawa, M.; Achiwa, N.; Hashimoto, Y.; Okawa, H. *J. Am. Chem. Soc.* **1992**, *114*, 6974.

(48) Okawa, H.; Matsumoto, N.; Tamaki, H.; Ohba, M. **1993**, *232*, 617.

(49) Ohba, M.; Tamaki, H.; Matsumoto, N.; Okawa, H. *Inorg. Chem.* **1993**, *32*, 538.

(50) Decurtins, S.; Schmalle, H. W.; Oswald, H. R.; Linden, A.; Ensling, J.; Gutlich, P.; Hauser, A. *Inorg. Chim. Acta* **1994**, *216*, 65.

Chapter 2

COMPUTATIONAL STUDY OF SINGLET-TRIPLET GAPS IN DERIVATIVES OF

1^{2-}

2.1. Introduction

Preliminary considerations concerning the electronic structure of 1^{2-} were based

on very simple Hückel theory. In order to look at this topic in a more quantitative way

extensive *ab-initio* computations had to follow, both on the parent 1^{2-} and on derivatives

of this dianion. The most straightforward modifications of 1^{2-} are (a) replacement of

hydrogen atoms with other substituents and (b) coordination of the semidione units to

different metal cations. An understanding of the relationship between electronic

properties and structural modifications of 1^{2-} should enable the design of derivatives,

which are most appropriate for assembly of molecular magnets. One of the most desirable

properties of such derivatives from the 'magnetic' point of view would be a strong

preference for a triplet ground state. The majority of our theoretical studies therefore

focused on correlation of structural modifications with the magnitude and sign of $\Delta E_{(S-T)}$.

Since the value of $\Delta E_{(S-T)}$ is directly linked to the degree of degeneracy of the frontier

orbitals (assuming that their spatial overlap remains relatively unperturbed), an attempt

was made to correlate these two factors.

Calculations were planned to be performed first at the CAS(2, 2) level of theory

also known as TCSCF (Two Configuration Self-Consistent Field), for singlet states and

ROHF (Restricted Open-shell Hartree-Fock) for triplets. To gain insight into influence of

correlation between π electrons they were also repeated at the CAS(14, 12) (fourteen

36

electrons in twelve orbitals) level. The set of calculated species included 'naked' dianion

1^{2-} and its complexes $1M_2$ with metal cations of increasing charge ($M=Li^+$, Be^{2+}, Al^{3+}). In

the latter two systems, fluoride anions were added to balance the charge and keep the

overall complexes neutral. The lithium complex was chosen to assess the influence of

substituents such as fluorine (F_41Li_2) and hydroxy groups ($(OH)_41Li_2$). CAS(2, 2) and

CAS(6, 6) calculations on model **DMCB** were also performed.

1^{2-} $1Li_2$ $1(BeF)_2$

$1(AlF_2)_2$ F_41Li_2 $(OH)_41Li_2$

DMCB
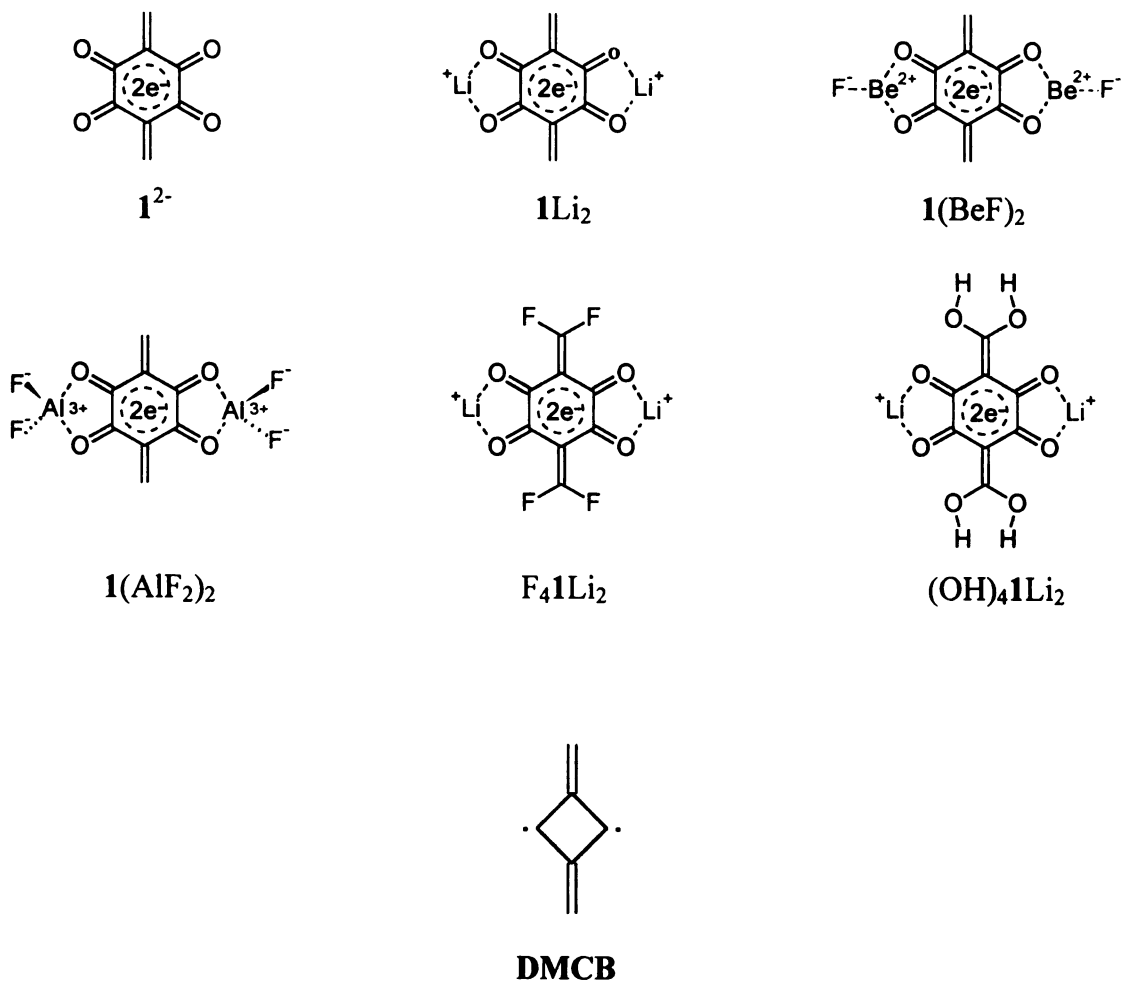
Theoretical Background. Hartree-Fock (**HF**), the most basic computational *ab-initio* method determines the best one-determinantal trial wave function of the molecule

$$\Psi = \Phi_0$$

where:

$$\Phi_0 = (n!)^{-1/2} \begin{vmatrix} \varphi_1(1) & \varphi_1(2) & \cdots & \varphi_1(n) \\ \varphi_2(1) & \varphi_2(2) & \cdots & \varphi_2(n) \\ \cdots & \cdots & \cdots & \cdots \\ \varphi_n(1) & \varphi_n(2) & \cdots & \varphi_n(n) \end{vmatrix}$$

and φ_n symbolizes spin-orbital.

The **HF** solution neglects electron correlation effects (**EC**). Those effects, although accounting for only ~1% of the total energy of a molecule may play an important role in some chemical problems (especially those involving bond breaking processes or diradicaloid species). To describe properly the exact wave function one should include also determinants of states excited with respect to Φ_0.

$$\Psi = a_0\Phi_0 + \Sigma \; a_i\Phi_i$$

Inclusion of all possible excited states would fully account for correlation of all electrons and the exactness of the found solution would be limited only by the size of the basis set used. The computational cost of determining such a function is, however, very high, even for moderate-size molecular systems. To shorten the time of calculation the Complete

38

Active Space Self-Consistent Field (CASSCF or CAS) method is often employed. This method takes into account all possible excitations only in the selected (chemically relevant) orbital subspace. CASSCF calculations optimize both a_i and the form of the orbitals used to define both Φ_0 and the selected excited configurations. The CASSCF method proved to be reliable for prediction of sign and magnitude of the singlet-triplet gaps of many of non-Keküle hydrocarbons, and therefore was selected for use in our calculations.

$$\Phi_0 \qquad \Phi_1 \qquad \Phi_2 \qquad \Phi_3 \qquad \Phi_4 \qquad \Phi_5$$
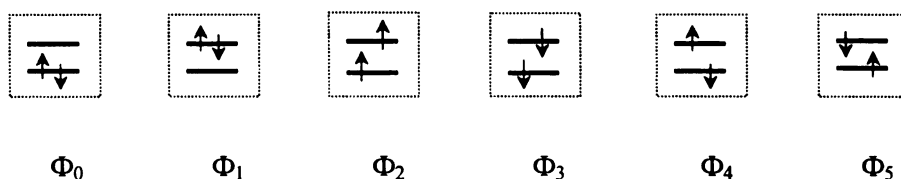
Figure 2.1. All possible determinants in CAS(2,2) active space

In the simplest two orbital scheme for two active electrons (CAS(2, 2)) six possible determinants may be written (figure 2.1). The first two determinants, Φ_0 and Φ_1, represent a singlet state while Φ_2 and Φ_3 form triplet configurations with corresponding values of 1 and -1, respectively, for M_s, the electron spin quantum number. Linear combinations of Φ_4 and Φ_5 lead to one singlet and one triplet ($M_s=0$) configuration. The only difference between the three triplet configurations is the alignment of their magnetic moments in the presence of an external magnetic field, so calculation of only one is required to find out its electronic energy. To describe the singlet state one should use three singlet configurations. However, those three configurations are not unique. In particular, calculations with only Φ_0 and Φ_1 (which is equivalent to the General Valence

39

Bond method) give exactly the same energy as is obtained from calculations with the three configurations.

This two electron, two-orbital level of theory, sometimes considered to be the minimal acceptable, provides relatively consistent results at modest computational cost.[1] It can not, however, be expected to accurately predict the exact energies of the S-T gaps. Correlation with other electrons of the molecule may substantially change the magnitude or even the sign of the calculated values. To account for correlation at least among the most important electrons for conjugated diradicals, an active space including all π electrons and all basic π orbitals is required. Although such a level of calculations describes energy differences rather accurately, further improvement may be achieved by inclusion of corrections for 'dynamic' correlation of the 'active' and inactive (in the case of π diradicals, σ bonds) electrons. The most common method of calculating this correlation is to use second-order Moller-Plesset (MP2) perturbation theory for the CAS wavefunction (CASPT2N method).[2] Although the resulting corrections are minimal, they are necessary for correct prediction of the orderings of closely spaced states (for example exited states for analysis of electronic spectra).

2.2. Results

Table 2.1 summarizes the total energies of the lowest lying singlet and triplet
states for all the species. Reported energies are for geometries optimized in D_{2h} symmetry
at the indicated computational level, except for the CAS(14,12)/6-31+G* energies which
were computed using the CAS(14,12)/6-31G* geometries. In most cases calculations
found ^1A_g and $^3B_{3u}$ to be the lowest lying singlet and triplet electronic states respectively.
The only exception was the naked dianion $\mathbf{1}^{2-}$ whose $^3B_{2u}$ ($|...2b_{3g}{}^2 3b_{1u}{}^1 3b_{3g}{}^1\rangle$) state was
found to be 0.2 kcal/mol below $^3B_{3u}$ ($|...2b_{3g}{}^2 3b_{1u}{}^1 2b_{2g}{}^1\rangle$). To keep all the comparisons
consistent, however, all orbital populations and geometry analyses for $\mathbf{1}^{2-}$ and congeners
(Tables 3 and 4) were based on the $^3B_{3u}$ state. Table 2.1 also contains values of S-T gaps
($\Delta E_{(S-T)}$) expressed in kcal/mol along with the ZPE corrections calculated at the
CAS(2,2)/6-31G* level. Figure 5 graphically depicts the ($\Delta E_{(S-T)}$) gaps as a function of
$\Delta E_{(B-A)}$, the difference between the one-electron energies of the singly occupied frontier
orbitals $\mathbf{B}$ and $\mathbf{A}$ in the ROHF triplets. The $\Delta E_{(B-A)}$ values and occupancies of $\mathbf{A}$ and $\mathbf{B}$ in
the TCSCF (CAS(2,2)) singlet wavefunctions are presented in Table 2.2.

Table 2.3 and 2.4 lists the occupancies of the π (active) orbitals in the CAS(14,12)
wavefunctions for the ^1A_g and $^3B_{3u}$ states, together with the CAS(2,3) results for ^1A_g.
Table 2.5 contains selected bondlengths; cartesian coordinates of the unique atoms and
vibrational frequencies in all calculated complexes may be found in the appendix A.

41

Table 2.1. Total energies of the investigated complexes in their lowest singlet (^1A_g) and triplet ($^3B_{3u}$) electronic states at all levels of the performed calculations.

Level of theory /6-31G*(d)	^1A_g Hartree	$^3B_{3u}$ Hartree	$\Delta E_{(S-T)}$ Kcal/mol
1^{2-}			
CAS(2,2)	-604.55602	-604.54691	-5.7
ZPE$_{CAS(2,2)}$	0.10740	0.10835	-0.6
CAS(2,3)/(2,2)	-604.56193	-604.54691	-9.4
CAS(14,12)	-604.67936	-604.65936	-12.6
		-604.65955*	-12.4
CAS(14,12) /6-31+G*(d)	-604.73282	-604.70526	-17.3
1Li$_2$			
CAS(2,2)	-619.72305	-619.72589	1.8
ZPE$_{CAS(2,2)}$	0.11678	0.11699	-0.1
CAS(2,3)/(2,2)	-619.72569	-619.72589	0.1
CAS(14,12)	-619.82437	-619.82360	-0.5
CAS(14,12) /6-31+G*(d)	-619.84374	-619.84055	-2.0

$*^3B_{2u}$

Table 2.1 (cont.). Total energies of the investigated complexes in their singlet (^1A_g) and tripet ($^3B_{3u}$) electronic states at all levels of the performed calculations.

Level of theory /6-31G*(d)	^1A_g Hartree	$^3B_{3u}$ Hartree	$\Delta E_{(S-T)}$ Kcal/mol
1(BeF)₂			
CAS(2,2)	-833.19055	-833.19756	4.4
ZPE$_{CAS(2,2)}$	0.12690	0.12694	0.0
CAS(2,3)/(2,2)	-833.19243	-833.19756	3.2
CAS(14,12)	-833.28259	-833.28859	3.8
CAS(14,12) /6-31+G*(d)	-833.30793	-833.31300	3.2
1(AlF₂)₂			
CAS(2,2)	-1486.76131	-1486.76908	4.9
ZPE$_{CAS(2,2)}$	0.12879	0.12877	0.0
CAS(2,3)/(2,2)	-1486.76282	-1486.76908	3.9
CAS(14,12)	-1486.85099	-1486.85871	4.8
CAS(14,12) /6-31+G*(d)	-1486.88976	-1486.89663	4.3
F₄lLi₂			
CAS(2,2)	-1015.11315	-1015.11899	3.7
ZPE$_{CAS(2,2)}$	0.08402	0.08419	-0.1
CAS(2,3)/(2,2)	-1015.11443	-1015.11899	2.9
CAS(14,12)	-1015.20809	-1015.21185	2.4
CAS(14,12) /6-31+G*(d)	-1015.23961	-1015.24196	1.5

Table 2.1 (cont.). Total energies of the investigated complexes in their singlet (^1A_g) and tripet ($^3B_{3u}$) electronic states at all levels of the performed calculations.

Level of theory /6-31G*(d)	^1A_g Hartree	$^3B_{3u}$ Hartree	$\Delta E_{(S-T)}$ Kcal/mol
(OH)₄1Li₂			
CAS(2,2)	-919.10912	-919.11529	3.9
ZPE$_{CAS(2,2)}$	0.13544	0.13521	0.1
CAS(2,3)/(2,2)	-919.10971	-919.11529	3.5
CAS(14,12)	-919.19130	-919.19899	4.8
CAS(14,12) /6-31+G*(d)	-919.22139	-919.22854	4.5
DMCB			
CAS(2,2)	-230.538275	-230.54967	7.2
ZPE$_{CAS(2,2)}$	0.09902	0.09846	0.4
CAS(6,6)	-230.587662	-230.61921	19.8
CAS(6,6) /6-31G*(d)	-230.59436	-230.62581	17.7

Table 2.2. Occupancies of orbitals **A** and **B** in the TCSCF singlet wavefunctions and values of $\Delta E_{(B-A)}$ in the ROHF calculations

| | $\Delta E_{(B-A)}$ | Occup. | |
| | ROHF | TCSCF | |
		B	**A**
1^{2-}	0.0453	1.59	0.41
$1Li_2$	0.0209	1.34	0.66
$1(BeF)_2$	0.0091	1.19	0.81
$1(AlF_2)_2$	0.0041	1.11	0.89
F_41Li_2	0.0043	1.08	0.92
$(OH)_41Li_2$	-0.0112	0.78	1.22
DMCB	0.0338	1.53	0.47

Table 2.3. Occupancies of the active orbitals of investigated complexes in the singlet ^1A_g CAS(14,12) and CAS(2,3) wavefunctions.

	^1A_g					
Orbital	1^{2-}	1Li$_2$	1(BeF)$_2$	1(AlF$_2$)$_2$	F$_4$1Li$_2$	(OH)$_4$1Li$_2$
I (b_{1u})	1.98	1.98	1.99	1.99	1.98	1.99
II (b_{2g})	1.96	1.98	1.98	1.99	1.98	1.98
III (b_{3g})	1.97	1.97	1.98	1.99	1.98	1.98
IV (a_u)	1.95	1.97	1.98	1.99	1.97	1.98
V (b_{1u})	1.92	1.91	1.91	1.92	1.92	1.93
VI (b_{3g})	1.94	1.92	1.92	1.92	1.93	1.94
VII **B** (b_{1u})	1.66*	1.41*	1.25*	1.17*	1.14*	0.82*
	1.68	1.56	1.44	1.26	1.37	1.20
VIII **A** (b_{2g})	0.28*	0.58*	0.74*	0.82*	0.86*	1.18*
	0.17	0.40	0.53	0.73	0.62	0.80
IX (b_{3g})	0.06*	0.02*	0.01*	0.01*	0.01*	0.00*
	0.29	0.17	0.15	0.12	0.12	0.09
X (b_{1u})	0.05	0.03	0.03	0.02	0.03	0.03
XI (a_u)	0.05	0.07	0.07	0.06	0.06	0.06
XII (b_{3g})	0.03	0.03	0.02	0.01	0.03	0.02

*CAS(2,3)

Table 2.4. Occupancies of the active orbitals of investigated complexes in the triplet $^3B_{3u}$ CAS(14,12) wavefunctions.

$$^3B_{3u}$$

Orbital	1^{2-}	$1Li_2$	$1(BeF)_2$	$1(AlF_2)_2$	F_41Li_2	$(OH)_41Li_2$
I (b_{1u})	1.98	1.99	1.99	1.99	1.99	1.99
II (b_{2g})	1.98	1.99	1.99	1.99	1.99	1.99
III (b_{3g})	1.96	1.98	1.98	1.98	1.98	1.98
IV (a_u)	1.96	1.98	1.98	1.98	1.98	1.98
V (b_{1u})	1.91	1.92	1.92	1.93	1.93	1.94
VI (b_{3g})	1.91	1.90	1.90	1.90	1.93	1.93
VII B (b_{1u})	1.02	1.01	1.00	1.00	1.00	1.00
VIII A (b_{2g})	1.01	1.01	1.01	1.00	1.01	1.01
IX (b_{3g})	0.11	0.11	0.11	0.11	0.08	0.08
X (b_{1u})	0.04	0.03	0.03	0.03	0.03	0.03
XI (a_u)	0.07	0.07	0.07	0.07	0.06	0.06
XII (b_{3g})	0.03	0.02	0.02	0.02	0.02	0.02

Table 2.5. Selected bond lengths (in Å) of $\mathbf{1}^{2-}$ and its complexes optimized at the

CAS(14,12)/6-31G* level.
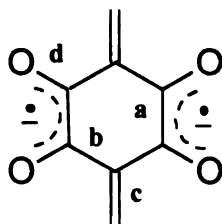
	a($^3B_{3u}$)	a(^1A_g)	b($^3B_{3u}$)	b(^1A_g)	c($^3B_{3u}$)	c(^1A_g)	d($^3B_{3u}$)	d(^1A_g)
$\mathbf{1}^{2-}$	1.436	1.487	1.501	1.457	1.356	1.383	1.252	1.240
$\mathbf{1}Li_2$	1.431	1.451	1.473	1.461	1.357	1.357	1.263	1.257
$\mathbf{1}(BeF)_2$	1.423	1.437	1.457	1.458	1.358	1.351	1.269	1.264
$\mathbf{1}(AlF_2)_2$	1.423	1.433	1.457	1.461	1.358	1.349	1.271	1.266
$F_4\mathbf{1}Li_2$	1.439	1.441	1.471	1.478	1.366	1.356	1.263	1.261
$(OH)_4\mathbf{1}Li_2$	1.433	1.441	1.474	1.474	1.351	1.345	1.259	1.256

48

a)
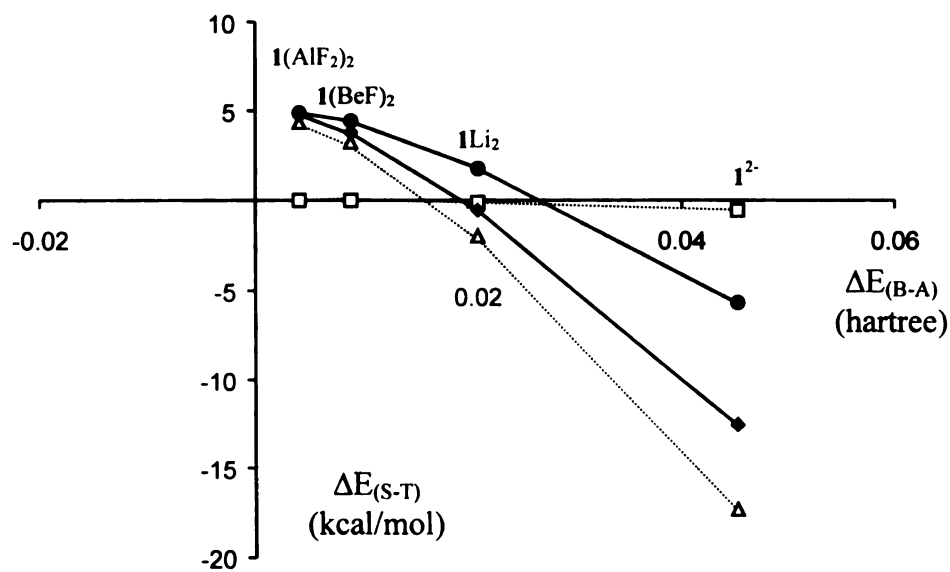
b)
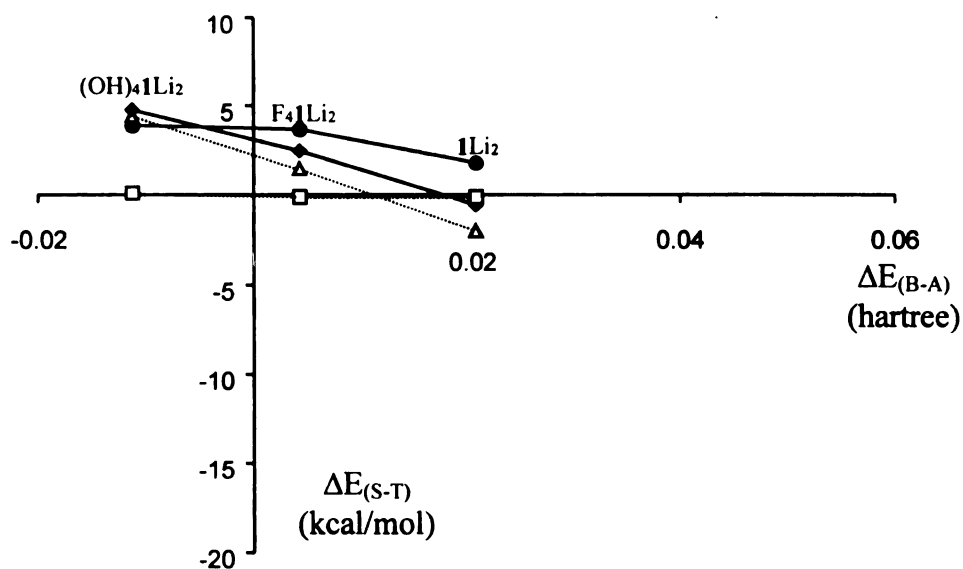
Figure 2.2. S-T gap calculated for a) 1^{2-} complexed by different metal cations b) $1Li_2$
with different substituents R, *vs.* $\Delta E_{(B-A)}$ at

(—●—) CAS(2,2)/6-31G*(d)

(—◆—) CAS(14,12)/6-31G*(d),

(----▲----) CAS(14,12)/6-31+G(d) level of the theory.

(----□----) Zero point corrections at CAS(2,2) level.

2.3. Discussion

Series (a): Effect of metal cation coordination. Electrostatic interactions of electrons with metal cations should lower the energies of all occupied MOs. Orbitals concentrated close to the cations should, however, be affected more strongly then those further away. With substantial density on the methylene carbons, orbital **B** ($3b_{1u}$) does not interact with the cations as strongly as orbital **A** ($2b_{2g}$), which is distributed only on the semidione units (fig 1). These disparate interactions lead to a decrease in the gap between **A** and **B** ($\Delta E_{(B-A)}$) as the cation charge increases. The more charged the cations the stronger an effect is observed; $\Delta E_{(A-B)}$ drops from 0.0453 through 0.0209 and 0.0091, to 0.0041 Hartree for 1^{2-}, $1Li_2$, $1(BeF)_2$ and $1(AlF_2)_2$ respectively. The values of $\Delta E_{(A-B)}$ are obtained at the single configuration ROHF level of theory, so their physical relevance to the CAS results is approximate. Nonetheless, a correlation between $\Delta E_{(A-B)}$ values and S-T gaps is expected, and indeed, an increasing preference for the triplet state tracks the shrinking interorbital gap. At the CAS(2,2) level of theory the ground state of 1^{2-} is a singlet lying 5.7 kcal/mol below the triplet; for $1Li_2$ the singlet already lies above the triplet by 1.8 kcal/mol, while for $1(BeF)_2$ and $1(AlF_2)_2$ this value increases to 4.4 and 4.9 kcal/mol, respectively. Extrapolation of the curve obtained leads to a predicted triplet preference of about 5 kcal/mol for $\Delta E_{(A-B)}=0$. At the current level of theory, this value is probably close to the maximum achievable by tuning of the relative energies of the orbitals.

Series (b): Effect of substitution. Unlike **B**, orbital **A** has no coefficients on the exocyclic methylene carbons in 1^{2-}. Replacement of the hydrogen atoms with other

substituents should thus affect the energy of **B** much more than that of **A**. Since orbital **B** lies lower than **A**, the desired decrease of the **A-B** gap should be achieved by substitution of 1^{2-} with electron donating groups. Figure 5b shows the effect of such structural modifications. Fluorine, a weak π donor, already has a substantial effect, lowering $\Delta E_{(B-A)}$ from 0.0209 for H-substituted $1Li_2$ to 0.0043 for F_41Li_2. The effect of the more strongly donating hydroxy groups is powerful enough to reverse the HOMO-LUMO orbital order ($\Delta E_{(A-B)}$= -0.0112). Although in both cases a strong preference for the triplet follows, the $\Delta E_{(S-T)}$~$\Delta E_{(A-B)}$ correlation can not be directly related to that obtained in series (a). For example, complexes $1(AlF_2)_2$ and F_41Li_2 have almost the same values for $\Delta E_{(A-B)}$ (0.0041 vs 0.0043 Hartree) but somewhat different $\Delta E_{(S-T)}$ values (4.9 vs 3.7 kcal/mol). Inspection of the MO coefficients confirms that replacement of hydrogens with heavy atoms causes more extensive delocalization of orbital **B** and lowers its spatial overlap with **A**. This in turn weakens the electrostatic interactions between the frontier orbitals and slightly lowers the triplet preference. The HOMO-LUMO gap for the model **DMCB** (0.0338 hartree) is larger than for $1Li_2$. Nonetheless, its triplet preference calculated at the CAS(2,2) level of theory is the highest of all the investigated species (7.2 kcal/mol). In this case the electrostatic interactions between the frontier electrons must by magnified by the small size and resulting strong spatial overlap of the two SOMOs.

Correlation effects. Examination of results obtained at the CAS(14,12) level of theory shows that the correlation energy corrections for the calculated species depend on their structures. The more charged are the cations coordinated to 1^{2-}, the lower is the magnitude of $(E_{CAS(2,2)}-E_{CAS(14,12)})$ for both singlet and triplet states. Apparently, with

51

increasing charge of the coordinated cation, the bonding electrons of the π system localize more on the carbonyl oxygens while the antibonding frontier electrons localize on the carbons, weakening their mutual interactions. Coordination also increases the gap between bonding and antibonding orbitals leading to lower polarizability (i.e. higher excitation energies) in the π system. Stabilization of the singlet drops faster than for the triplet. Thus, the improvement in correlation description favors singlet versus triplet for 1^{2-}, the first member of series (a), by 6.9 kcal/mol but for the last member, $1(AlF_2)_2$, by only 0.1 kcal/mol. A similar tendency is observed for the substituent effects in series (b) (2.3 kcal for $1Li_2$ vs. -0.9 for $(OH)_4 1Li_2$). One of the factors contributing to this covariation must be the fact that leveling of the HOMO-LUMO gap results in singlets having more diradical and less ionic character, but it has no analogous effect on triplets. Since correlation generally favors more ionic wavefunctions,[2] the relative stabilization by correlation of the singlet vs. the triplet by correlation thus decreases.

Especially impressive is the relative stabilization of the triplet state in the case of the model **DMCB**, where the triplet preference rises from 7.2 for CAS(2,2) to 19.8 kcal/mol for CAS(6,6). Additional inclusion of all π-SD and σ-S, π-SD CI from the CAS multireference wavefunction were reported to yield preferences of 20.2 and 18.2 kcal/mol, respectively.[3] The authors attributed this large correction to a higher degree of delocalization of the frontier electrons in the triplet compared to the singlet and consequently their stronger interaction with other electrons. The second value reflects the correlation of π with σ electrons, which usually provides extra stabilization for singlets. Unfortunately, the species described herein were too large for such studies via CASPT2N or MR SD CI methods with the software available to us.

Examination of the partial occupancies of the active orbitals in the CAS(14,12) wavefunctions of both singlet and triplet states (tables 2.3 and 2.4), shows high occupation of $3b_{3g}$, especially for 1^{2-}. For this dianion, a triplet state of different symmetry, $^3B_{2u}$ ($|...2b_{3g}{}^2 3b_{1u}{}^1 3b_{3g}{}^1\rangle$), is slightly lower in energy than the $^3B_{3u}$ ($|...2b_{3g}{}^2 3b_{1u}{}^1 2b_{2g}{}^1\rangle$) state. In this doubly charged situation, the low lying $3b_{3g}$ orbital could be electrostatically preferred over $\mathbf{A}$ ($2b_{2g}$) due to the more disjoint relationship of $\mathbf{B}$ and $3b_{3g}$, than of $\mathbf{B}$ and $\mathbf{A}$. The less complete CAS(2,3) ($\mathbf{B}$, $\mathbf{A}$, $3b_{3g}$ and 2 frontier electrons) calculations, however, show rather low populations of $3b_{3g}$ indicating that in the full π space, it is mostly excitations from orbitals other than $\mathbf{A}$ and $\mathbf{B}$ that fill this orbital.

To more accurately describe the anionic character of the organic core 1^{2-} of the species studied here, single point CAS(14,12) calculations with the 6-31+G* basis set were performed on the geometries optimized at the CAS(14,12)/6-31G* level. Addition of the diffuse "+" sets of s and p functions on heavy atoms generally favors singlets. The corrections, however, are not dramatic (see table 1) and as expected, they decrease with tighter coordination of the metal ions.

<u>Molecular Geometry</u>. Potential degeneracy in non-disjoint frontier orbitals does not necessarily assure that a molecule will have a triplet ground state. The degeneracy may be lifted by Jahn-Teller distortion. For example, lowering of the symmetry from threefold or higher to pseudo D_{2h} stabilizes singlet states of $4n\pi$ electron 'antiaromatic' annulenes.[1,4] In the present systems evidence for such distortions was sought at the CAS(2,2) level by vibrational analysis of the D_{2h} optimized structures.

All frequency values for series (a) (1^{2-}, $1Li_2$, $1(BeF)_2$ and $1(AlF_2)_2$) turned out to be real in both singlet and triplet states. Values for some modes of bending out of plane were however very low, showing that the planar geometry is a rather shallow minimum. This finding is unsurprising, in light of the nonplanar geometries we have found for the neutral tetraketone, both computationally and experimentally (with Ph substituents).

In series b, for triplet state $F_4 1Li_2$ all the frequencies are real, while there is one (16 cm^{-1}) imaginary mode for the singlet state. For $(OH)_4 1Li_2$, there are three imaginary frequencies for each state. Two of them in each state (426, 425 cm^{-1} (s) and 458, 457 cm^{-1} (t)) belong to combinations of out of plane torsions of the hydrogens of the OH groups. The third ones (18 cm^{-1}(s) and 23 cm^{-1}(t)) similar like the imaginary frequency of singlet state $F_4 1Li_2$, represent boat-like out of plane bending of the molecular frame. Presumably these distortions arise from the steric interactions introduced when H was replaced by the larger F and OH groups.

While OH torsions may easily be attributed to the artificially high D_{2h} symmetry chosen for the molecules, bending of the whole molecule must reflect an intrinsic characteristic. Does it indicate a tendency to Jahn-Teller distortions or just high flexibility of the molecular frame? Optimization of singlet $F_4 1Li_2$ in the boat-like C_{2v} geometry indicated by imaginary vibration led to energy being less then 15 cal/mol lower then in the D_{2h} one. At the same time occupation numbers of the frontier orbitals change only slightly (from 0.92(A), 1.08(B) to 0.91(A), 1.09(B)), suggesting that the distortion that may be caused more by geometry difference rather then an energetic splitting of the singlet frontier orbitals. Whatever is nature of this distortion the magnitude is negligible in comparison with the value of the S-T gap.

To probe further the flexibility of the molecular frame of $1Li_2$, single point CAS(14,12) calculations on the triplet at the optimal geometry of the singlet (and vice versa) were performed. The energy of the triplet at the singlet geometry was only 1.6 kcal/mol higher then at its own optimum, but for the less forgiving singlet state molecule The analogous increase was 2.8 kcal/mol.

Based on the bond lengths of both singlet and triplet state complexes (table 2.5), it appears that the molecular frame is best described as two semidione units connected through vinylidene bridges. Shortening of bond **a** and elongation of **d** with increasing charge of the coordinated cation may be understood as arising from increasing recruitment of the unpaired electron density to the semidione fragment, wherein the SOMOs are C-C bonding and C-O antibonding. Besides the previously discussed deviation from planarity of F_41Li_2, some bond length differences were found between singlet and triplet geometries. For singlet structures bonds **a** and **b** are longer while **c** and **d** are shorter than for the corresponding triplets. Those variations can be understood in terms of the calculated shifts in electron occupancy from orbital **B** to **A**.

2.4 Computational details

All calculations with the 6-31G*[5] basis set were performed using the GamessD98[6] program running on a SGI/CRAY Origin 2000 computer. Geometries of all complexes in both electronic states were fully optimized in D_{2h} symmetry at each level of calculation. The lowest energy orbitals with the symmetries listed in table 2.3 and 2.4 were selected as the active space. Due to the very low electron occupation of the

LUMO+1 in the triplet CAS(2,3), calculations were automatically terminated by the program. Since GamessD98 can not calculate analytical derivatives at the MCSCF level, vibrational frequencies were calculated only at the CAS(2,2) level with the use of the GVB method for singlet and ROHF for triplet (these methods gave the same single point energies as CAS(2,2)). The symmetry adapted CAS(14,12) active space generates 70 840 configurations for the triplet state and 42 756 for the singlet state. Multiconfigurational Gamess calculations that were attempted with the 6-31+G* basis set failed to converge. They were, however, successfully completed by use of the Molpro package[7,8] after verification that this software yielded identical results to Gamess D98 for the 6-31G* basis set.

BIBLIOGRAPHY

(1) Borden, W. T. in *Diradicals*; Borden, W. T., Ed.; Wiley: New York, **1982.**

(2) Borden, W. T.; Davidson, E. R. *Accounts Chem. Res.* **1996,** *29,* 67.

(3) Du, P.; Hrovat, D. A.; Borden, W. T. *J. Am. Chem. Soc.* **1989,** *111,* 3773.

(4) Breslow, R. *Pure Appl. Chem.* **1982,** *54,* 927.

(5) Hariharan, P. C.; Pople, J. A. *Theor. Chim. Acta* **1973,** *28,* 213.

(6) Schmidt, M. W.; Baldridge, K. K.; Boatz, J. A.; Elbert, S. T.; Gordon, M. S.; Jensen, J. H.; Koseki, S.; Matsunaga, N.; Nguyen, K. A.; Su, S. J.; Windus, T. L.; Dupuis, M.; Montgomery, J. A. *J. Comput. Chem.* **1993,** *14,* 1347.

(7) Werner, H. J.; Knowles, P. J. *J. Chem. Phys.* **1985,** *82,* 5053.

(8) Knowles, P. J.; Werner, H. J. *Chem. Phys. Lett.* **1985,** *115,* 259.

Chapter 3

SYNTHESIS OF THE PRECURSORS OF 1^- AND 1^{2-}

3.1. Introduction

Before starting synthetic work, the crucial question 'What to synthesize' had to be answered. The main goal of the experimental studies is to investigate properties of the derivatives of 1^{2-}. Two hypothetical modes of generation of dianion 1^{2-} might be envisioned. One is reduction of the tetrone **1**, the other deprotonation of the 'acid ' $1H_2$ (Figure 3.1).
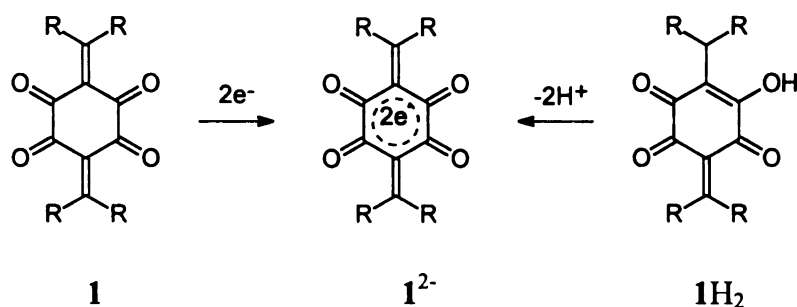
Figure 3.1. Two hypothetical modes of generation of 1^{2-}

Since reduction of **1** gives access cleanly to both radical anion and dianion, this tetrone was given higher priority then the acid as the main target of the synthetic work. The other factor which also had to be determined before beginning the synthesis was selection of appropriate substituents on the methylene group. Both anion, dianion, and their precursors should possess reasonable stability so they can be handled and investigated with relative ease.
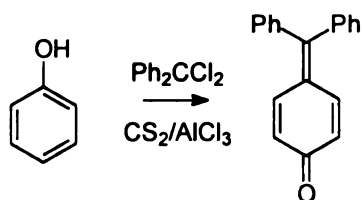
a) Direct condensation of phenols and derivatives of benzophenones
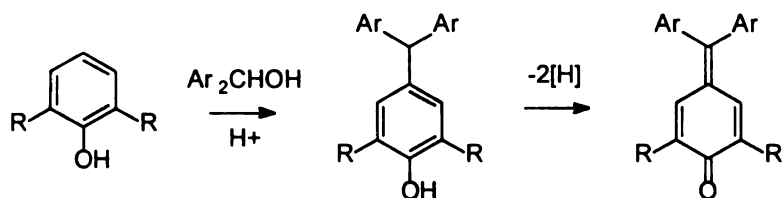
b) Dehydrogenation of diarylmethyl phenols
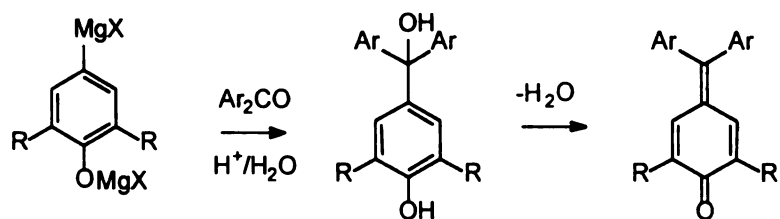
c) Dehydration of triarylmethyl alcohols

Figure 3.2. Three main methods of synthesizing quinone methides

A very common method of stabilizing radical intermediates is to sterically protect then with phenyl rings. Indeed the first known radicals and diradicals were stabilized that way.[1] Phenyl rings are however not only bulky spectators. Their conjugated π systems may transfer electronic perturbations induced by various substituents and electronically tune the tetrone unit. Many synthons necessary for synthesis of such ring substituted compounds are readily available. Phenyl rings also have beneficial effects on the solubility of compounds in non-polar solvents. Considering all those practical factors, a specific precursor **2** (**1**, R=Ph) and **2H$_2$** (**1H$_2$**, R=Ph) and their derivatives were selected as initial synthetic targets.

Preparation of **2** has no precedent. There are, however, some records describing preparation of related fuchsones, diphenyl substituted derivatives of quinone methides.[2] Such compounds were investigated as early as the end of the XIX century and attracted some attention due to their potential application as dyes. Preparation of fuchsones can be classified into three main methods (Figure 3.2): (**a**) Condensation of phenols with benzophenone derivatives; (**b**) alkylation followed by dehydrogenation and (**c**) dehydration of triarylmethyl alcohols. In this work all three methods were tried in an attempt to synthesize **2**.

3.2. Results

Since the first strategy is the most straightforward, investigations were started

with the reaction between dihydroxybenzoquinone and benzophenone.

No reaction however was observed either in alkaline ($3Na_2$ as a substrate) nor acidic

conditions (H^+, $TiCl_4$, $BF_3\cdot THF$ as catalysts).
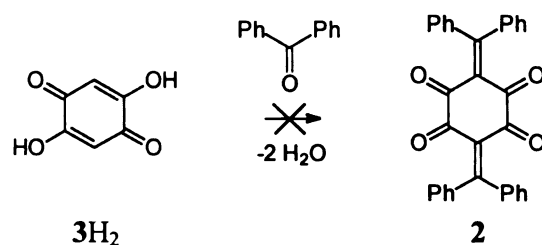
Figure 3.3. Attempt to prepare **2** from $3H_2$ and benzophenone

Apparently, the highly conjugated carbonyl group of the benzophenone was not active

enough toward weakly nucleophilic 3^{2-}(pK_2=5.2). In order to increase the nucleophilicity

of the tetraoxalane unit, the more electron rich tetrahydroxybenzene ($3H_4$) was prepared

by reduction of $3H_2$ (Figure 3.4).[3]
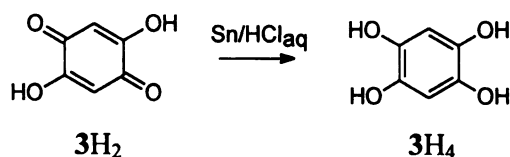
Figure 3.4. Preparation of 1,2,4,5-tetrahydroxy benzene from dihydroxybenzoquinone

Replacement of 3H$_2$ by 3H$_4$ did not bring any breakthrough and unreacted benzophenone

was recovered from reaction mixtures under all conditions investigated. The more

reactive benzophenone equivalent dichlorodiphenylmethane was then prepared from

benzene and tetrachloromethane following the procedure of Gomberg (Figure 3.5).[4]
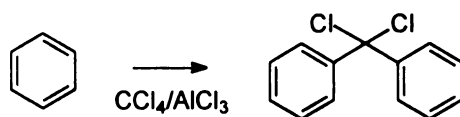
Figure 3.5. Preparation of dichloro-diphenylmethane

Although 3H$_2$ reacted with diphenyldichloromethane, the reaction did not produce 2.

Basic catalysts like NEt$_3$ or pyridine (neat or in DMF or DMSO) led to tars or solids that

were insoluble in common solvents. Acidic conditions (heating in H$_2$SO$_4$/AcOH, AcOH,

CF$_3$COOH or just a neat mixture of reagents) led to evolution of HCl and formation of

benzophenone as a main product. It has been concluded that even if 2 was formed as an

intermediate, it was too delicate to survive such strenuous conditions and reacted further

to form the thermodynamically more stable products. Apparently milder conditions were

required for preparation of 2. Reactions between 3H$_4$ and dichlorodiphenylmethane were

also investigated. When both compounds were heated neat a in 1:2 stoichiometry, HCl

evolved and a yellowish solid identified as 5 was produced (Figure 3.6). Given the above

failures, the one-step strategy for the synthesis of 2 had to be discarded. A new

preparation was attempted by the substitution-dehydrogenation sequence presented on

Figure 3.7.
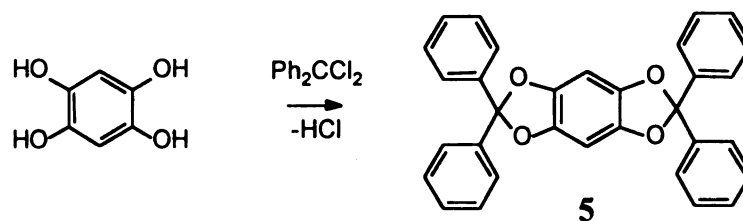
Figure 3.6. Reaction between tetrahydroxybenzene and dichlorodiphenylmethane
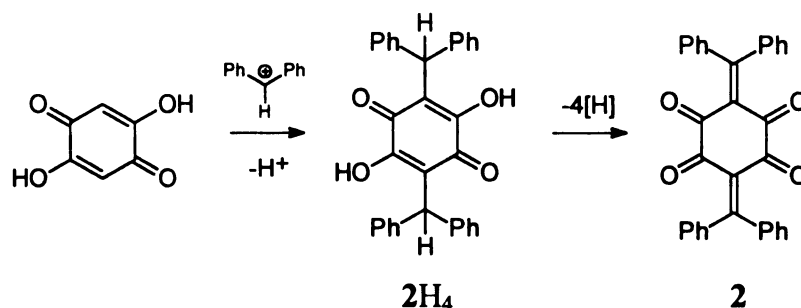
Figure 3.7. Preparation of **2** by a substitution-dehydrogenation sequence

The attempt to prepare **2H₄** turned out to be successful. When **3H₂** and benzhydrol where

refluxed in hot acetic acid with a few drops of H_2SO_4, orange needles of a new compound

separated after cooling. Spectroscopic analysis determined its structure to be **2H₄**. After

some optimization this reaction turned out to give a high yield (96%) of product that was

convenient to isolate and purify. Dehydrogenation turned out to be a much more difficult

task. Out of the many oxidizing agents which were tried, only high-potential quinones

(DDQ and o-chloranil) proved to be effective. Metal salts ($Pb(OAc)_4$, $K_3Fe(CN)_6$,

$Ce(NH_4)_2(NO_3)_6$ and oxides (Ag_2O, activated MnO_2, PbO_2) did not react or formed

insoluble and unreactive salts of $2H_4$. Boiling of $2H_4$ with DDQ in toluene led to a

mixture in which **2** and $2H_2$ (Figure 3.8) could be identified with other side products. The

more expensive and hard to handle o-Chloranil was less effective, while p-Chloranil did

not react at all.
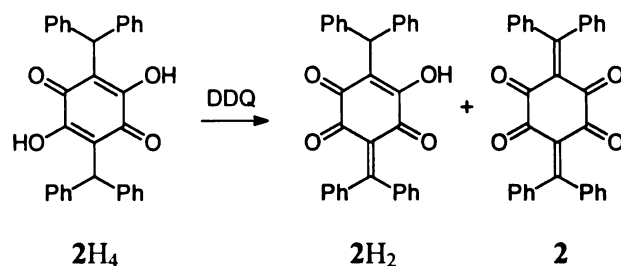
Figure 3.8. Dehydrogenation of $2H_4$ to $2H_2$ and **2**

Separation and purification of products was an unexpectedly difficult task. In addition to

the fact that **2** is a minor product of the reaction, most of the compounds present in the

mixture could be donors or acceptors (or both!) in donor-acceptor charge-transfer

complexes. This situation led to a complicated mixture of such complexes from which

separation of pure components could not be achieved by such standard techniques as

chromatography. Additionally compound **2** proved too delicate to be sublimed or handled

with protic or electron donating solvents. In order to separate the mixture special care had

to be taken that no DDQ (a particularly effective acceptor) remained in solution by

driving the reaction to completion. Precipitation from dichloromethane solution of the

reaction mixture with ether and recrystallization from hot acetonitrile finally achieved

isolation of **2**. The structure of the isolated compound was confirmed by X-ray

crystallography (Chapter 8)

A method to isolate **2H$_2$** was also developed. After reaction of DDQ with excess

of **2H$_4$**, **2H$_2$** was isolated from remaining **2H$_4$** by extraction with Acetic acid and then

purified by recrystallization from cyclohexane.

The simplicity of this two-step synthetic procedure, once developed, encouraged

us to apply it for preparation of phenyl ring substituted derivatives of the parent tetrone **2**

(figure 3.9). Since *ab-initio* calculations indicated that electrondonating substituents

should stabilize the triplet state of the dianion diradical relative to the singlet state, we

focused on such derivatives. Condensation of commercially available 4,4'-

dimethoxybenzhydrol and 4,4'-bis(dimethylamino)benzhydrol with **1H$_2$** led to

(MeO)$_4$**2H$_4$** and (Me$_2$N)$_4$**2H$_4$** under significantly milder conditions than required for **2H$_4$**

Dehydrogenations were also much more facile for the substituted compounds.

The shorter reaction times and the higher stability of the substituted tetrones minimized

side reactions, increasing their yields and simplifying work-up procedures. A new

problem, however, appeared with the new compounds. Donation of electron density from

the phenyl substituents to the tetrone moieties increased the polarity of the compounds

and consequently lowered their solubility in organic solvents. To overcome this problem

a tetrone with eight *t*-butyl groups attached to the phenyl rings was prepared. The

benzhydrol **9** required for this synthesis was prepared from readily available 4,4'-

Methylenebis(2,6-di-t-butyl-phenol) (**6**) following figure 3.10.
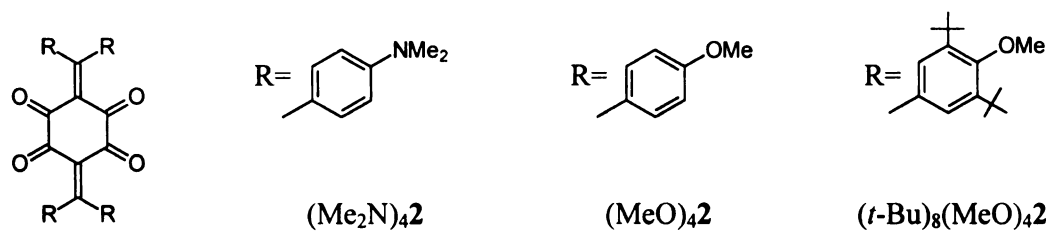
Figure 3.9. Prepared phenyl substituted derivatives of **2**.
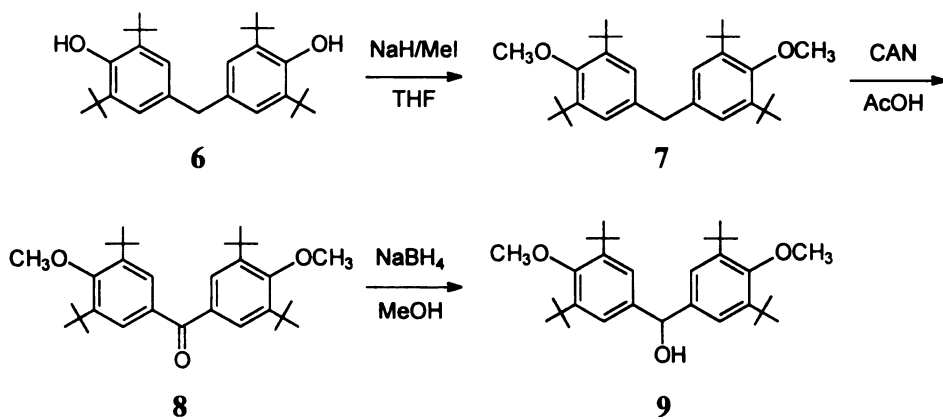
Figure 3.10. Preparation of benzhydrol **9**
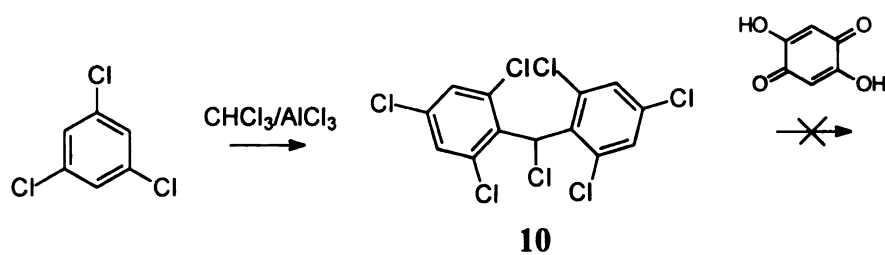
Figure 3.11. Preparation of **10** and its attempted condensation with dihydroxy-

quinone.
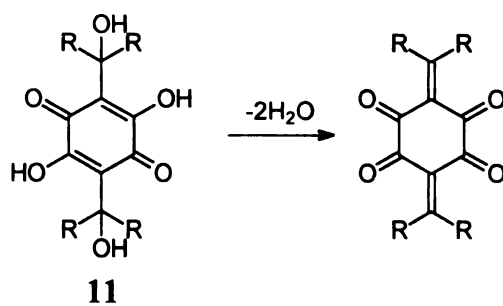
Figure 3.12. Possible Preparation of **1** by dehydration of tetrol **11**

This strategy proved to be successful and $(t\text{-Bu})_8(\text{MeO})_4\mathbf{2}$ was the most soluble out of all the tetrones prepared. It dissolved well even in such a relatively nonpolar solvent as toluene. In addition the bulky t-butyl groups are expected to stabilize the radical against covalent bond-forming processes by providing steric hindrance.

Replacement of the hydrogens by chlorine atoms on the phenyl ring in the *ortho* and *para* positions has been reported to be a very effective protection strategy for triphenylmethyl radicals.[5] Such chlorinated radicals are even air stable. To prepare analogous tetrone condensation of 3H_2 with benzhydrochloride **10** was attempted (figure 3.11). This promising looking reaction failed despite the fact that the benzhydylic chlorineof **10** exchanged for an acetoxy group in the AcOH solvent.

An alternative method for preparation of additional tetrones based on dehydration of tetrol **11** was also attempted (figure 3.12). The protected adamantane substituted diol **13** was prepared following figure 3.13. Intermediate **13** was designed to be deprotected to **15**, then oxidized to **11** and then dehydrated. Deprotection however turned out not to work as planned. Product analysis showed **14** instead of **15** as a main product (Figure 3.14).
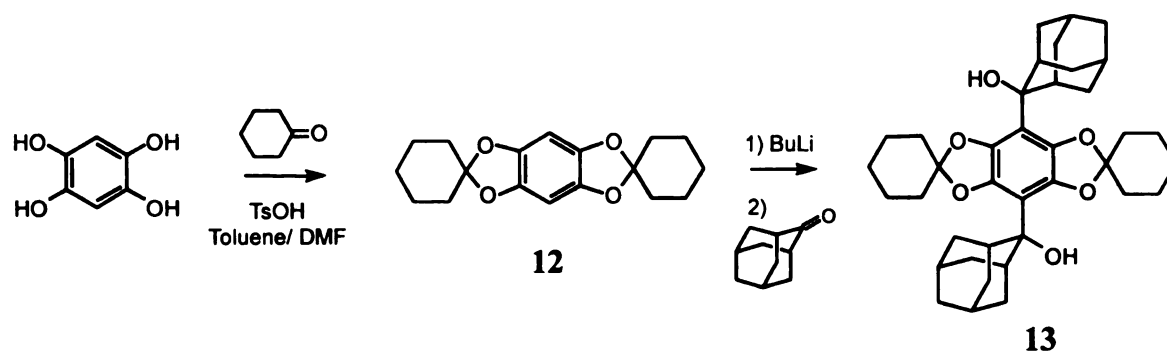
Figure 3.13. Preparation of diol **13**
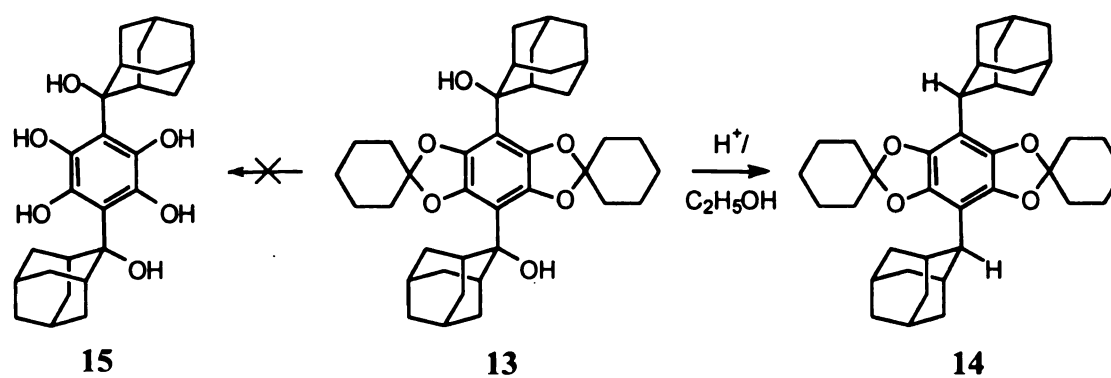
Figure 3.14. Reduction of **13** to **14** instead of its attempted deprotection to **15**
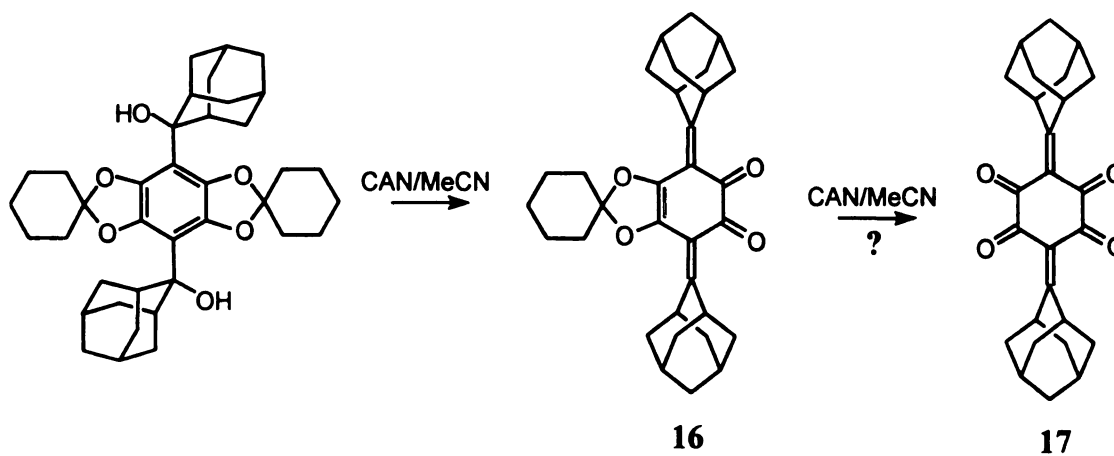
Figure 3.15. Oxidative deprotection of **13** with CAN

Protonation of the hydroxyl group probably leads to formation of a very stable benzylic carbocation, which eventually abstracts hydride from the solvent (EtOH). Attempts at oxygenative deprotection were also stunning. After stirring of 13 with an acetonitrile solution of CAN an orange product precipitated which could be identified as 16 (Figure 3.15). What is interesting is that the oxidation state of molecule did not change. This means that Ce^{4+} cations were apparently acting as a catalyst, not an electron acceptor. The other explanation may be that oxidation took place at the dioxy substituted carbon of the cyclohexyl group instead of at the π system. Further stirring of 16 with the CAN/MeCN solution produced a mixture of products. Although MS showed a peak corresponding to the molecular mass of 17, peaks with higher mass were also present, some of them with odd molecular weights, suggesting the presence of nitrogen.

3.3. Discussion

This work has shown that derivatives of tetrone 2 can be prepared in a simple two-step procedure from readily available substrates. The simplicity of these reactions allows preparation of multigram quantities of target molecules in a matter of days (or even hours). The rate of the first step (electrophilic substitution) clearly correlates with the higher stability of the intermediate carbocation, pointing to its concentration rather than reactivity as a limitation of the reaction. The other reason my be that lower acid concentration used in later synthesis prevents protonation of the dihydroxyquinone. The condensation step did, however, show some limitations. The lack of reaction between $3H_2$ and chlorinated benzhydrol 10 suggests that electrophilic attack of diarylmethylcarbenium ions on 2,5-dihydroxy-1,4-benzoquinone is rather sensitive to the

steric hindrance. This fact impedes preparation of tetrones with *ortho*-substituted phenyl rings, a substantial disadvantage since the resulting mono and dianions would be potentially oxygen stable. As a means to overcome this problem, the use of **18** instead of **10** may be examined. Due to the electron donating methoxy groups (in contrast to the electron withdrawing chlorines) the substitution reaction should be accelerated. In addition the methoxy groups, with their smaller size than chlorine, should also hinder the reaction less, but still be big enough to protect final anion radicals from oxygen.

18

The rate of dehydrogenation in the second step of the scheme developed also positively correlates with the electron-donating abilities of the substituents. This is not surprising since electron-donating substituents stabilize both transient cation and electron-deficient tetrone ring of the final product.[6] Thus to prepare **2,** 24h reflux is required and the yields are generally poor, while the methoxy substituted derivatives require only a couple of hours of reflux; and reaction for $(Me_2N)_4$**2** is almost instantaneous.

DDQ appears to be the only effective dehydrogenating agent in this reaction. Its biggest advantage besides high oxidizing power is its ability to dissolve in mild nonprotic organic solvents. Compounds **2H$_2$** and **2** are unstable in the presence of nucleophilic solvents which excludes many water-soluble metal-ion based oxidizers.

71

The main disadvantage of the developed two step sequence is the limitation to substituents **R** that do not rearrange in the vicinity of the carbocationic center during the first step of electrophilic substitution. The synthetic scheme developed for preparation of **13** was an attempt to overcome that problem. Unfortunately, the oxidative deprotection, which would complete the scheme, probably did not succeed because of the high reactivity of the final product. Its is very likely that the alkyl substituted tetrone, lacking the stabilization provided by phenyl groups, is too electrophilic to survive in the presence of the ammonium cations introduced with CAN. Conceivably, Ce^{+4} triflate may be effective as an alternative to that more traditional reagent.

3.4. Experimental Section

General Methods. Melting points were determined on a Thomas-Hoover apparatus and are uncorrected. ^1H and $^{13}C\{1H\}$ spectra were obtained at 300 and 75.5 MHz, respectively on Varian GEMINI 300 spectrometer. The ^1H NMR shifts are referenced to residual ^1H resonances in the deuterated solvents: $CDCl_3$ (δ 7.24); DMSO-d_8 (δ 2.49). The ^{13}C shifts are referenced to those of the deuterated solvents: $CDCl_3$ (δ 77.0); DMSO-d_8 (δ 39.5).

Toluene, Benzene and THF were dried by refluxing over sodium/benzophenone under nitrogen; acetonitrile by refluxing over CaH_2 under nitrogen. The rest of the reagents and solvents were used as supplied (Aldrich). Ketone **9** was prepared following ref 7, compound **12** following ref 3.

Synthesis of 2H$_4$. 2g of 2,5-dihydroxy-1,4-quinone (14.3 mmol), 5.5 g of

benzhydrol (29.9 mmol) and 0.5 ml of conc. H$_2$SO$_4$ were refluxed for 1h in 20ml of

AcOH and then left at room temperature to cool. The crystalline mass obtained was

crushed with a spatula and vacuum-filtered through a glass frit. The collected yellow

crystals were washed with a small amount of AcOH and then thoroughly with water.

Crystals were dried overnight at ca. 90 °C in air giving 6.5 g (96.5%) of orange powder.

The purity of the resulting 2H$_4$ proved to be sufficient for the next step. It could, however,

be recrystallized from 20 ml of AcOH giving 6g (89% yield) of the product: mp 190-192

°C, ^{1}H NMR (CDCl$_3$, 300 MHz): δ=5.69 (s; 1 H), 7.2-7.3 (m; 10 H), 7.95 (s; 1 H), ^{13}C

NMR (CDCl$_3$, 75 MHz): δ=45.6, 117.3, 126.75, 128.4, 129.0, 140.6 (Broadening caused

by concerted proton shift makes it difficult to detect signals of C=O and C-OH carbons).

Synthesis of 2H$_2$. 2H$_4$ (6g, 12.7 mmol), DDQ (1g, 4.4 mmol) and benzene (30 ml)

were gently refluxed with magnetic stirring for 18h under a nitrogen atmosphere. The

benzene was evaporated, 75 ml of CHCl$_3$ were added to the flask, and after a few minutes

of stirring at room temperature, the solution was suction filtered. The separated solid of

2,3-dichloro-5,6-dicyano-1,4-hydroquinone was washed with more CHCl$_3$ and the

combined chloroform solutions were evaporated to dryness. After addition of 25ml of

Acetic acid to the flask, the solution was refluxed until the entire solid dissolved. It was

then left to cool. The precipitated 2H$_4$ (which can be reused) was filtered off and washed

with more acetic acid. The combined acetic acid solutions were concentrated on vacuum

to a dark red oil, cold water was added, and mixture stirred until the oil solidified. The

resulting orange-brown solid of crude 2H$_2$ was filtered off, washed with water and dried.

73

The dry solid was then crushed, refluxed with 800 ml of cylohexane for about 25 min and the solution was cooled, filtered and concentrated to about 80 ml of volume. The precipitated orange crystals of $2H_2$ (1.2g, 58%yield based on DDQ) were filtered off, dried, and once again recrystallized from cyclohexane; mp 115-116 °C (dec.), ^1H NMR (CDCl$_3$, 300 MHz): 5.93 (s; 1 H), 7.1-7.6 (m; 20 H), 8.0-8.2 (broad; 1H), ^{13}C NMR (CDCl$_3$, 75.5 MHz): 46.3, 126.8, 128.0, 128.4, 129.1, 131.4, 132.1, 132.6, 140.3, 140.9, 157.4, 177.2, 179.4, 180.3.

Synthesis of **2**. 10g of **2H$_4$** (21.2 mmol), 10g of DDQ (44.1 mmol) and 70 ml of dry benzene were gently refluxed with stirring for 24h under a nitrogen atmosphere, the solvent was evaporated, and the solid washed with ca. 200 ml of Et$_2$O and air dried. The resulting red powder was dissolved in 200 ml of CHCl$_3$ and filtered. The separated solid DDQH$_2$ was washed with more CHCl$_3$ and combined chloroform solutions were concentrated to about 25 ml. When 300 ml of Et$_2$O was poured into the concentrate, after a while red crystals of crude **2** separated. The product was purified by recrystallization from hot MeCN (Yield 2-10%); mp 288-290 °C (dec.), ^1H NMR (CDCl$_3$, 300 MHz): 7.2-7.6 (m; 20 H), ^{13}C NMR (CDCl$_3$, 75.5 MHz): 128.1, 132.0, 132.5, 140.0, 180.1, 186.6. Analysis: calc. C82%, H 4.3%, found C 81.04%, H 4.55%.

Synthesis of (MeO)$_4$2H$_4$. To the well stirred refluxing solution of 2g of **3H$_2$** (14.3 mmol) in 100 ml of AcOH containing a few drops of conc. H$_2$SO$_4$ was added 7.0g (28.7 mmol) of 4,4'-dimethoxybenzhydrol. Solution first became red and after a while yellow product precipitated. The suspension obtained was refluxed for about 15 min more,

cooled to room temperature and filtered. The collected powder was washed first with AcOH, then water, and dried giving 8g (13.5 mmol 94.4%) of crude product which was recrystallized from dioxane; mp=263-4°C, ^{1}H NMR (DMSO-d_6, 300 MHz): δ=3.71 (s; 6 H), 5.46 (s; 1 H), 6.82 (d; J=8.7 Hz, 4 H), 7.07 (d; J=8.7 Hz, 4 H), 11 (broad; 2 H), ^{13}C NMR (DMSO-d_6, 75.5 MHz): δ=43.4, 55.0, 113.5, 118.0, 129.6, 133.9, 157.5.

Synthesis of (MeO)$_4$2. 1.3 g of (MeO)$_4$2H$_4$ (2.2 mmol) and 1g of DDQ (4.4 mmol) were refluxed in 50 ml of toluene for 3h. The solvent was evaporated and the solid extracted in a soxhlet extractor with 100ml of CH$_2$Cl$_2$. The resulting dark purple solution of tetrone was diluted with 100ml of Et$_2$O and, left aside for ca. 1h and filtered giving 0.9 g (70%) of product: mp>300; ^{1}H NMR (CDCl$_3$, 300 MHz): δ=3.87 (s; 3 H), 6.88 (d; J=10 Hz, 2 H), 7.28 (d; J=10 Hz, 2 H), Analysis: calc. C73.5%, H 4.8%, found C 72.52%, H 5.06%.

Synthesis of (Me$_2$N)$_4$2H$_4$ 2g of 3H$_2$ (14.3 mmol) and 7.8 g (28.9 mmol) of 4,4'-Bis(dimethylamino)-benzhydrol was refluxed with stirring in 100ml of absolute EtOH for 15 min, the solution was cooled and the purple (zwitteronic) product of spectroscopic purity (8.7g, 13.5 mmol, 94.3%) filtered off, washed with ethanol and dried: mp=169-170 °C (dec.), ^{1}H NMR (CDCl$_3$, 300 MHz): δ=2.90 (s; 12 H), 4-4.5 (broad; 1 H), 5.49 (s; 1 H), 6.64 (d; J=9 Hz, 4 H), 7.10 (d; J=9 Hz, 4 H), ^{13}C NMR (CDCl$_3$, 75.5 MHz): δ=40.7, 43.8, 112.5, 117.7, 129.6, 129.75, 148.9, 168.4.

Synthesis of (Me$_2$N)$_4$2 To the well stirred solution of 1 g (1.55 mmol) of

(Me$_2$N)$_4$2H$_4$ dissolved in 100 ml of CH$_2$Cl$_2$ was added slowly 0.7g (3.1 mmol) of DDQ

dissolved in 100 ml of CHCl$_3$. During addition the solution turned dark blue. It was left

stirring for ca. 20 min more and the solvent was removed by evaporation. Separation of

the product from DDQH$_2$ was achieved on a glass frit by slow dissolving of the

protonated product with conc. HCl until the acid no longer was yellow. The resulting

acidic solution was neutralized first with NaOH and then with sodium bicarbonate until

solution reached pH 7-8. The precipitated blue suspension of product was suction filtered,

washed with water, dried, and recrystallized from hot DMSO giving 0.9 g (67%) of

(Me$_2$N)$_4$2•((CH$_3$)$_2$SO)$_3$: mp>300 (dec.), ^{1}H NMR (DMSO-d$_6$, 300 MHz): δ=3.13 (s; 12

H), 6.76 (d; J= 9 Hz, 4 H), 7.20 (d; J= 9 Hz, 4 H). Analysis: calc C 63.1% H 6.7% N

6.4%, found C 62.43%, H 6.94% N 6.61%.

Synthesis of benzhydrol 9. To the well stirred suspension of 30 g (71.7 mmol) of

benzophenone 8 in 250 ml of MeOH, was slowly added 7g of NaBH$_4$. During the process

the mixture warmed up, become homogenous and started to froth. When the reaction

slowed down it was refluxed for ca. 30 min more. After cooling, 250 ml of water was

added and the milky solution was extracted with three 100 ml portions of CH$_2$Cl$_2$. The

combined extracts were dried over Na$_2$SO$_4$ and evaporated to dryness. The waxy residue

was recrystallized from a small volume of hexanes giving 26 g of 9: mp=115-116.5, H^1

NMR (CDCl$_3$, 300 MHz): δ=1.38 (s; 36 H), 2.2 (s broad; 1 H), 3.66 (s; 6 H), 5.72 (s; 1

H), 7.22 (s; 4 H), C^{13} NMR (CDCl$_3$, 75.5 MHz): δ=32.0, 35.8, 64.2, 76.7, 125.1, 137.6,

143.4, 158.8.

Synthesis of $(t\text{-Bu})_8(\text{MeO})_4\text{2H}_4$.To the well stirred refluxing suspension of 1.4g of 3H_2 (10 mmol) in 100 ml of AcOH containing a few drops of conc. H_2SO_4 was added 10.0g (21.3 mmol) of benzhydrol **9**. The solution was refluxed for about 15 min, 40 ml of water was added, and the mixture was cooled to room temperature and filtered. The collected yellow crystals were washed first with water, then MeOH, and dried giving 10 g (9.7 mmol, 97 %) of crude product which was recrystallized from AcOH: mp=232-3°C, H^1 NMR (CDCl$_3$, 300 MHz): δ=1.36 (s; 72 H), 3.68 (s; 12 H), 5.51 (s; 2 H), 7.11 (s; 8 H), 8 (s broad; 2 H), C^{13} NMR (CDCl$_3$, 75 MHz): δ=32.1, 35.7, 45.2, 64.1, 117.9, 127.2, 134. 8, 142.9, 157.9.

Synthesis of $(t\text{-Bu})_8(\text{MeO})_4\text{2}$. 4.6g of $(t\text{-Bu})_8(\text{MeO})_4\text{2H}_4$ (4.425 mmol), 2g of DDQ (8.8 mmol) and 50 ml of dry toluene were gently refluxed with stirring for 5h. The hot solution was filtered and the filtrate evaporated to dryness. The resulting dark red solid was triturated with two 50ml portions of hexane giving the crude product which could be recrystallized from toluene/hexane giving 2.6g (56%) of tetrone: mp>300 (dec.), H^1 NMR (CDCl$_3$, 300 MHz): δ=1.35 (s; 36 H), 3.71 (s; 6 H), 7.15 (s; 4 H), C^{13} NMR (CDCl$_3$, 75 MHz): δ=31.9, 35.8, 64.6, 129.8, 133.3, 134.5, 143.1, 165.0, 178.4, 184.2. Analysis: calc. C 78.7%, H 8.9%, found C 77.77%, H 9.58%.

BIBLIOGRAPHY

(1)   Gomberg, M. *Ber. Deutsch. Chem. Ges.* **1900**, *33*, 3150.

(2)   Grunanger, P. *Methoden Der Organischen Chemie*; Vol. 7/3b Chinone; Houben-Weyl: Stuttgart Thieme, 1979; pp 395. (b) Wagner, H.-U.; Gompper, R. *Chemistry of functional groups.*; The chemistry of the quinonoid compounds; Interscience: London ; New York, 1974; pp 1145.

(3)   Orlemans, E. O. M.; Lammerink, B. H. M.; Vanveggel, F.; Verboom, W.; Harkema, S.; Reinhoudt, D. N. *J. Org. Chem.* **1988**, *53*, 2278.

(4)   Gomberg, M.; Jickling, R. L. *J. Am. Chem. Soc.* **1915**, *37*, 2575.

(5)   Ballester, M. *Accounts Chem. Res.* **1985**, *18*, 380.

(6)   Becker, H.-D. *Chemistry of functional groups.*; The chemistry of the quinonoid compounds; Interscience: London ; New York, 1974; pp 335.

(7)   Anderson, K. K.; Shultz, D. A.; Dougherty, D. A. *J. Org. Chem.* **1997**, *62*, 7575.

Chapter 4

GENERATION AND EPR/ENDOR STUDY OF THE DERIVATIVES OF 1- AND 1^{2-}

4.1 Introduction

The main aim of conducting EPR/ENDOR studies of radical monoanions was to gain basic information concerning their structure (especially the symmetry of the spin delocalization) and their stability. The related study of the dianion focused also on determination of its ground state (singlet *vs*. triplet). The required samples of anions and dianions were prepared by reduction of the parent tetrones with alkali metals (Scheme 3.1). EPR/ENDOR spectroscopic characterization started with investigation of 'naked' anions (non-coordinated to metal cations). Generation of such species is possible when the metal cation is trapped inside the cage of a tightly coordinating organic ligand such as a crown ether or cryptand. Use of the cryptand c(2.2.2) as an additive in potassium mirror reductions not only traps potassium cations but also facilitates the whole dissolution process. The dissolved macrocycle, upon contact with the potassium surface, forms a solution of potassium potasside [K@c(2.2.2)]$^{+}$K^{-}, a strong and effective reducing agent,[1] which then may reduce substances that are themselves insoluble in the reaction solvent.
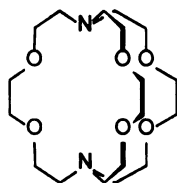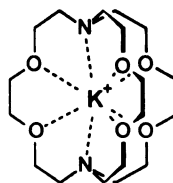
c(2.2.2)   K@c(2.2.2)$^{+}$

Although *ab-initio* calculations (Chapter 2) showed tight coordination should increase the chances of the triplet being the ground state of the dianions, the strategy of using naked anions allows the acquisition of information about them free of complication caused by ion pairing. Aggregation phenomena can often obscure spectroscopic results by allowing intermolecular spin-spin interactions and decreasing the solubility of the investigated species. Studies of the reduction products without macrocyclic co-ligands were also performed.

Theoretical Background. EPR (*electron paramagnetic resonance*) and the closely related ENDOR (*electron-nuclear-double-resonance*) spectroscopies are the most direct spectroscopic methods for characterization of paramagnetic organic molecules.[2] In particular they can map delocalization of the unpaired electron(s) over the atoms of the molecule and in the case of polyradicals, provide information about the strength of the magnetic spin-spin interactions of the unpaired electrons.

Electron Paramagnetic Resonance spectra of monoradicals (S=1/2, doublets) are usually split into many lines. This splitting of the resonances, known as hyperfine structure, is caused by interactions of the unpaired 'resonating' electron with the magnetic moments of the nuclei of the molecule (usually H^1, N^{15}, F^{19}, C^{13}, P^{31} for organic molecules). The strenght of these electron nuclear spin interactions is quantified via the hyperfine coupling constant (a) and may be obtained directly from the EPR spectra by measuring the separation between the lines of the spectrum. The value of a depends linearly on the probability of finding the unpaired spin of the electron on the interacting nuclei (Fermi contact $|\Psi(0)|^2$) and may be expressed as:

$$\mathbf{a}=(2/3)\mu_o g_e \mu_\beta \gamma |\Psi(0)|^2$$

where:

μ_o- magnetic permeability of vacuum, g_e-Lande's factor, μ_β-Bohr magneton γ-gyromagnetic ratio of the nucleus.

For a group of structurally related atoms or molecular units a linear correlation exists between the Fermi contact and the spin population localized on that unit. One such correlation is the McConnell relation:[2-3]

$$\mathbf{a}_H = Q\rho_\pi$$

where the spin population localized on an sp^2 hybridized carbon (ρ_π) is related to the hyperfine splitting at hydrogen ($\mathbf{a}_H$) directly attached to it, via the constant Q. This relation is often used for estimating spin distribution over π conjugated systems.

Other important information besides the strength of the hyperfine coupling is its multiplicity (number of lines signal is split into). For proton hyperfine splitting, the variety most commonly encountered, the multiplicity of the splitting relates to the number of interacting nuclei n, as n+1 (generally interpretation of the splitting of the electron EPR signal is similar to that for NMR spectra). In the case when the electron interacts with a large number of nuclei (highly delocalized radicals) interpretation of the spectrum by inspection is difficult and computer simulation of the spectra are needed in the analysis. If this approach fails, ENDOR spectroscopy must be used. In the ENDOR experiment, the intensity of the EPR signal of the radical is measured as a function of the frequency of electromagnetic irradiation in the NMR region while the electron resonance frequency is kept constant. When such irradiation reaches a resonant value for nuclei 'coupled' to the unpaired electron (usually protons) the intensity of the measured EPR

81

signal increases. Each coupled nucleus will resonate with two frequency values, corresponding to its splitting by the unpaired electron's spin-i.e: depending whether spin of the unpaired electron is parallel or antiparallel to the field of the instrument. The difference between those two resonances (usually measured in MHz) linearly relates to the value of the hyperfine coupling constant. The main advantage of the method is that one can measure very small hyperfine splittings under conditions where the hyperfine structure of the EPR spectrum contains so many lines that they can overlap.

In principle EPR spectra of triplet diradicals in solution do not differ significantly from those of monoradicals. The most notable difference is a broadening of the hyperfine pattern caused by the diradical molecule's spin-spin interactions between the unpaired electrons, averaged by tumbling. A large difference may be observed in powder or glass solid matrices. In this case tumbling of the molecules is impossible and the anisotropic spin-spin interactions of the two unpaired electrons of the molecule do not average. As a consequence the external magnetic field felt by each electron is strongly perturbed by the magnetic moment of the other unpaired electron. The degree of such perturbation depends on the position of the molecule vs. the external magnetic field. Since the distribution of diradicals is random, a very broad (usually hundreds of Gauss) EPR spectrum may be observed.[4] Figure 4.1 displays a typical example of such a triplet spectrum. The D value reflects the magnetic interaction between the unpaired spins and is proportional to r^{-3} where r is an average distance between unpaired electrons. The E value, in turn, relates to the deviation from threefold or higher symmetry of the diradical.
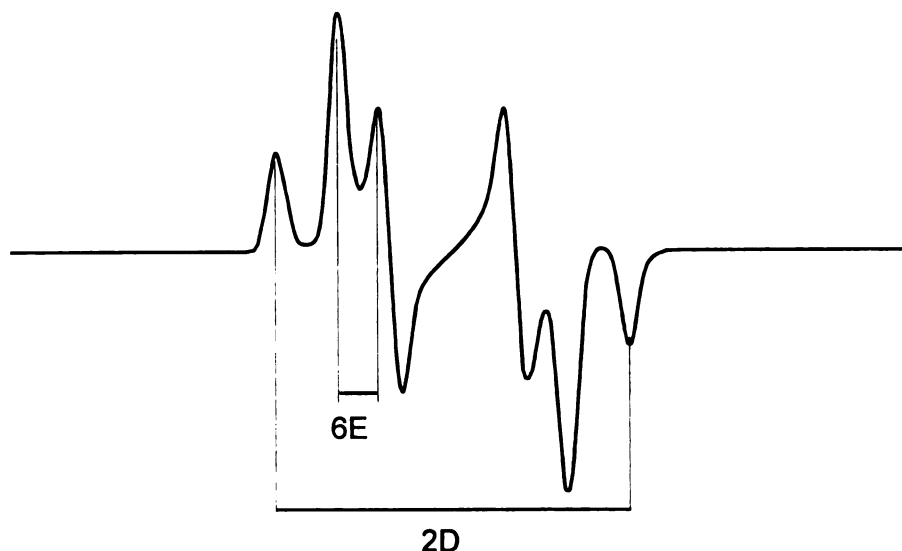
Figure 4.1. A typical solid state spectrum of triplet diradical

Another characteristic feature of the triplet state diradical is the presence of the so-called half-field transition. This is a weak signal (for organic diradicals in ca. 1600 G, g=4) indicating formally forbidden $\Delta S=2$ (from spin S=-1 to S=1) transition. In the case of doublet radicals, neither a half-field transition nor anisotropic spin-spin interactions may be observed and frozen solutions produce only a sharp peak in the regular field (ca. 3200 G, but depends on the instrument used) intensity. Of course singlet state molecule will not produce any EPR signal at all.

4.2 Results

Monoanions. All para substituted monoanions, in the present work could be handled at room temperature without noticeable decomposition. Under these conditions, however, 2^- decayed slowly with a half-life of ca. 1h, so it was handled below –20 C. All prepared monoanions were air sensitive. Monoanions in solution produced strong EPR signals with g values characteristic for organic radicals. Values of hyperfine coupling constants of the phenyl rings were determined for all anion radicals by ENDOR and are presented in table 4.1. The ENDOR spectra are also reproduced in figures 4.(2,4,6,8). Experimental EPR spectra of those anion radical could be successfully simulated (figures 4.(3,5,10) by assigning a_1 values to all 8 *ortho* (and in the case of 2^-, 4 *para*) protons and a_2 to all 8 *meta* protons of the four phenyl groups. Simulation of the signal of $(Me_2N)_4 2^-$ (figure 4.7) was not attempted, due to the low resolution of the experimental EPR spectrum and the inability to find values of the coupling constants for the $-NMe_2$ protons by ENDOR. The monoanion t-$Bu_8(MeO)_4 2^-$ showed strong temperature dependence of its ENDOR and EPR spectra. At low temperature (197 K), its ENDOR spectrum (fig 4.8) showed two couplings caused by its *ortho* hydrogens (5.4 and 1.5 MHz). Raising the temperature to 223 K decreased those signals intensities with simultaneous appearance of a new averaged single value of 3.39 MHz. At 263 K only the latter one may be observed.

The general TRIPLE experiment (nuclear-nuclear-electron resonance) has determined that for all of the investigated monoanions the spin population on the *ortho* and *para* hydrogens has the opposite from that that on the *meta* sites. Assuming that each phenyl ring has three carbons with negative spin density (two *orto* and 1 *para*) and three with positive (two meta and 1 *ipso*) and assuming the spin population on the *ipso* carbon

is equal to the one on *meta*, population of unpaired electron residing outside the tetrone

ring may be estimated with use of the McConnell's relation (Q=-70MHz) as:

$$4*(3*a_2-3*a_1)/-70=0.3$$

where: 4-numer of phenyl rings, 3-number of carbon atoms, with the same spin density,

on each phenyl ring.

Table 4.1. Values of the hyperfine constants for monoanions of **2** and its derivatives

Radical anion	a_1 (ortho) (MHz)	a_2 (meta) (MHz)	a_3 (para) (MHz)
2⁻	3.23	1.43	3.23
(MeO)$_4$**2**⁻	3.24	1.31	0.36
(NMe$_2$)$_4$**2**⁻	3.26	1.08	-
(*t*-Bu)$_8$(MeO)$_4$**2**⁻	3.39	-	-
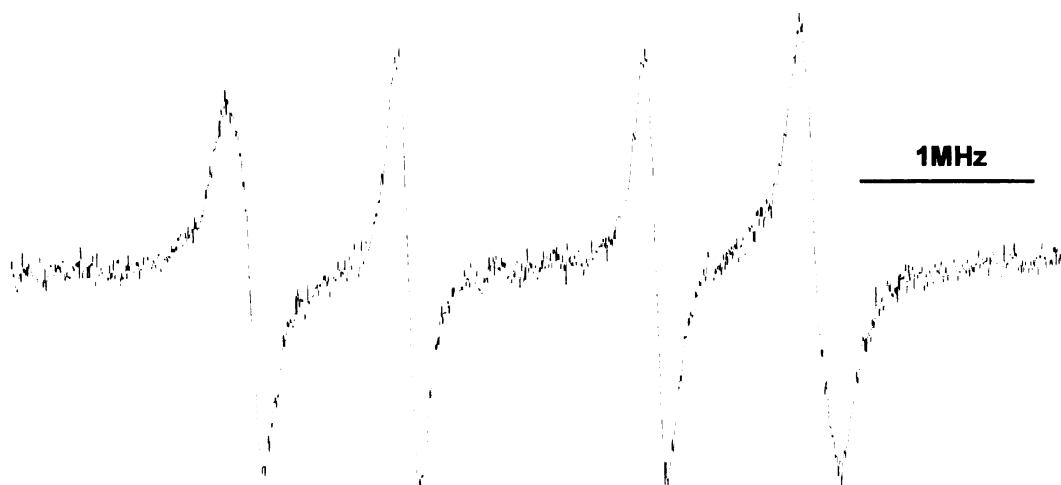
Figure 4.2. ENDOR of $2^-[K@c(2.2.2)]^+$/THF recorded at 246K (a_1=3.23; a_2=1.43 MHz)
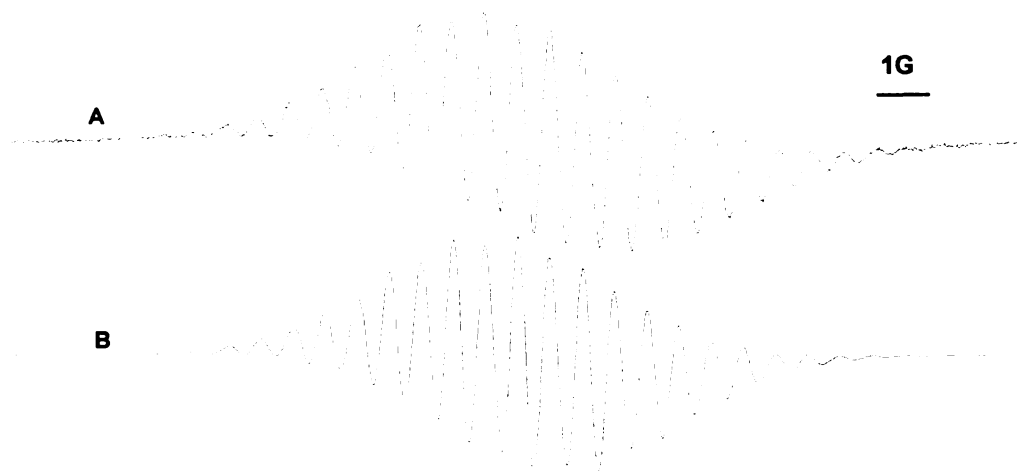
Figure 4.3. A) EPR of $2^-[K@c(2.2.2)]^+$/THF recorded at 246K.

B) Simulation with parameters obtained from ENDOR.
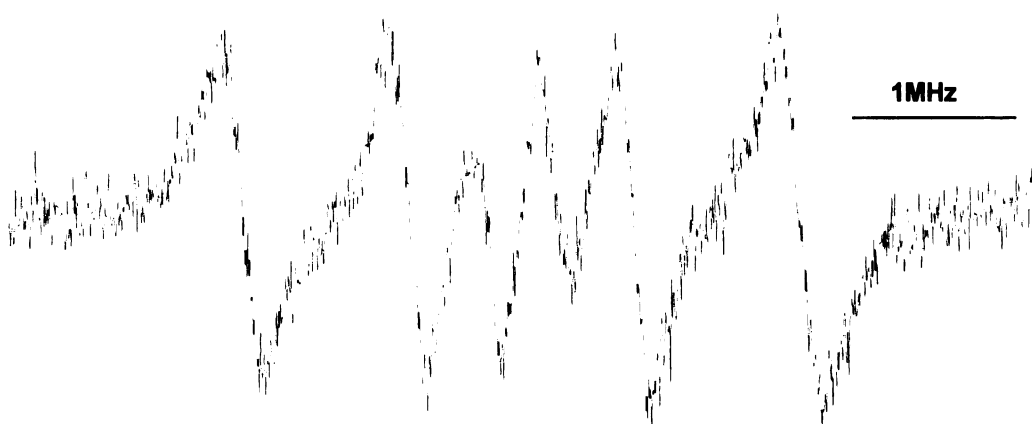
Figure 4.4. ENDOR of (MeO)$_4$2$^-$[K@c(2.2.2)]$^+$/THF recorded at 215K, (a$_1$=3.24; a$_2$=1.31

MHz).
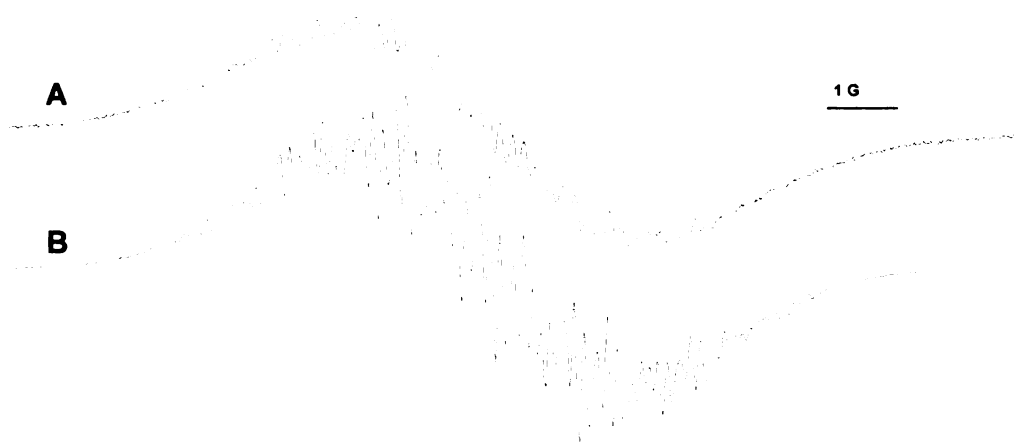
Figure 4.5. A) EPR of (MeO)$_4$2$^-$K@c[2.2.2]$^+$/THF recorded at 215 K.

B) Simulation with parameters obtained from ENDOR.
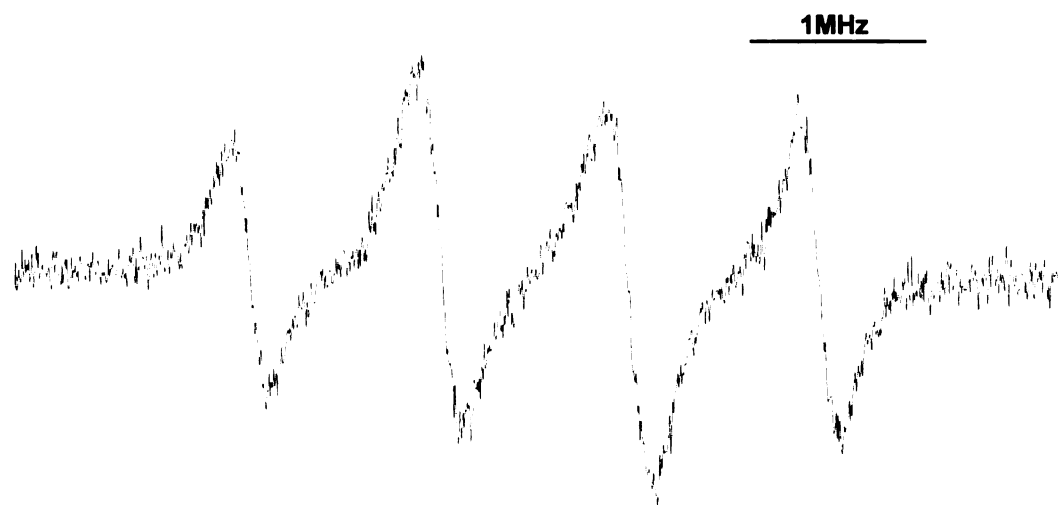
Figure 4.6. ENDOR of $(NMe_2)_42^-[K@c(2.2.2)]^+$/THF recorded at 210 K, (a_1=3.26;

a_2=1.08).
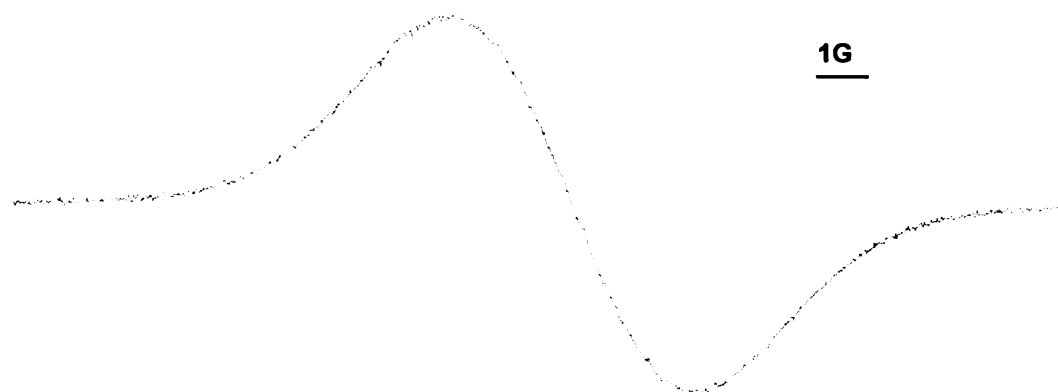
Figure 4.7. EPR of $(NMe_2)_42^-[K@c(2.2.2)]^+$/THF recorded at 243 K.
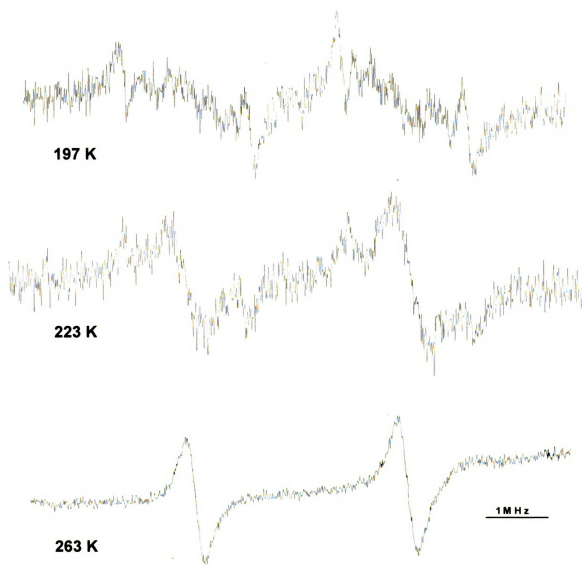
Figure 4.8. ENDOR of (*t*-Bu)$_8$(MeO)$_4$**2**$^-$[K@c(2.2.2)]$^+$/THF recorded at 197, 223 and

263K, a$_{1a}$=5.4 MHz; a$_{1b}$=1.5 MHz (197K), a$_1$=3.39 (263 K).

Figure 4.9. EPR of $(t\text{-Bu})_8(\text{MeO})_4 2^-K@c[2.2.2]^+/$THF recorded at 180 K

1G

A

B
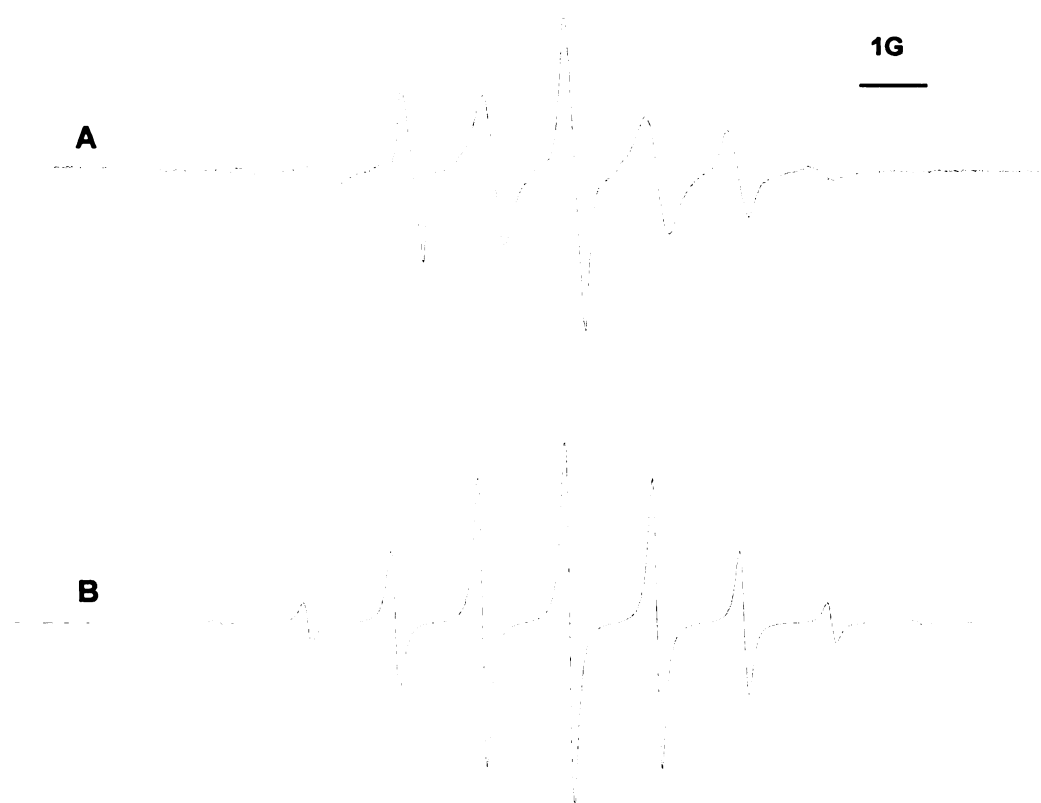
Figure 4.10. **A**) EPR of $(t\text{-Bu})_8(\text{MeO})_4 2^-K@c(2.2.2)^+/$THF recorded at 263 K

B) Simulation with parameters obtained from ENDOR.

Table 4.2. Values of the hyperfine constants of species present in the solution of dianions

Dianion	a_1 (*ortho*) (MHz)	a_2 (*meta*) (MHz)	a_3 (*para*) (MHz)
2^{2-}	7.87	3.22	7.87
$(t\text{-Bu})_8(MeO)_4 2^{2-}$	8.30		

Dianions. The main goal of EPR studies of the dianions was to observe signals of

their triplet states. Frozen solutions of 2^{2-} did not show any broad signals characteristic

for typical triplet diradicals nor did they show a half-field transition peak. Only narrow

monoradical peaks could be observed. Analysis of the solution spectrum showed that the

species responsible for that signal is not simply the monoanion. A clean signal of a new

radical was obtained for the sample of 2^{2-} (fig. 4.12). The ENDOR spectrum was also

obtained (fig. 4.11), showing two values of proton hyperfine splitting, approximately

twice as big as those of the monoanion. Attempted simulation of EPR spectrum with all

the protons of the tetrone molecule did not produced satisfying results. Halving the

number of interacting protons, however allowed however a simulation much closer to

the experiment (although still not perfect and thus not reproduced). The signal produced

by paramagnetic species in the solution of $(t\text{-Bu})_8(MeO)_4 2^{2-}$ was much easier to

interpret.
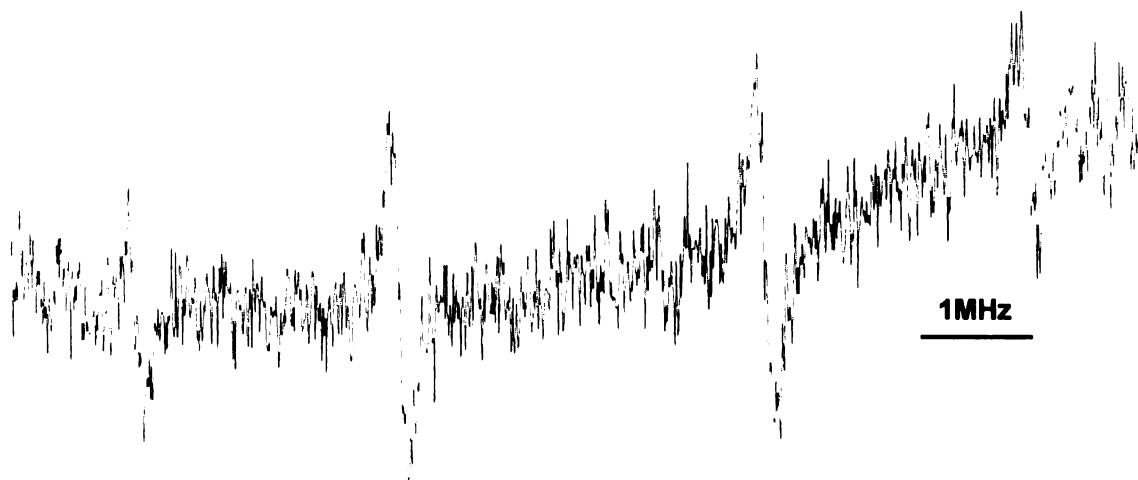
Figure 4.11. ENDOR of $\mathbf{2^{2-}}[K@c(2.2.2)^+]_2$/THF recorded at 240 K ($a_1$=7.87 MHz,

a_2=3.22 MHz)
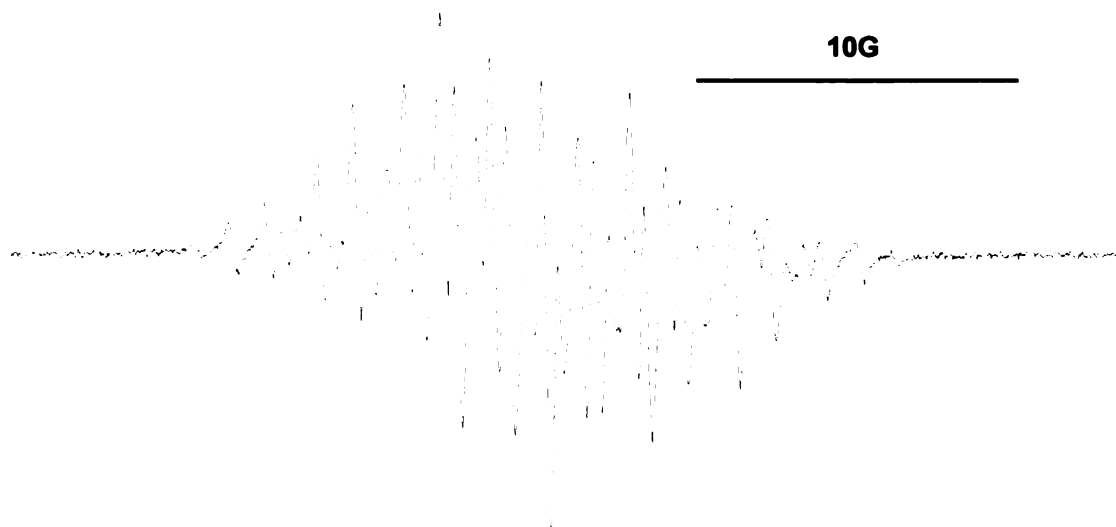
Figure 4.12. EPR of $\mathbf{2^{2-}}[K@c(2.2.2)]^+_2$/THF recorded at 247 K.
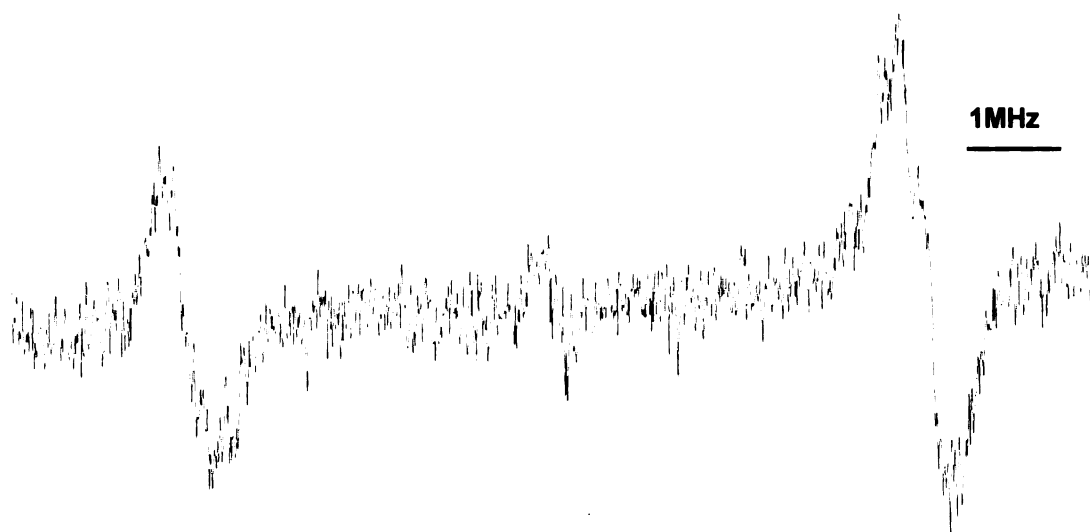
Figure 4.13. ENDOR of $(t\text{-Bu})_8(\text{MeO})_4\mathbf{2}^{2-}[\text{K@c}(2.2.2)^+]_2/\text{THF}$ recorded at 263 K, $(a_1=8.30 \text{ MHz})$
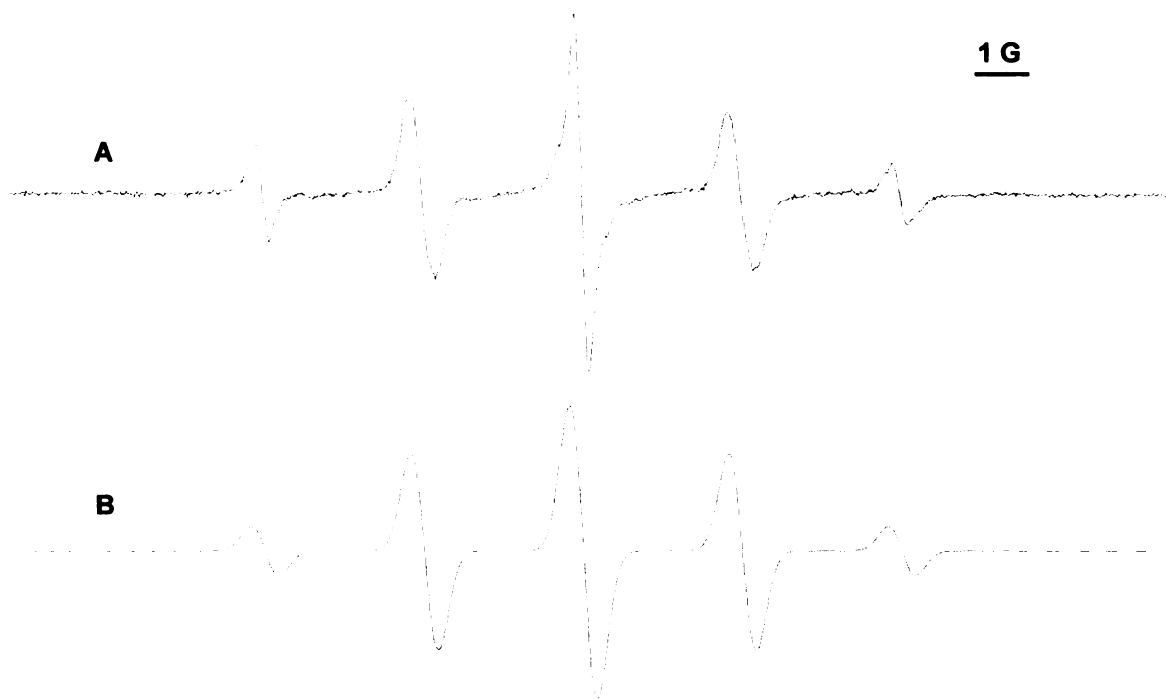
Figure 4.14. **A)** EPR of $(t\text{-Bu})_8(\text{MeO})_4\mathbf{2}^{2-}(\text{K@c}[2.2.2]^+)_2/\text{THF}$ recorded at 290 K

B) Simulation with parameters obtained from ENDOR.

Lack of the *meta* and *para* protons simplified the spectrum and ENDOR (fig. 4.13) has shown only one hyperfine coupling which could be assigned to the *ortho* protons. EPR simulation unambiguously assigned it to 4 rather than 8 protons (fig. 4.14)

Aggregates of 2^- and Cs^+. Reduction of tetrones with alkali metals in the absence of macrocycles was hampered by their low solubility in THF. Out of the three tetrones initially synthesized (2,$(MeO)_4 2$ and $(Me_2N)_4 2$) only 2 dissolved in THF to the extent that reduction could be carried out. But even if this precursor could be dissolved, the potassium mirror quickly covered with a film of insoluble reduction products, which prevented further reaction. A cesium mirror appeared to form more soluble products of reduction than potassium. When solution of 2 contacted this mirror, color of the solution darkened and an EPR signal of 2^- could be detected. The only difference between the solution spectra of $2Cs$ and $2^-[K@c(2.2.2)]^+$ was the much broader linewidth of the first one. A large change, however, could be observed for the powder spectra. While frozen $2[K@c(2.2.2)]$ produced only the sharp peak of the monoradical, the spectrum of $2Cs$ had the structure characteristic for the triplet state species. Figure 4.15 shows the signal of $2Cs$ as a function of reduction progress. A clear change of the spectrum's appearance was observed during the reduction. At first, the spectrum seemed to consist almost entirely of a pure triplet signal with a D value of ca. 90G. Then as the reduction progresses, a stronger and stronger doublet spectrum overlapping with the triplet one could be observed. Unfortunately, even with Cesium, after a while the reaction stops and no sample of dianion can be prepared.
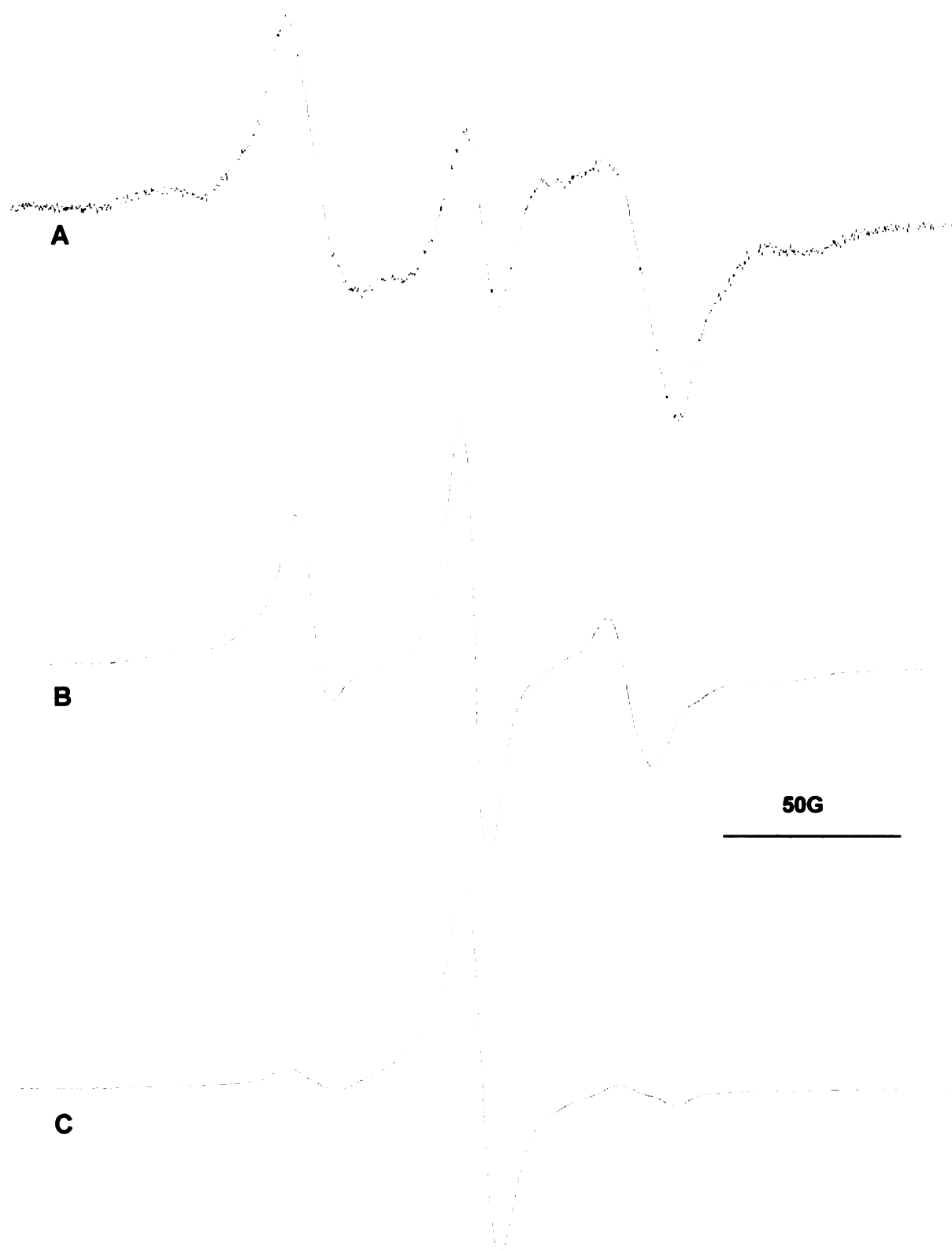
Figure 4.15. Progress (from **A** to **C**) of reduction of **2** with Cs mirror monitored by EPR.

Spectra collected at 4.2 K (**A**), 3.9 K (**B**), 4.2 K (**C**).

4.3 Discussion

'Naked' monoanions. The experimental spectra of monoanion radicals may be interpreted rather unambiguously. The data obtained agrees with the simplest most symmetric model of hyperfine interactions, pointing to high degree of symmetry (on the EPR timescale) of spin delocalization over the whole molecule. Temperature dependent study of $(t\text{-Bu})_8(\text{MeO})_4 2^-$ shows however that this symmetry can be broken. Separation of the *ortho* protons into two nonequivalent groups at low temperature may be explained by substituent induced inhibition of rotation and freezing of the phenyl groups into conjugated and non-conjugated groups (fig. 4.16a), or localization of the electron on one methylene site (fig. 4.16b).

Para-substituted monoanions are much more stable, what points to this location as being the most reactive of the whole molecule, as it is in the simple triphenylmethyl radical.
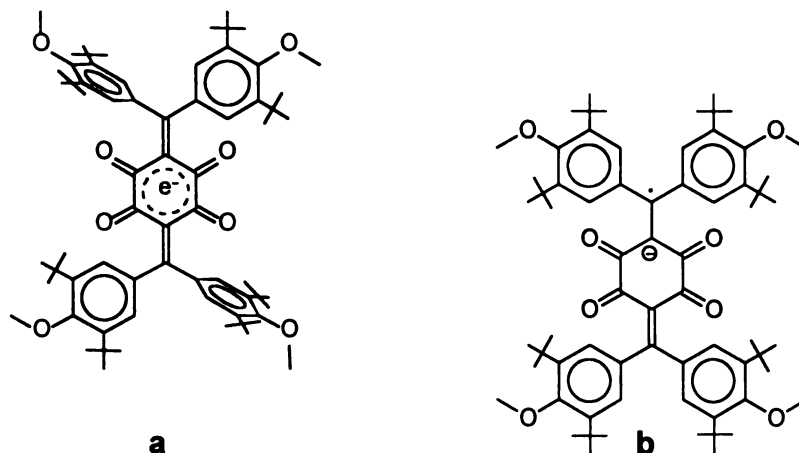
Figure 4.16. Possible reasons for splitting of the ENDOR signal of the meta protons of the $(t\text{-Bu})_8(\text{MeO})_4 2^-$.

'Naked' Dianions. No signal of the triplet state dianion could be observed in the whole range of investigated temperatures for 'naked' dianions. What was surprising was the observation of a new 'monoradical'. Various types of species may be assigned to it (Figure 4.17). Products of dimerization (**a**) at first seem to be the most appealing explanation. Further analysis however shows certain drawbacks to that hypothesis. First, 2^{2-} could dimerize in one of three ways: 'head to head', 'head to tail', or 'tail to tail'. As in the case of the triphenylmethyl radical, tail to head coupling should prevail. ENDOR shows however signals of only two types of protons, consistent with 'head to head' coupling only. The other hard-to-explain fact is the presence of the related signal in the case of $(t\text{-Bu})_8(\text{MeO})_4 2^{2-}$. Due to the effective steric protection this dianion should not dimerize easily. Formation of the dimer peroxide (**b**) would require the presence of oxygen. Although it can not be absolutely ruled out, the greatest care has been taken to eliminate such possibility. The diradical peroxide would also be expected to be unstable. A weak oxygen-oxygen bond might break easily and the free oxygen is valence couple with the radical part of the molecule producing diamagnetic compounds like epoxides. Other modes of formation of a new radical may be protonation of monoanion or abstraction of the hydrogen from the solvent (THF) by a photo-exited dianion (**c**). The first case is very unlikely since the monoanion should not be a very strong base and the solvents were carefully dried before the use as well as being continually dried by the presence of the metal mirror.
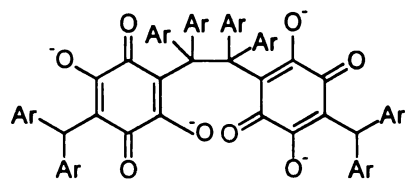
a) Dimers of dianions
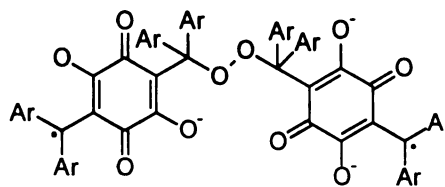
b) Peroxides
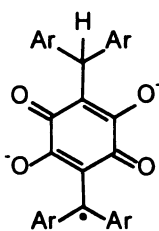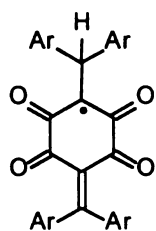
c) Products of protonation or hydrogen
abstraction
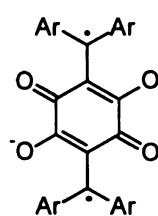
d) Localized diradicals
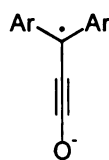
e) Products of fragmentation

Figure 4.17. Possible species responsible for EPR signal found in the solution of dianions

In addition in both cases some of the spin density should be delocalized onto the newly acquired proton which in turn should be observable in EPR and ENDOR spectra. The signal may also be attributed to a localized diradical (d). It is however difficult to imagine why the conjugated dihydroxy-quinone anion spacer should isolate the radical centers.

The most plausible explanations seems to be fragmentation of the dianion. Concerted or stepwise processes (figure 4.18) may be imagined as a way of getting there. Radical anions such as (e) would easily explain both the high-spin density and the spin delocalisation on only two of the phenyl rings, as well as the presence of only one type of species.
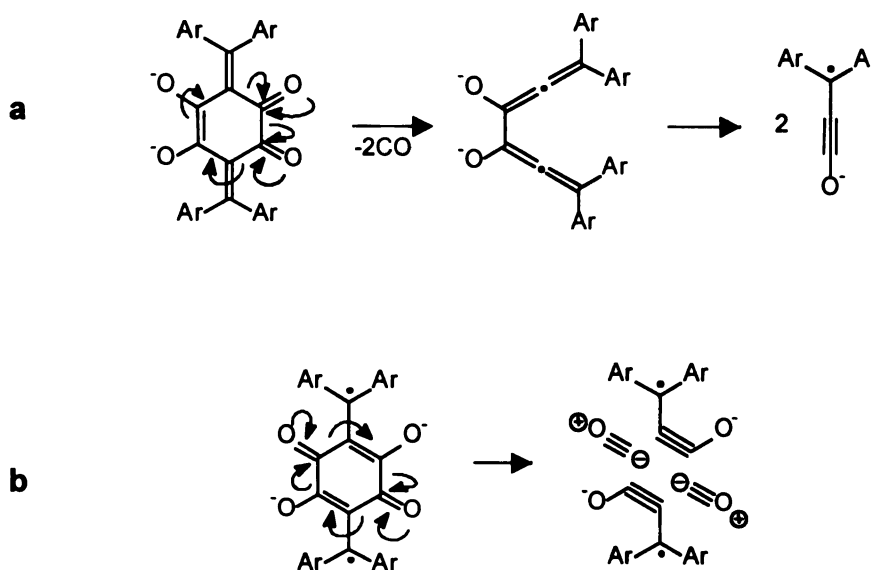
Figure 4.18. Proposed concerted (a) and stepwise (b) paths of fragmentation of 2^{2-} and its derivatives.

99

Ion aggregates. The low solubility of the complexed anion shows that **2** and its derivatives may have the desired ability to form extended structures in the solid state. Similar conclusions may be deduced from observation of the powder EPR spectra. A triplet signal detected in frozen solutions of the 2Cs points to strong intermolecular spin-spin interactions, probably through the metal cation. This proposed origin for the signal is supported by the fact that in the presence of the cryptand, only a sharp signal of the monoanion doublet may be seen and that similar signals were recorded for analogous complexes of quinones.[5] It is interesting is that while the reaction proceeds the signal of the triplet disappears and the doublet signal seems to be more and more intense. This observation seems to contrast with the expectation that a higher concentration of anions should lead to a higher degree of aggregation. Problem this may be easily solved if we assume that predominating later signal is quartet or higher multiplet rather than doublet. Out of two modes of aggregation which may be expected (Figure 4.19). Solid state crystallographic study (Chapter 7) seems to support structure **b**).
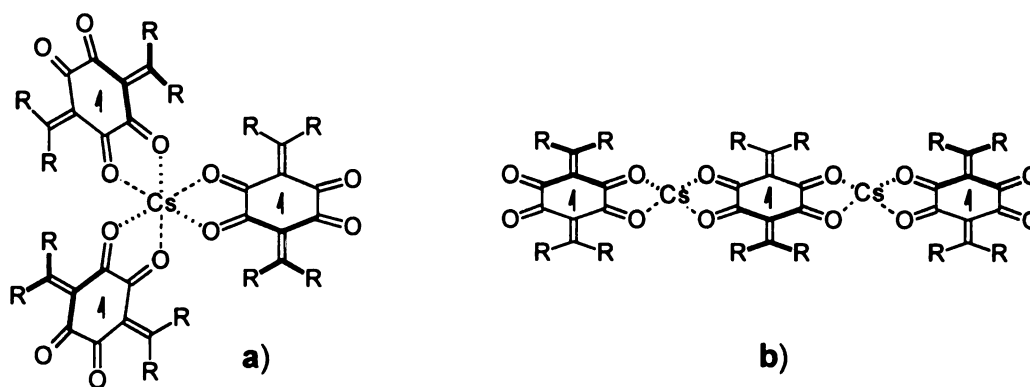
Figure 4.19. Two possible modes of aggregation of 2Cs

4.4. Experimental

Purification and Handling of THF. Anhydrous THF (Aldrich) was placed in a
Shlenk bottle with a few drops of NaK_2 alloy, degassed through a few of freeze-pump-
thaw cycles and left to sit until occasional shaking turned its color to blue. Solvent was
then freeze-pump-thawed until vacuum over the frozen solid reached $1*10^{-5}$ torr and high
vaccum distilled to the storage bottle. Just before the experiment the needed quantity of
the solvent was distilled to a bottle containing a few drops of NaK_2, shaken until blue,
and distilled back to the H-Cell.

Preparation of the EPR/ENDOR samples of mono and dianions. In a typical
experiment tetrone (ca. 10mg) and stoichiometric amount (1:1) of cryptand were placed
in chamber A of the H-cell (figure 4.20), evacuated on a high-vacuum line, and placed in
a Helium filled glove box. A small piece of potassium (ca. 5mg) was placed in chamber
B. Then the H-cell was sealed, put back on the vacuum line, and evacuated until the
vacuum reached ~$5*10$-6 torr. In order to minimize the possibility of an oxygen leak, the
pyrex glass tube leading to chamber B was sealed off just below the swagelock joint.
Potassium mirror was then prepared in chamber B by heating the potassium with a small
gas flame. Chamber A was immersed in liquid nitrogen and THF (ca. 30ml) distilled into
it. After thawing of the solvent, the H-cell was placed in an isopropanol/dry ice bath (–
40-50°C) and the solution was sloshed between chambers A and B through the glass frit.
The progress of the reduction was monitored by Vis-NIR spectroscopy in the opticall cell
attached to the sidearm. Control over the degree of reduction was facilitated by the fact
that after depletion of the cryptand, reduction considerably slowed down.
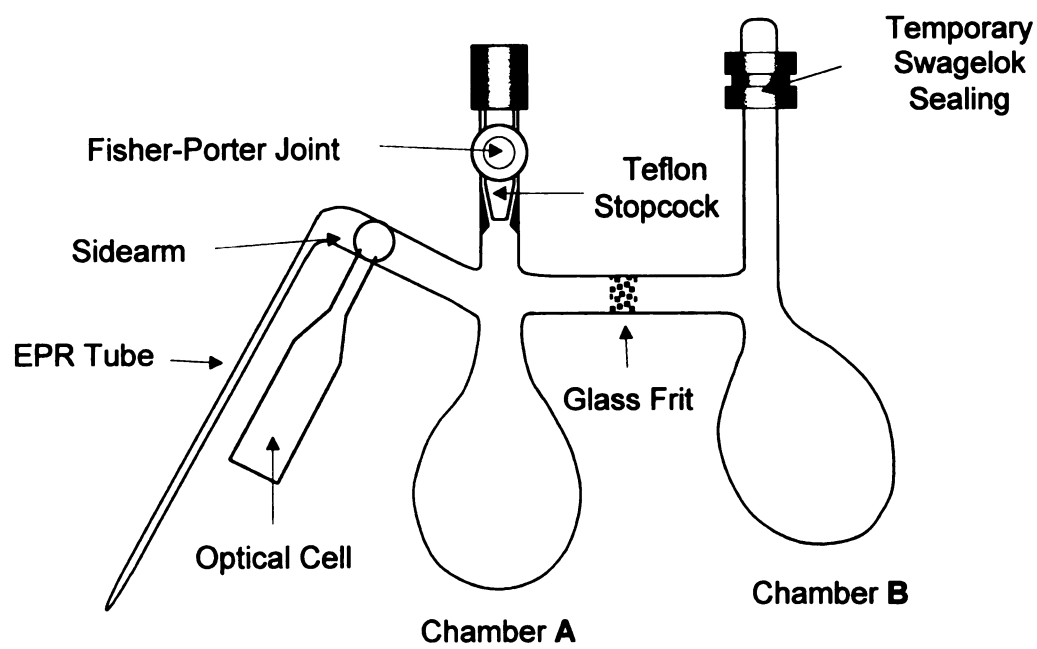
Figure 4.20. A typical H-cell used for preparation of EPR samples.

A small amount of solution was then transferred to the quartz EPR tube and the tube sealed off while the sample was kept in liquid nitrogen.

Spectroscopy. EPR and ENDOR spectra were recorded on a Bruker ESP300E spectrometer equipped with a DICE ENDOR unit. Typical conditions for EPR were: modulation frequency 100kHz, modulation amplitude 0.1 gauss, power 0.1mW, gain 10^5. Typical conditions for ENDOR were: modulation frequency 12.5 kHz, microwave power 20-32 mW, Rf power 200-300 W, modulation depth 100kHz, gain 10^5.

BIBLIOGRAPHY

(1)   (a) Jedlinski, Z. *Accounts Chem. Res.* **1998,** *31*, 55. (b) Dye, J. L.; Jackson, J. E.;
        Cauliez, P. In *New Aspects of Organic Chemistry, Organic Synthesis for
        Materials and Life Sciences*; Yoshida, Z., Ohshiro, Y., Eds.; VCH Publishers:
        New York, **1992.**

(2)   (a) Carrington, A.; McLachlan, A. D. *Introduction to magnetic resonance with
        applications to chemistry and chemical physics*; Harper & Row: New York, **1967.**
        (b) Atherton, N. M. *Principles of electron spin resonance*; Ellis Horwood : PTR
        Prentice Hall: New York, **1993.**

(3)   McConnell, H. M.; Chesnut, D. B. *J. Chem. Phys.* **1958,** *28*, 107.

(4)   (a) Dougherty, D. A. In *Kinetics and Spectroscopy of Carbenes and Biradicals*,
        Platz. M. S., Eds.; Plenum Press: New York, **1990,** pp. 117-143. (b) Berson, J. A.
        In *The Chemistry of Quinonoid Compounds*, Vol II, Patai, S.; Rappoport, Z.,
        Eds.;Wiley: New York, **1988,** pp. 455-536. (c) Berson, J. A. In *Diradicals*,
        Borden, W. T., Eds.;Wiley: New York, **1982,** pp. 151-194.

(5)   Brown, M. A.; McGarvey, B. R.; Ozarowski, A.; Tuck, D. G. *J. Am. Chem. Soc.*
        1996, *118*, 9691.

Chapter 5

NMR

5.1 Introduction

Since EPR studies did not indicate the presence of triplet state tetrone dianions, a complementary NMR study was performed to gain some information about the structures of the species generated by reduction of tetrones. NMR signals can not be observed for most paramagnetic organic molecules. The reason is that the unpaired spin of the radicals delocalized over the molecule interacts with the NMR active nuclei leading to their fast relaxation and consequently extreme broadening. In most cases the broadening is so strong that no signal may be observed at all. If dianions of the investigated tetrones could be observed by NMR, it would mean that their ground state is singlet and give additional insight into their structure.
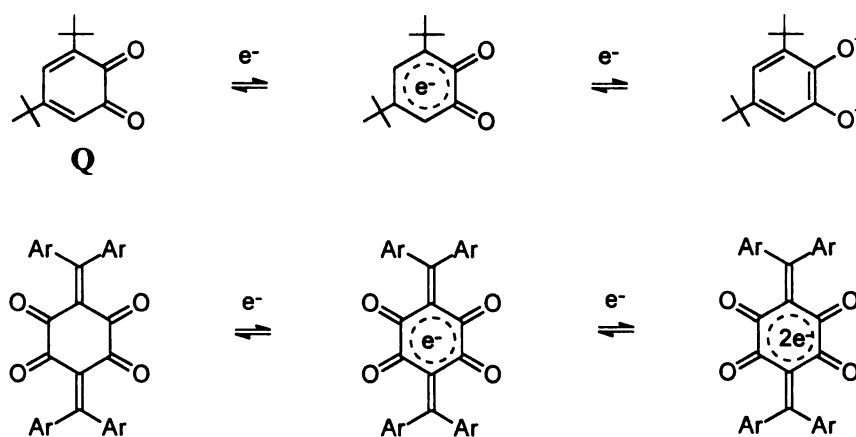
Figure 5.1. Reductions investigated by H^1 NMR

In these studies tetrone/c(2.2.2) mixtures in d_8-THF were reduced with potassium mirrors and the progress of reduction was monitored by the NMR spectroscopy. In addition to derivatives of **2** reduction of model quinone **1** was also investigated under the same conditions. (Figure. 5.1)

Singlet state species with low HOMO-LUMO gaps possess a substantial admixture of the low-lying Triplet State (through a spin-orbit coupling mechanism). This in turn leads to local perturbation of the magnetic field, which, in analogy to the diamagnetic ring current of aromatic compounds, is called a 'paramagnetic ring current'. The effect of such a perturbation is 'paratropic', yielding an upfield shift of the exocyclic ring protons.

Extensive study performed on 'antiaromatic' dianions of fused polycyclic hydrocarbons has shown a correlation between the HOMO-LUMO gap and the degree of the paratropic shift.[1-4] The lower the HOMO-LUMO gap the higher the contribution of the triplet and consequently the higher the shift. In the case of very low HOMO-LUMO gaps, in addition to the paratropic chemical shift, paramagnetic broadening of the NMR lines can also be observed. In some cases spectra are highly temperature dependent. Raising the temperature leads to a higher triplet admixture and higher paramagnetism of the molecule. This in turn leads to broadening of the peaks relative to the low temperature case.

5.2. Results

<u>Reduction of quinone **Q**</u>. After very short contact of the c(2.2.2)-quinone solution with a potassium mirror, its yellow color turned green. At the same time the signals of all the quinone protons disappeared, including even the protons of the *t*-Butyl groups. The only observable signals left were those of the solvent and broadened lines belonging to the cryptand. Further reduction did not dramatically change the spectrum besides broadening of the cryptand lines. During that process the color of the solution gradually changed from green to blue, which is presumably the color of the 'pure' semiquinone. Continuation of the reduction process bleached that color, resulting finally in a faintly yellowish almost transparent solution. At that stage the sample became diamagnetic and sharp lines of diamagnetic products could be observed by proton NMR. Further reduction led to generation of the transient blue color of $[K^+@c(2.2.2)]K^-$ which at room temperature decomposed after a while.

<u>Reduction of the tetrone (*t*-Bu)$_8$(MeO)$_4$**2**</u>. Brief contact of the dark red solution of (*t*-Bu)$_8$MeO$_4$**2** with the potassium mirror led to quick disappearance of the signals of the phenyl and methoxy protons. The signal of the *tert*-butyl protons remained, although it became somewhat broader (figure 5.2). Further reduction broadened the *t*-Butyl line more and more (figure 5.3) and at the same time the center of the peak slowly moved downfield from its initial shift of 1.36 ppm (A$_1$) to ca. 1.5 ppm (A$_3$). Upon longer contact with the mirror, the behavior of the *t*-Butyl peak reversed. The line became sharper and moved back to the position of ca. 1.4 ppm (A$_4$). At the same time the color of the solution changed from purple to green. Further reduction of the green solution did not change the

position of the peak. The signal, however, became broader (A₅) again while the solution became red.
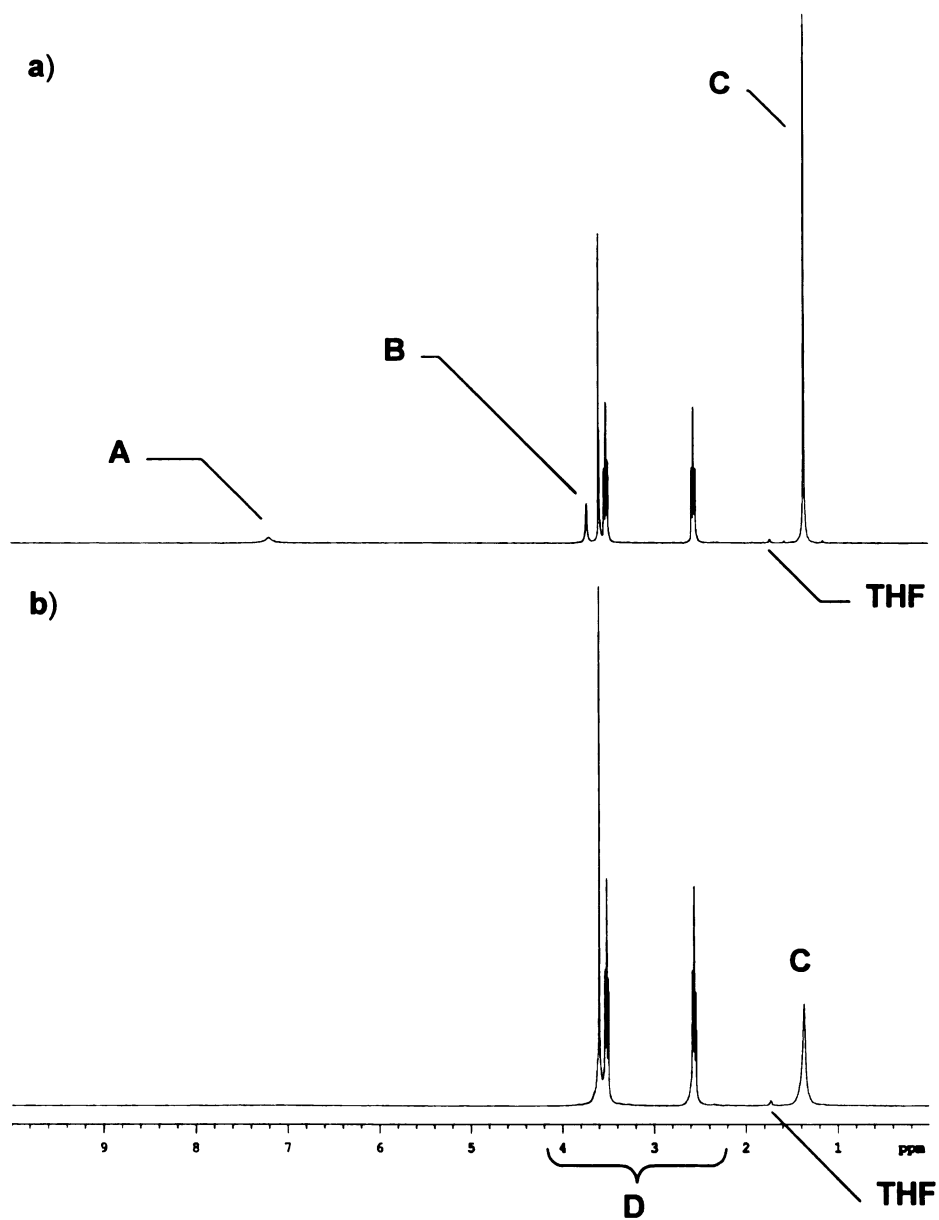
Figure 5.2. ^{1}H NMR of the mixture of $(t\text{-Bu})_8(\text{MeO})_42$ and c(2.2.2) (THF-d_8, RT)

a) Before and b) After a very short reduction time
A) o-hydrogens of the phenyl group, B) metoxy protons, C) t-Bu protons,
D) c(2.2.2) peaks.
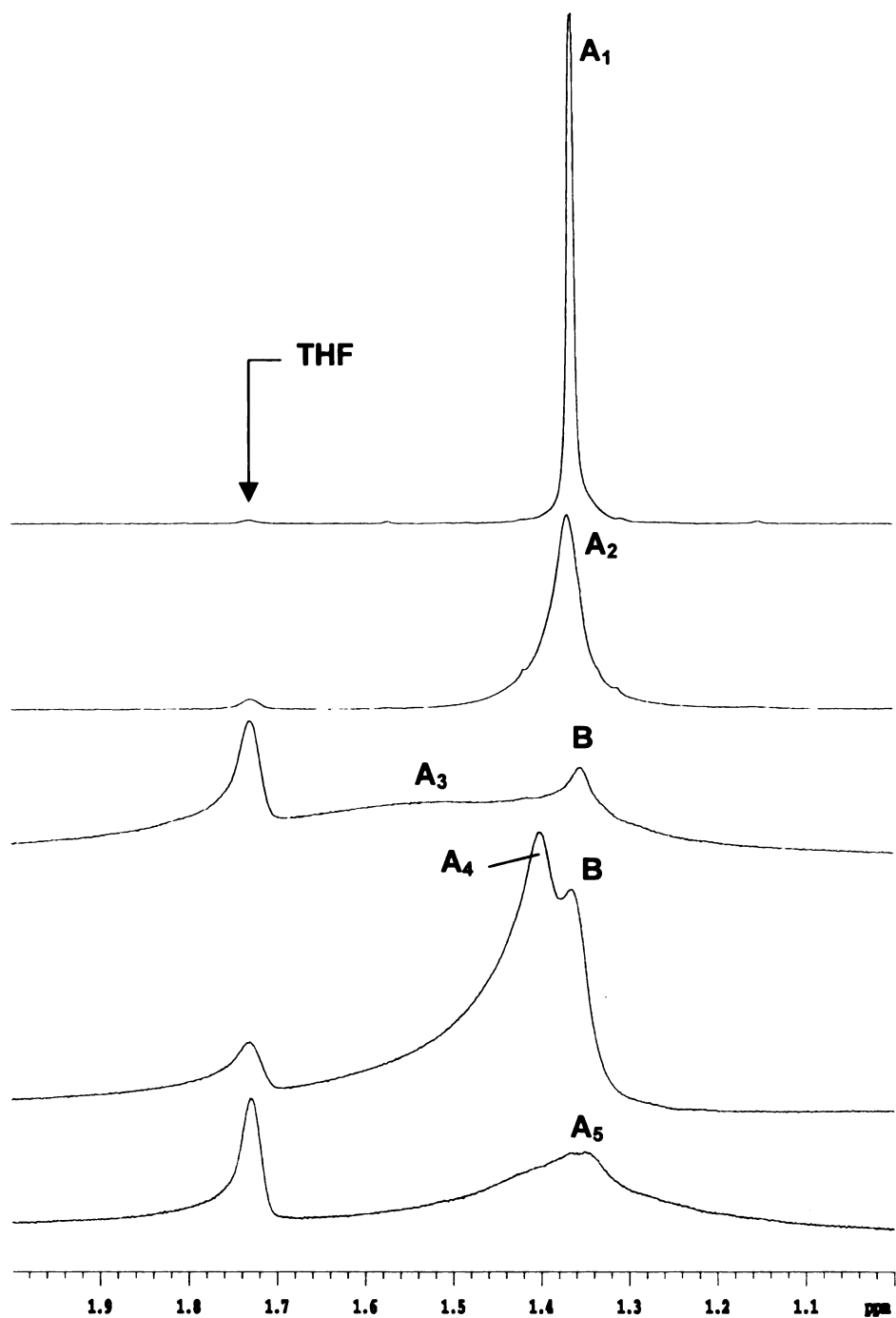
Figure 5.3. Progress of the reduction of (*t*-Bu)$_8$(MeO)$_4$**2** observed in the 1-2 ppm range, THF and. **A)** *t*-Butyl protons may be observed. **B)** probably belongs to small diamagnetic impurity.
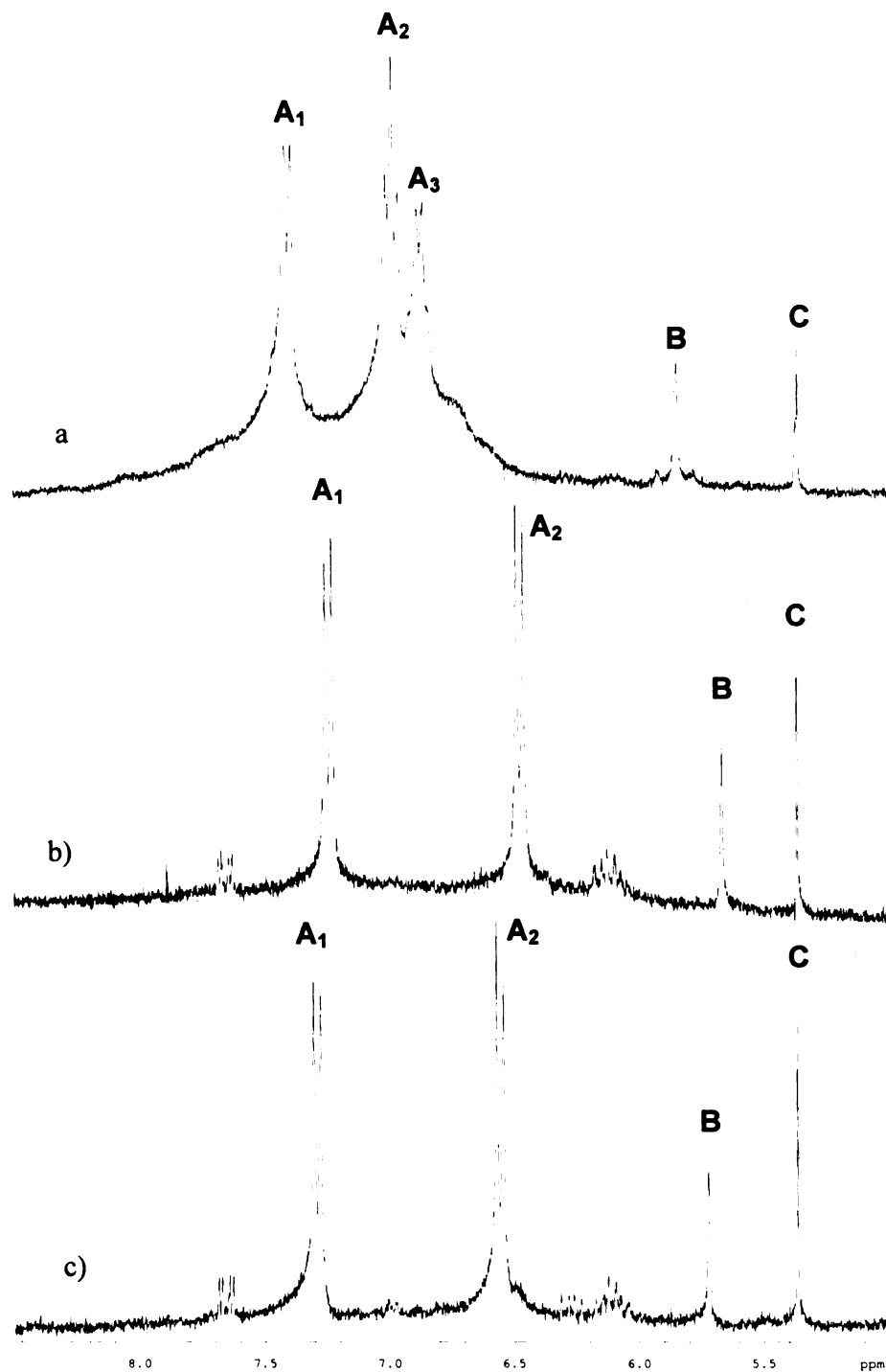
Figure 5.4. Aromatic region of the ^{1}H NMR spectrum of the diamagnetic products obtained by decomposition of the solutions of a) 2^{2-}, b) $(MeO)_4 2^{2-}$ and c) $(Me_2N)_4 2^{2-}$.

Reductions of the tetrones 2, (MeO)$_4$2 and (NMe$_2$)$_4$2. Unlike (t-Bu)$_8$(MeO)$_4$2, 2 does not possess t-Butyl groups. The signal of 2 thus disappears completely at a very early stage of the reduction experiment and does not reappear (at low temperature) at any other stage of the reduction. However when the solution of the dianion 2^{2-}(as judged by its green color) is warmed up to room temperature, a relatively clean spectrum of a new diamagnetic compound appears in the aromatic region (Figure 5.4). Similar behavior may be observed for the other two tetrones (MeO)$_4$2 and (NMe$_2$)$_4$2 with the main difference being that no signal of the starting material may be observed since these compounds are insoluble in THF. In both cases, the final room temperature formation of a diamagnetic product may be seen (Figure 5.4). In all three cases, attempts at further reduction of the dianion led to precipitation of the solid.

No ^{13}C NMR signal could be observed for any of the tetrones at any stage of the reduction besides the neutral precursor.

5.3. Discussion

Even short contact of the THF soluble quinone and tetrones leads to dramatic changes in the NMR spectra of those compounds. Presumably electron transfer between reduced and unreduced molecules

$$Q + Q^{\cdot -} \rightleftharpoons Q^{\cdot -} + Q$$
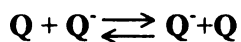
is fast on the NMR time-scale, leading to observation of the averaged signal of tetrone and its radical anion. Even a minimal concentration of the unpaired electrons leads to intensive broadening of the lines and finally disappearance of the ^1H NMR signals. In the case of $(t\text{-Bu})_8(MeO)_4\mathbf{2}$, the signal of the saturated t-Butyl groups, with their weak couplings to the paramagnetic π-regions, are still observable even for a pure anion radical.

When both monoanion and dianion are present in the solution, an analogous process must happen since no separate signal of the dianion can be observed. Unlike the behavior of the model quinone no sharp signal of the dianion is observed for any tetrone. Only the broad signal of the t-Butyl groups can be seen for $(t\text{-Bu})_8MeO_4\mathbf{2}^{2-}$. The broadness and the position of this signal indicate that $(t\text{-Bu})_8MeO_4\mathbf{2}^{2-}$ (or immediate products formed from it) are 'less paramagnetic' then the monoanion, which seems to decrease the likelihood of it being a triplet under those conditions. The best explanations of the tetrone dianions at that stage is that they are probably strongly paratropic compounds with a low HOMO-LUMO gap and consequently high admixture of the triplet into the ground singlet state even at low temperatures.

The other important issue is the further fate of the dianions. Their slow decomposition leads to the formation of diamagnetic compounds that are cleary related to each other. Analysis of the multiplicity of the aromatic NMR signals allows for generalizations like: (a) There is only one major product (b) The product has one type of phenyl rings only. The relative positions of the signals of the *ortho-* and *meta-* protons prompts the conclusion that the phenyl rings are conjugated to the π system of the product.
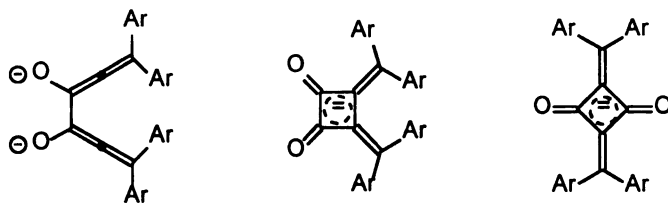
Figure 5.5. Proposed species responsible for NMR signals presented on figure 5.4

Having in mind the radical intermediates proposed in chapter 4, one of its diamagnetic dimers may be responsible for the observed NMR signals (figure 5.5). Besides phenyl ring signals, additionally two sharp peaks (**B** and **C**) may be observed in figure 5.4. The only source of the non-aromatic protons in the solution may be C(2.2.2) (if the presence of water is completely excluded). Those peaks may belong to the products of its decomposition.

5.4. Experimental

NMR reduction experiments were performed in high precision pyrex NMR tubes attached to the high vacuum line through a swagelock connection, Teflon stopcock and Fisher-Porter joint (figure 5.6). Tetrone (ca. 5mg) and C(2.2.2) cryptand (more then 2:1 stoichiometric excess with respect to tetrone) were placed in the tube, the tube was evacuated and left to a pressure of ca.10^{-5} torr, the stopcock was closed, and the whole device was introduced into a helium-filled dry box. Inside the box, the NMR tube was detached and a small quantity of potassium metal was smeared with a pipet inside the

upper part of the tube (in the place where the tube was supposed to be sealed off later with a torch). The tube was then reattached to the stopcock and put back on vacuum line. After 10^{-5} torr was reached again, the NMR tube was immersed into liquid nitrogen and ca. 0.5-0.75 ml of previously dried and degassed THF-d_8 was distilled into it. While still in liquid nitrogen and under vacuum, the tubewas sealed-off with the torch in such a way that at the same time the potassium formed a mirror in the upper part. After slow thawing of the THF, the tube was stored and manipulated vertically so no contact of solution with the mirror was allowed prior to spectroscopic studies

Between NMR measurements, the solution in the tube was briefly allowed to contact with the mirror while remaining in the isopropanol-dry ice bath (below $-60°C$). It was then quickly dried off with a cloth and inserted into the pre-cooled probe of the NMR instrument
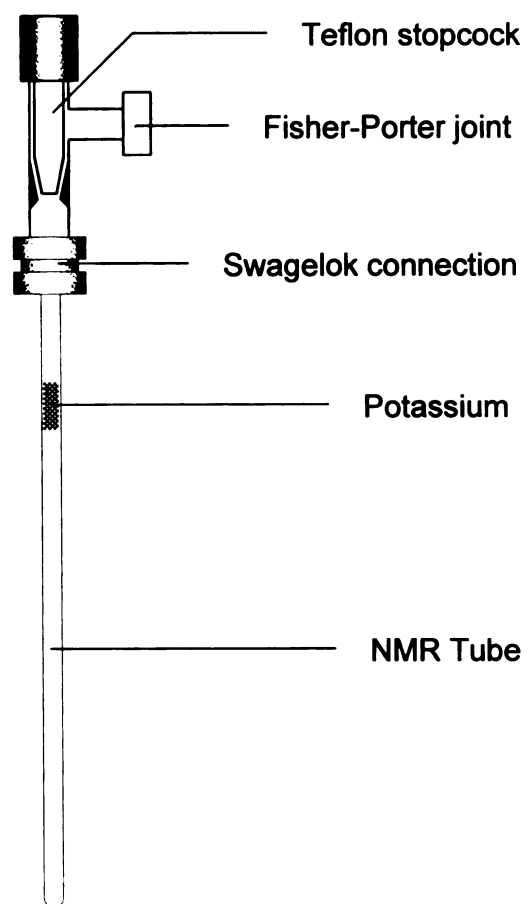
Figure 5.6. Instrument used for preparation of the NMR samples.

BIBLIOGRAPHY

(1)   Minsky, A.; Meyer, A. Y.; Rabinovitz, M. *Tetrahedron* **1985,** *41*, 785.

(2)   Rabinovitz, M.; Cohen, Y. *Tetrahedron* **1988,** *44*, 6957.

(3)   Rabinovitz, M. *Top. Curr. Chem.* **1988,** *146*, 99.

(4)   Rabinovitz, M.; Cohen, Y. *Adv. Chem. Ser.* **1988,** 53.

Chapter 6

CYCLIC VOLTAMMETRY

6.1 Introduction

In order to get detailed insight into the process of formation of mono- and dianions of tetrones **2**, their redox behavior was investigated by means of cyclic voltammetry (CV). This technique allows determination of reduction potentials (E°) of the investigated tetrones and provides some information concerning the chemical behavior of produced from them reduced species.[1] Our main interest was focused on verification of whether mono- and dianions are indeed stable products of reduction. The study was performed in non-polar THF (for **2** and (t-Bu)$_8$(MeO)$_4$**2**) and polar DMF (for **2**, (MeO)$_4$**2** and (Me$_2$N)$_4$**2**).

6.2 Results

Figure 6.1 presents a voltammogram of (t-Bu)$_8$(MeO)$_4$**2**/THF as a typical example; the rest of the tetrones produced similar patterns. Four reduction waves (E$_1$°, E$_2$°, E$_3$°, E$_4$°) could be observed for these species. The first two waves appeared to be reversible, with corresponding oxidations waves E$_1$'° and E$_2$'°, while the third and fourth were irreversible. The values of the measured reduction potentials (versus ferrocene/ferrocenium couple) are collected in the table 6.1.

Table 6.1. Cyclic voltammograms of the 1 mM solutions of the tetrones with 0.1M of (n-Bu)$_4$N(PF$_6$) as supporting electrolyte. Swept rate 0.1V/s, glassy carbon working electrode, platinum wire counterelectrode, silver wire quasireference calibrated to FeCp$_2$/FeCp$_2^+$ couple (0.46V).

	$E_1°$	$E_2°$	$E_3°$	$E_4°$	$\Delta E_{1,2}°$	$\Delta E_{2,3}°$	$\Delta E_{3,4}°$
			THF				
2	-0.39	-1.10	-	-2.01	0.71	-	-
(*t*-Bu)$_8$(MeO)$_4$**2**	-0.57	-1.22	-2.58	-2.41	0.65	0.36	0.83
			DMF				
2	-0.28	-0.91	-1.23	-1.82	0.63	0.32	0.59
(MeO)$_4$**2**	-0.39	-0.96	-1.29	-1.85	0.57	0.33	0.51
(Me$_2$N)$_4$**2**	-0.78	-1.27	-1.51	-2.03	0.49	0.24	0.52
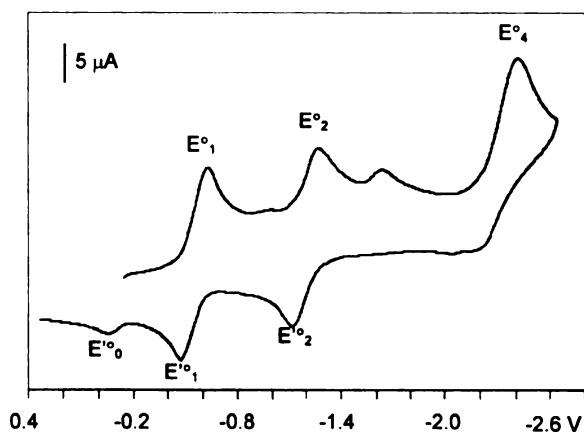
Figure 6.1. Cyclic voltammogram of (*t*-Bu)$_8$(MeO)$_4$**2** in THF

6.3 Discussion

The first wave apparently corresponds to the reduction of the tetrone to its monoanion. These species are stable reduction products, as has been firmly established by both EPR spectroscopy and the X-ray diffraction study.

A clear correlation between the strength of the electron-donating abilities of the phenyl substituents and the reduction potential may be established. As may be expected, substituents with stronger donating abilities make the tetrone more difficult to reduce. For example the difference between $E_1°$ for **2** and $(Me_2N)_4$**2** (in DMF) is 0.50 V. The lower reduction potential $E_1°$ of **2** in DMF than in THF (-0.28 vs. -0.39V) may be rationalized by its better solvating abilities for the charged anion. Oxidizing abilities of the most electron-deficient **2** are better then for simple p and o-benzoquinones (-0.43 V and –0.47 V for benzoquinone in DMF and 3,5-Di(*tert*-butyl)-o-quinone in THF respectively)[2, 3] measured in similar conditions but due to electron donation from the conjugated phenyl ring are lower then for some other systems containing four conjugated carbonyl groups.[2] Apparently tetrone **1** meant to be strong electron acceptor will require electron-withdrawing substituents R.

The second wave $E_2°$ most likely corresponds to the reduction of the monoanion to the dianion. Supporting this assigment are (a) the fact that the values of i_p (peak current) of $E_2°$ is similar to that for $E_1°$ (so it is likely to be a one electron process) and (b) the presence of the oxidation wave $E_2'°$, corresponding to $E_2°$. This well-behaved electrochemistry points to the reversibility of the reduction with regeneration of the monoanion. If the dianion produced by one-electron reduction of monoanion underwent prompt decomposition, regeneration of the monoanion would be impossible.

119

The separation between the first and the second reduction waves is rather high (in the range of ~0.5 V and more). This shift points to the strong interactions between the two frontier electrons in the dianion and rules out their localization on separate parts of the molecule. Such a high separation between the first and second reduction potentials precludes disproportionation of the monoanion to the dianion and neutral tetrone. It is significant that the gap between the first two waves decreases with increasing electron-donating abilities of the phenyl ring substituents (0.63, 0.57, 0.49 V for **2**, (MeO)$_4$**2**, (Me$_2$N)$_4$**2** in DMF respectively). At first, one might expect that more electron-rich phenyl rings would confine the frontier electrons to the tetrone unit and consequently strengthen their mutual electrostatic interactions. Electron donation may, however (see chapter 2) decrease electron-electron repulsion of frontier electrons by formation of the more and more open-shell singlets.

The origins of the third and fourth waves cannot be assigned easily. The third one is separated from the second by about 0.3V and is usually of much lower intensity (which varies from tetrone to tetrone). For **2** it is especially small and can be observed only as a shoulder. A physical phenomenon such as ion pairing or film deposition on the electrode, may be responsible for this peak. Another explanation may be protonation of the dianion by traces of water (or by the ethanol used for recrystallization of the supporting electrolyte). The protonated dianion with its negative charge may then be quickly be reduced, producing this extra third wave. The fourth wave has a much higher intensity than the second one and two electrons are probably transferred (which would lead to the formation of the tetraanion). This wave (like the third one) in all cases appears to be irreversible. Apparent irreversibility must be caused by slow rate of the oxidation rather

than chemical decomposition of the formed species since dianion and monoanion are recovered. An additional small oxidation wave $E'_0{}^\circ$ can also be observed sometimes. Oxidation of the carbon protonated anion may be responsible for this peak.

6.4 Experimental

THF was purified as described in Chapter 3. Anhydrous DMF (Aldrich) was used as supplied. Supporting electrolyte [(n-Bu)$_4$N](PF$_6$) (Aldrich) was recrystallized three times from absolute ethanol and dried in vacuum. A calculated amount of [(n-Bu)$_4$N](PF$_6$) (to produce 0.1M solution) and a magnetic stirring bar was placed in a main chamber of an electrochemical cell, and the tetrone (to obtain ca.1mM solution) was placed in the side chamber. The cell was evacuated on a vacuum line and ca. 2ml of THF was condensed into the main chamber. When DMF was used as a solvent, it was transferred to the cell with a syringe inside a glove bag, and then degassed in the cell via several freeze-pump-thaw cycles. Vacuum distillation of DMF into the cell lowered its quality, probably through its partial decomposition (to dimethylamine and carbon monoxide). Cyclic voltammograms were recorded on a BAS CV-50W Voltammetric Analyzer with a glassy carbon working electrode, platinum wire counterelectrode and silver wire as a quasi-reference. Before each experiment the carbon electrode was polished with an alumina paste, and sonicated. A sweep rate of 0.1V/s was used in most cases and 100% IR compensation was achieved before each run. Before the tetrone was dissolved into the electrolyte solution, a few blank sweeps were done until no change in the background current could be seen. After the runs with tetrone a small amount of

ferrocene was added to the solution in the glove bag in order to calibrate the potentials to the $FeCp_2/FeCp_2^+$ couple.

BIBLIOGRAPHY

(1)   (a) Southampton Electrochemistry Group. *Instrumental methods in electrochemistry*; E. Horwood; Halsted Press: Chichester New York, **1985**. (b) Chambers, J. Q. In *The chemistry of the quinonoid compounds;* Patai, S., Eds; Interscience: London ; New York, **1974**; p 737.

(2)   Almlof, J. E.; Feyereisen, M. W.; Jozefiak, T. H.; Miller, L. L. *J. Am. Chem. Soc.* **1990**, *112*, 1206.

(3)   Bock, H.; Hierholzer, B.; Jaculi, D. *Z.Naturforsch.(B)* **1988**, *43*, 1247.

Chapter 7

X-RAY DIFFRACTION STUDIES

7.1 Introduction

No other method of characterization of chemical systems can give a more complete structural description than single crystal X-ray (or neutron) diffraction. Growths of single crystals of both neutral and reduced forms of the tetrones were attempted in the course of this study. In the case of the air stable neutral tetrones, this effort was a relatively simple task. Crystallizations of the mono- and dianions were more challenging, due to the low solubility of their metal salts in organic solvents, as well as their air sensitivity. The solubility problem was solved by synthesis of $(t\text{-Bu})_8(\text{MeO})_4\mathbf{2}$, a derivative 'decorated' with lipophilic t-Butyl groups. Use of Schlenk techniques allowed a slow diffusion of hexane into a THF solution of $(t\text{-Bu})_8(\text{MeO})_4\mathbf{2}\text{K}$, under oxygen-free conditions and produced crystals of $(t\text{-Bu})_8(\text{MeO})_4\mathbf{2}\text{K}\bullet(\text{THF})_4$. Growing of the crystals of dianions still requires some effort.

7.2 Results and discussion

The most important crystallographic data are summarized in tables 7.1-4 and Appendix B. Tetrone **2** crystallized from hot acetonitrile as dark red monoclinic needles in $P2_1/n$. The unique atoms of the unit cell comprise half of the tetrone molecule **2**, which contains an inversion center. Molecules of **2** are arranged in π stacks with an intermolecular separation equal to b (4.61 Å).

124

Table 7.1. Selected crystallographic data for **2**, $(NMe_2)_42 \bullet (Me_2SO)_3$, ($t$-Bu)$_8(MeO)_4$2K$\bullet$(C$_4H_8$O)$_4$ and (t-Bu)$_8$(MeO)$_4$2Na$\bullet$(C$_6$H$_{10}$O$_2$)$_4$.

	2	(NMe$_2$)$_4$2 $\bullet$(Me$_2$SO)$_3$	(t-Bu)$_8$(MeO)$_4$2K $\bullet$(C$_4$H$_8$O)$_4$.	(t-Bu)$_8$(MeO)$_4$2Na $\bullet$(C$_6$H$_{10}$O$_2$)$_4$
chem formula	C$_{32}$H$_{20}$O$_4$	C$_{46}$H$_{58}$N$_4$O$_7$S$_3$	C$_{84}$H$_{124}$O$_{12}$K	C$_{168}$H$_{264}$O$_{32}$Na$_2$
fw	468.48	875.16	1364.99	2841.90
cryst syst	Monoclinic	Monoclinic	Triclinic	Triclinic
space group	P2$_1$/n	P2$_1$/n	P1	P1
λ, Å (Mo Kα)	0.7107	0.7107	0.7107	0.7107
a, Å	13.8607(14)	21.092(4)	9.5055(2)	16.1411(4)
b, Å	4.6091(5)	8.0588(16)	13.0026(2)	16.3146(2)
c, Å	19.121(2)	26.781(5)	17.1668(2)	18.8482(4)
α, deg	90	90	77.2809(11)	64.4540(10)
β, deg	109.922(2)	101.31(3)	85.5001(12)	72.4140(10)
γ, deg	90	90	77.6417(10)	88.4470(10)
V, Å^3	1148.4(2)	4463.7(15)	2020.64(7)	4238.05(15)
Z	2	4	1	1
d_{calcd}, g cm^{-3}	1.355	1.302	1.384	1.114
μ, mm^{-1}	0.089	0.176	0.182	0.085
T, K	173(2)	293(2)	293(2)	293(2)
R	0.0493	0.0690	0.0844	0.0728
R$_{WF}$2	0.0952	0.1743	0.2430	0.2082
GOF	1.046	0.856	0.910	0.932
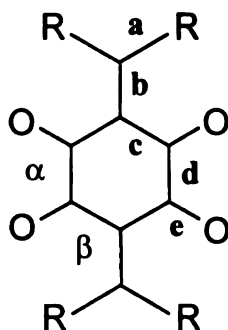
Figure 7.1 Symbols of bonds and dihedrals used in tables 7.2 and 7.3.

125

Table 7.2 Selected bond distances for tetrones and their monoanions.

	2		$(NMe_2)_42$		$(t\text{-Bu})_8(MeO)_42Na$		$(t\text{-Bu})_8(MeO)_42K$	
a	C4-C5	1.480(3)	C11-C1	1.464(4)	C11-C12	1.481(9)	C7-C8	1.477(7)
	C4-C11	1.472(3)	C11-C2	1.453(4)	C11-C28	1.502(9)	C7-C28	1.465(8)
			C30-C3	1.458(4)	C44-C45	1.477(9)	C44-C4	1.482(7)
			C30-C4	1.475(4)	C44-C61	1.463(9)	C44-C6	1.457(8)
					C87-C88	1.490(9)		
					C87-C104	1.469(8)		
					C120-C121	1.482(8)		
					C120-C142	1.486(9)		
b	C3-C4	1.388(3)	C1-C11	1.440(4)	C2-C11	1.393(9)	C1-C44	1.440(8)
			C4-C30	1.429(4)	C5-C44	1.442(8)	C4-C7	1.398(8)
					C78-C87	1.442(8)		
					C81-C120	1.408(9)		
c	C1-C3A	1.471(3)	C1-C2	1.455(4)	C1-C2	1.478(8)	C1-C6	1.470(7)
	C2-C3	1.476(3)	C1-C6	1.459(4)	C2-C3	1.486(9)	C1-C2	1.434(8)
			C4-C3	1.464(4)	C4-C5	1.453(9)	C4-C5	1.464(9)
			C4-C5	1.477(4)	C5-C6	1.452(9)	C3-C4	1.449(7)
					C77-C78	1.457(8)		
					C78-C79	1.478(8)		
					C80-C81	1.479(9)		
					C81-C82	1.451(9)		
d	C1-C2	1.540(3)	C2-C3	1.559(4)	C1-C6	1.529(9)	C2-C3	1.547(8)
			C5-C6	1.545(5)	C3-C4	1.549(8)	C5-C6	1.492(8)
					C77-C82	1.512(9)		
					C79-C80	1.572(8)		
e	C1-O1	1.226(2)	C2-O7	1.240(4)	C1-O7	1.219(7)	C2-O25	1.236(7)
	C2-O2	1.212(2)	C3-O8	1.237(4)	C3-O10	1.207(7)	C3-O27	1.228(7)
			C5-O9	1.231(4)	C4-O9	1.258(7)	C5-O24	1.229(7)
			C6-O10	1.234(4)	C6-O8	1.263(8)	C6-O26	1.233(7)
					C77-O84	1.254(7)		
					C79-O85	1.228(7)		
					C80-O86	1.219(7)		
					C82-O83	1.245(8)		

Table 7.3 Selected dihedrals for tetrones and their monoanions.

	2		(NMe$_2$)$_4$**2**		(t-Bu)$_8$(MeO)$_4$**2**K		(t-Bu)$_8$(MeO)$_4$**2**Na	
α	O1-C1-C2-O2	26.9	O7-C2-C3-O8	-20.2	O24-C5-C6-O26	-1.7	O8-C6-C1-O7	8.2
			O9-C5-C6-O10	-20.9	O27-C3-C2-O25	3.6	O10-C3-C4-O9	-6.2
							O85-C79-C80-O86	7.8
							O83-C82-C77-O84	-6.8
β	O2-C2-C3-C4	-26.2	O10-C6-C1-C11	15.2	O24-C5-C4-C7	-0.8	O7-C1-C2-C11	-14.0
	O1A-C1A-C3-C4	37.6	C11-C1-C2-O7	10.4	C7-C4-C3-O27	-11.6	C11-C2-C3-O10	2.6
			O8-C3-C4-C30	8.4	O25-C2-C1-C44	2.1	O9-C4-C5-C44	14.4
			C30-C4-C5-O9	3.3	C44-C1-C6-O26	8.2	C44-C5-C6-O8	-5.3
							O86-C80-C81-C120	-3.5
							C120-C81-C82-O83	13.1
							O84-C77-C78-C87	6.5
							C87-C78-C79-O85	-16.9

Table 7.4 Angles of the mean ring planes vs. the planes of the methylene centers of

tetrones and their monoanions.

2	C[3-5,11]	
C[5,10]	38.8	
C[11,16]	43.9	
C[1-3,1A-3A]	35.0	
(NMe$_2$)$_4$2	C[4,30,31,40]	C[1,11,12,21]
C[40-45]	36.4	
C[31-36]	31.3	
C[1-6]	43.1	30.4
C[12-17]		34.0
C[21-26]		28.5
(t-Bu)$_8$(MeO)$_4$2K	C[4,18,28,7]	C[1,44,45,61]
C[8-13]	30.5	
C[28-30,35,38,43]	33.5	
C[1-6]	40.9	41.3
C[45-50]		34.6
C[61-6]		29.8
(t-Bu)$_8$(MeO)$_4$2Na	C[2,11,28,12]	C[5,44,45,61]
C[12-17]	31.5	
C[28-33]	36.8	
C[1-6]	36.1	35.9
C[45-50]		38.6
C[61-6]		31.1
(t-Bu)$_8$(MeO)$_4$2Na	C[78,87,88,104]	C[120,121,142,81]
C[88-93]	37.5	
C[104-109]	28.3	
C[77-82]	37.1	37.5
C[121-126]		28.2
C[137-142]		38.2

Tetrone $(NMe_2)_42$ crystallized from DMSO as dark blue blocks of

$(NMe_2)_42\cdot(DMSO)_3$. The unique atoms of the unit cell include one molecule of $(NMe_2)_42$

and three solvent molecules of DMSO. Molecules of $(NMe_2)_42$ are arranged into sheets

with relatively short intermolecular contacts (O8-N37A 3.256Å and O10-N27B 3.260Å)

between two of their carbonyl oxygens and nitrogen atoms of two neighboring tetrones.

Additionally two of its own nitrogen atoms (N37 and N27) interacts in similar manner

with carbonyl oxygens of the another two neighbors. The change of the packing mode of

2 *vs.* $(NMe_2)_42$ may be explained by the transfer of charge between the electron-donating

nitrogens and the electron-accepting oxygen and electrostatic polarization of the

molecule. Intermolecular coulombic interactions in the crystal of $(NMe_2)_42$ also explain

its, contrasting to **2,** low solubility in non polar solvents. The geometry of single

molecules of **2** and $(NMe_2)_42$ are presented on figure 7.2 and 7.3. The central 3,6-

dimethylene-1,2,4,5-tetraoxocyclohexane ring of **2** is puckered into a chair-like

conformation, with the unique dicarbonyl dihedral OCCO angle being 26.9°. These

distortions are probably driven by coulombic repulsion between the exocyclic C=O bond

dipoles. The tetrone ring of $(NMe_2)_42$ is slightly different than that of **2**. Instead of

adopting a pseudo-chair conformation, this molecule twists around the axis defined by

the two methylene carbons. The values of the OCCO dicarbonyl dihedral angles (20.9°

and 20.2°) are however similar to that of **2**. Aryl and tetroxalane rings of **2** and $(NMe_2)_42$,

which are connected to the same methylene carbon centers form a propeller-like

arrangement. The steric and electronic differences between the phenyl rings and the one

of tetrone, which is formally doubly bonded to the methylene center, do not seem to have

great influence on their out-of-plane twists.
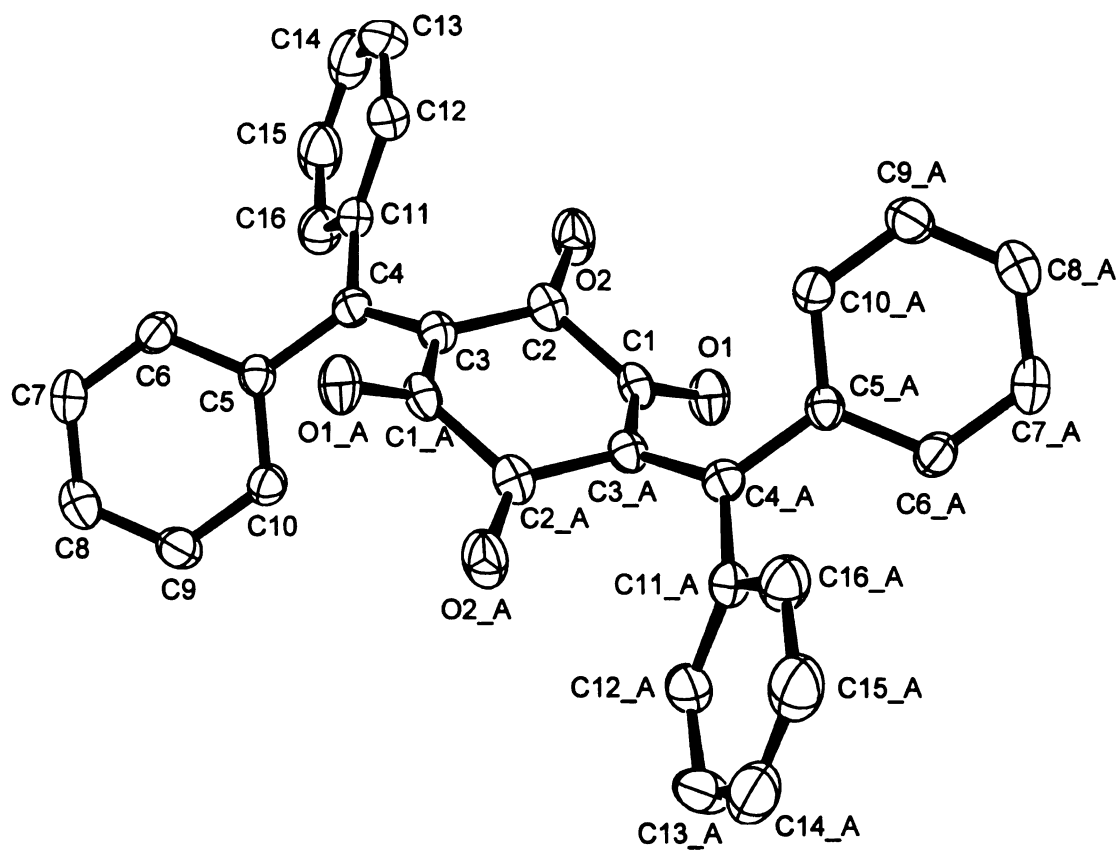
Figure 7.2 ORTEP drawing (50% probability) of **2**. Hydrogen atoms are not shown.
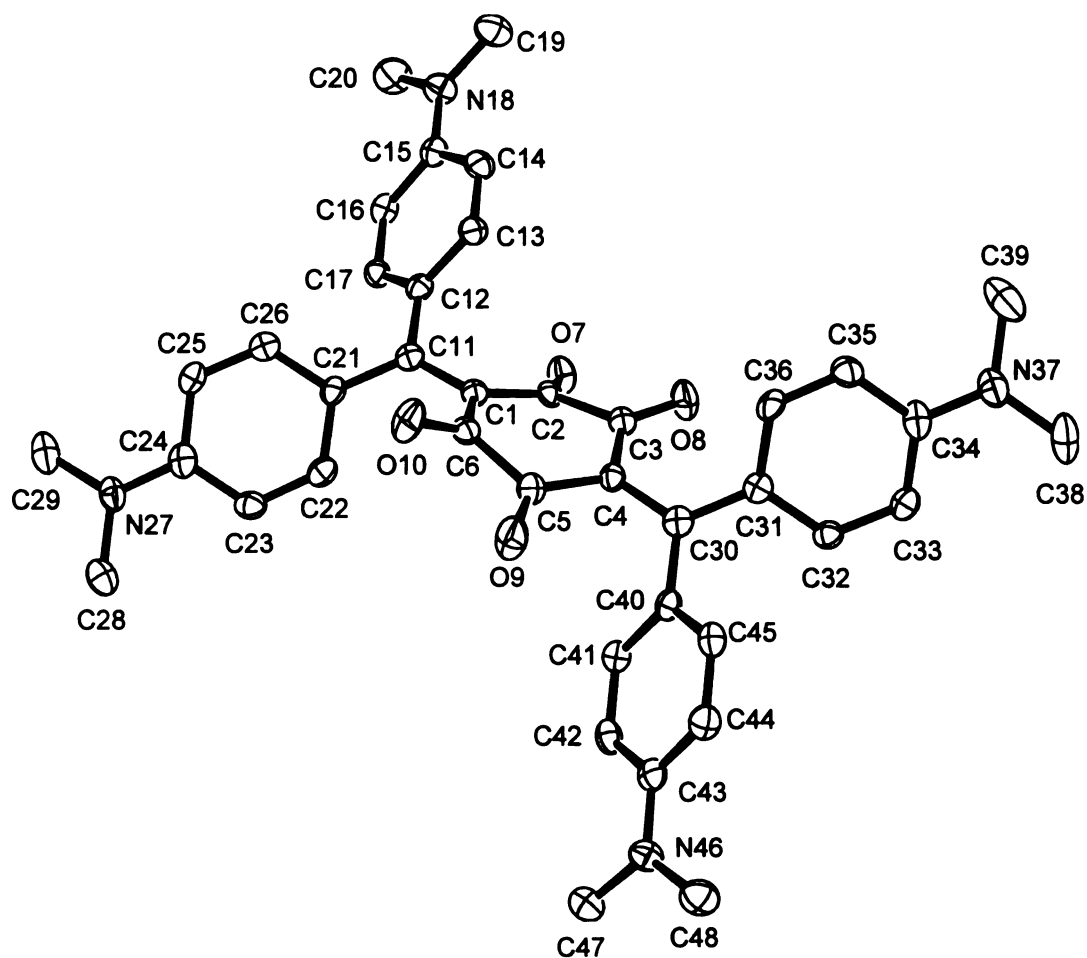
Figure 7.3 ORTEP drawing (50% probability) of (NMe₂)₄2•(Me₂SO)₃. Hydrogen atoms and DMSO molecules are not shown.

The angles defined as that between mean plane of all carbons of the rings and mean plane of four carbons of the 'methylene center' are around 30°-40° (table 7.4).

Slow diffusion of n-pentane into a THF solution of (t-Bu)$_8$(MeO)$_4$2K, under oxygen-free conditions produced purple needle-like triclinic (P1) crystals of (t-Bu)$_8$(MeO)$_4$2K•(THF)$_4$ with one molecule of the complex in the cell space group. A similar technique (using n-pentane/DME) produced crystals of (t-Bu)$_8$(MeO)$_4$2Na•(DME)$_4$* with the same color and symmetry but two unique molecules of the complex in asymmetric unit. In both of the above structures, the organic anions link alkali metal cation to form 1-D chains (figures 7.4 and 7.5). In these chains, the anions display the hoped-for chelating and bridging modes of coordination. In (t-Bu)$_8$(MeO)$_4$2K each potassium cations in the chain forms a pseudo-cubic sphere coordinating with four carbonyl oxygens from two tetrone molecules and four THF oxygens. Periodicity of the crystal implies that the central 'tetrone' rings of all of the anions are parallel to each other. There is however a 'zig-zag' angle of 148.2 ° between mean planes defined by four oxygens of tetrone rings and four carbonyl oxygens coordinated to the potassium cation. The sodium salt forms similar structure. In this case, however, there are two independent alternating monoanions in the chain and the pseudo-cubic coordination sphere of the sodium cation (containing four tetrone oxygens four oxygens of two chelated DME molecules) is distorted to form a pseudo square antiprism. This distortion rotates plane of one of the unique monoanions around the chain axis so the angle between its central mean planes and that of the neighbor is 37.6°.

---

* The crystal of the sodium salt was grown by Robert Gentner

132
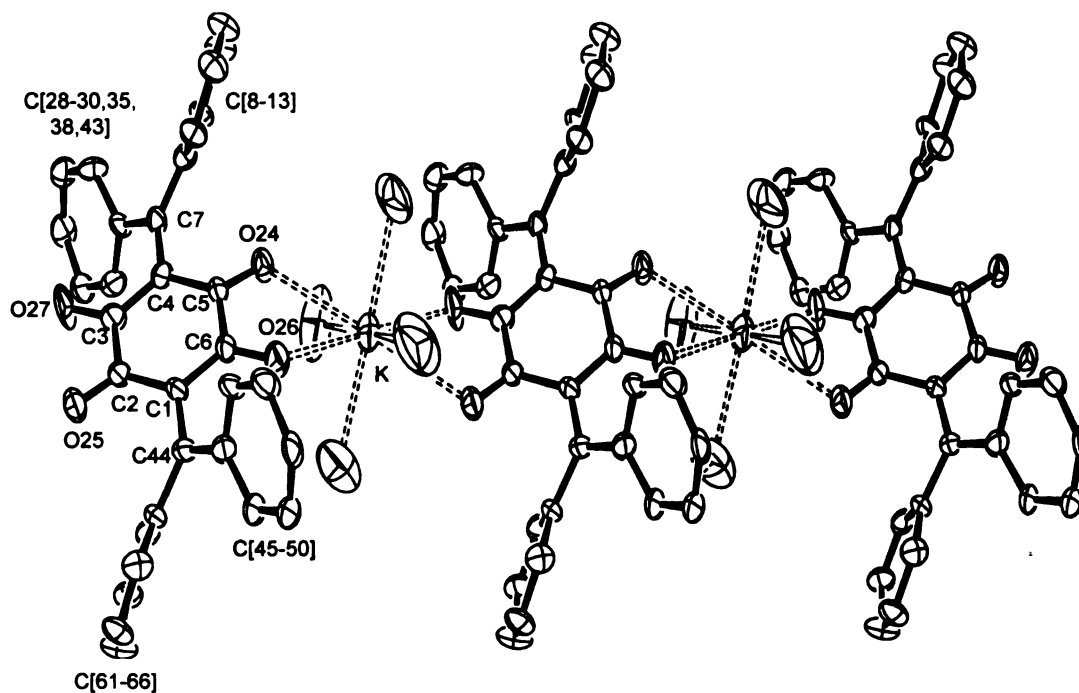
Figure 7.4 ORTEP drawing (50% probability) of chains formed in the solid state by

radical anion salt (t-Bu)$_8$(MeO)$_4$2K•(THF)$_4$ with one unique molecule of

complex. Hydrogen atoms, THF molecules (excluding coordinated oxygen

atoms) t-butyl and metoxy fragments, are not shown.
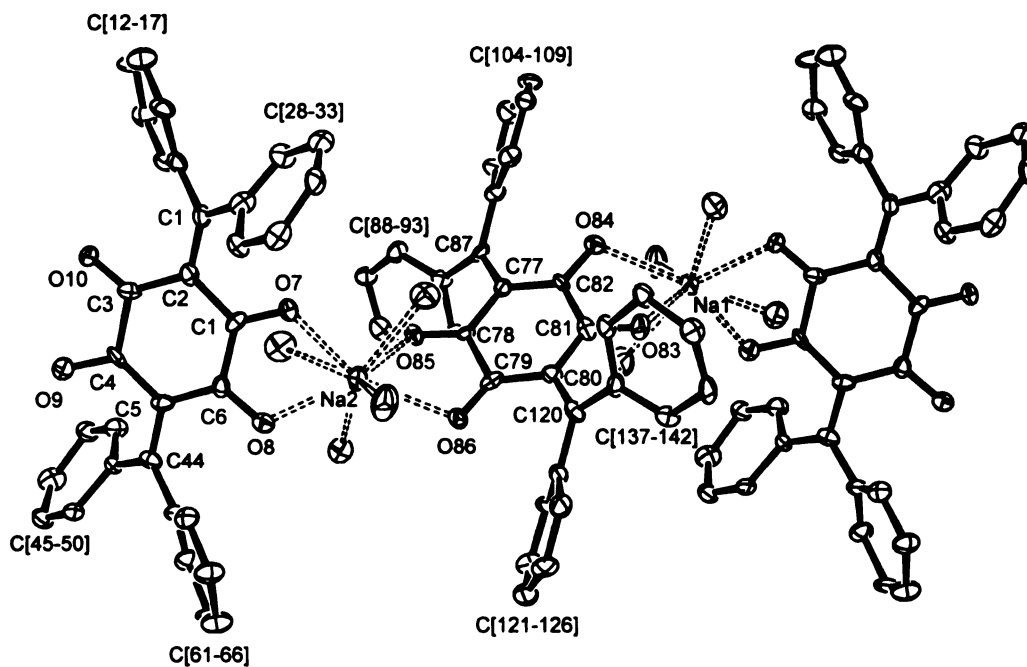
Figure 7.5 ORTEP drawing (50% probability) of chains formed in the solid state by

radical anion salt $(t\text{-Bu})_8(\text{MeO})_4 2\text{Na} \bullet (\text{DME})_4$ with two unique molecules of

complex. Hydrogen atoms, DME molecules (excluding coordinated oxygen

atoms), t-butyl and metoxy fragments are not shown.

In addition to four unique coordinated molecules of DME there are also four noncoordinated ones located in the cavities between the chains. Similar modes of coordination found in both crystals confirms, as expected, that the negatively charged pocket formed by two oxygen atoms on one side of the anion is the preferred place for metal cation binding. Both potassium and sodium salts have also polymeric nature. It may be attributed not only to the design of anion but also to relatively low coordinating power of solvents used for crystallization. THF and DME are probably too weak Lewis bases to compete for coordination sphere with chelating anions of **2**. Use of strongly donating solvent could break chains into separate ion aggregates. Such behavior has been observed for potassium radical anion salt of 2,3-bis(2-pyridyl)quinoxaline, which from THF crystallized as 1-D chains of (dpq)K•(THF)$_2$ but from methylamine as discrete solvent separated ion-pair dimmers of (dpq)K•(MeNH$_2$)$_2$.[1] Obtained organometallic structures have charge balance of the coordination equal to zero. We hope that increasing of the cation charge will force more of the anions to coordinate to it in order to preserve zero or as close to zero as possible balance. This in turn may induce formation of 2-D networks based on chessboard or honeycomb motifs.

Reduction of the tetrone notably flattens out its central ring and the values dicarbonyl dihedrals are now below 8.2° (table 7.3). There is however not much change in the propeller-like arrangements of the rings with angles of twist retaining values of 30-40° (table 7.4). Selected bond lengths of neutral and reduced forms of tetrone are presented in table 7.2. Relatively low changes of the bond lenghts of the monoanions vs. tetrones does not allow for unambiguously localize of distribution of the unpaired electron. Despite repeated attempts, so far we were unable to grow crystals of dianions of

2 and monovalent alkali metal cations suitable for X-ray analysis. Hopefully use of doubly divalent cations will lead to chains of dianions analogous to that of monoanions.

7.3 Experimental

Crystals of compound **2** were grown by slow cooling of its acetonitrile solution. Crystals of $(NMe_2)_4$**2**•$((CH_3)_2SO)_3$ formed over time from oversaturated DMSO solution of $(NMe_2)_4$**2**. To produce crystals of $(t\text{-Bu})_8(MeO)_4$**2**K•$(C_4H_8O)_4$, 50 mg of tetrone was dissolved in 30-50 ml of degassed THF and reacted wit potassium mirror following the procedure described for preparation of EPR samples. Solution of the potassium salt of anion was then transferred to two 9mm diameter Pyrex glass tubes attached to the K-cell. Pentane was condensed over it and and allowed to diffuse for a couple of days in room temperature. Crystals of $(t\text{-Bu})_8(MeO)_4$**2**Na•$(C_4H_{10}O_2)_4$ were grown similarly but DME was used instead of THF.

BIBLIOGRAPHY

(1)   Ichimura, A. S.; Szajek, L. P.; Xie, Q. S.; Huang, R. H.; Huang, S. Z.; Wagner, M. J.; Dye, J. L.; Jackson, J. E. *J. Phys. Chem. B* **1998**, *102*, 11029.

Chapter 8

ELECTRONIC SPECTROSCOPY

8.1 Introduction

The tetrones and their anions described in earlier chapters were also characterized

by means of electronic spectroscopy. UV-VIS (ultraviolet and visible) spectra in the

range of 200-1000 nm were recorded for neutral tetrones in acetonitrile. In addition, their

reduction with *in-situ* prepared [K^+@C(2.2.2)]K^- in THF was monitored by VIS-NIR

(visible and near-infrared) spectroscopy (400-2000 nm).

8.2 Results

<u>Neutral tetrones.</u> The electronic absorption profiles of neutral tetrones in the UV-

VIS region (table 8.1, figure 8.1) comprise of a set of peaks in the UV region and intense

visible absorption bands. In the case of **2**, the two bands coalesce into a single broad

band.

<u>Monoanions and dianions.</u> VIS-NIR spectra of mono- and dianions prepared by

reduction of tetrones with [K@c(2.2.2)]$^+K^-$ in THF were also recorded (figures 8.2, 8.3;

table 8.1). Solutions of **2**$^-$ are dark wine-red; $(MeO)_4$**2**$^-$ and $(t\text{-}Bu)_8(MeO)_4$**2**$^-$are purple

(similar to aqueous solutions of permanganates) while solutions of $(Me_2N)_4$**2**$^-$ are green.

In addition to the bands in the visible region, all monoanions possess a distinctive broad

absorption band in the near infrared region, with the maximums at 1000, 1100, 1150,

1500 nm for **2**$^-$, $(MeO)_4$**2**$^-$, $(t\text{-}Bu)_8(MeO)_4$**2**$^-$, and $(Me_2N)_4$**2**$^-$, respectively. The main

absorptions in the VIS-NIR spectra of the dianions are concentrated around 800 nm and

are much less affected by the phenyl rings' substituents, so the color of all dianion

solutions is emerald-green.

Table 8.1. Absorption maxima of tetrones their mono- and dianions.

Tetrone	λ_{max} (nm)		
	Neutral	Monoanion	Dianion
	(MeCN)	(THF)	(THF)
2	354	430	485,
		525	800
		1000	
(MeO)$_4$**2**	498,	530	745
	580 (shoulder)	600 (shoulder)	
		1100	
(t-Bu)$_8$(MeO)$_4$**2**	480	525,	770
		610 (shoulder)	
		1150	
(Me$_2$N)$_4$**2**	602,	425,	770
	674	635,	
		1500	

8.3 Discussion

Neutral tetrones. Since all tetrones possess electron-donor and electron-acceptor

moieties, the visible wavelength absorption may be assigned to an intramolecular charge-

transfer transition from the donor diarylmethylene fragment to the acceptor tetrone unit.

The bathochromic shift in the series **2**, (MeO)$_4$**2** and (Me$_2$N)$_4$**2** can be explained by the

increase in the electron-donating abilities of substituents in the order -H, -OMe, -N(Me)$_2$.

A similar trend can be seen for example in the case of substituted diphenylmethyl

carbocations (λ_{max} = 440(H-), 507(MeO-), 610(Me$_2$N-) nm).[1]

139
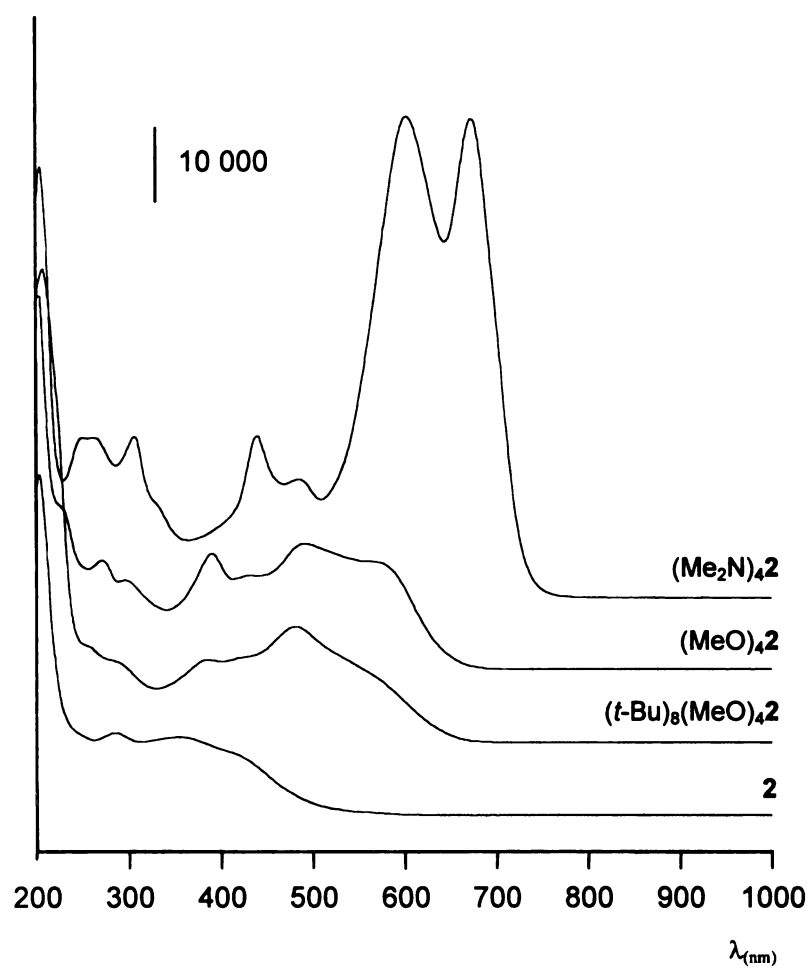
Figure 8.1. UV-Vis absorption spectra of neutral tetrones (acetonitrile)
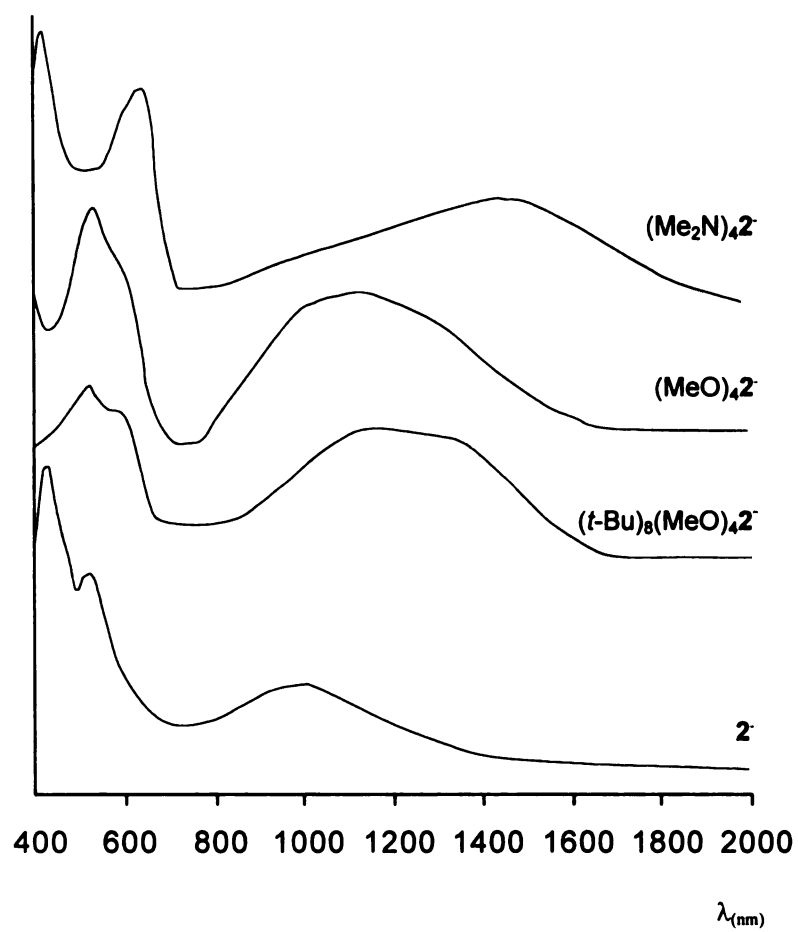
Figure 8.2. Vis-NIR spectra of the THF solutions of monoanions.

141
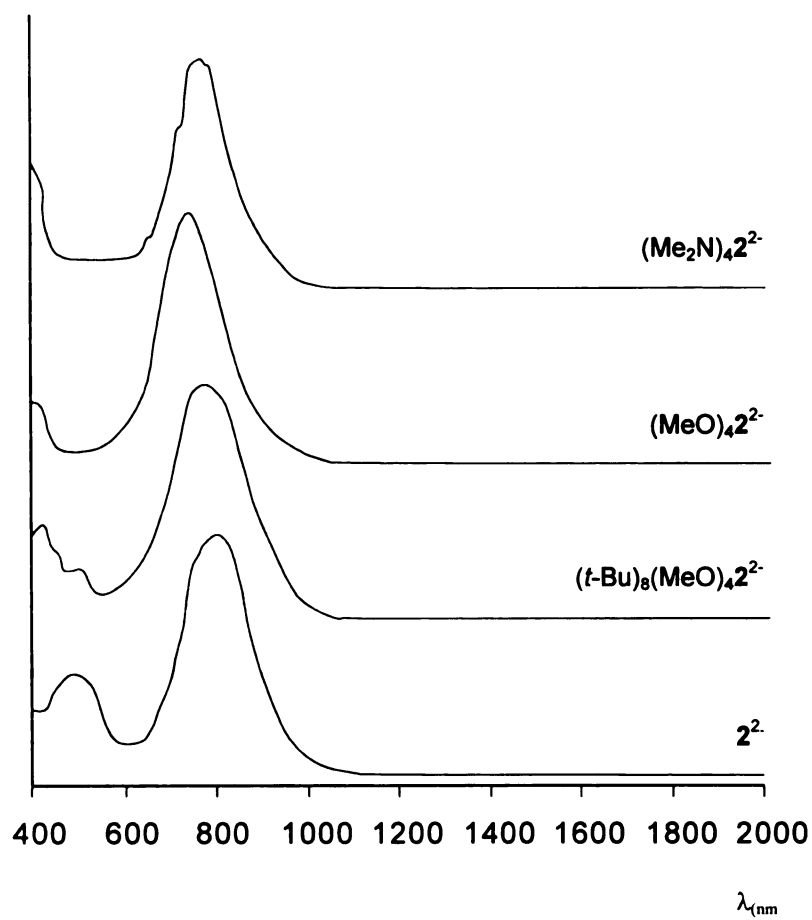
Figure 8.3. Vis-NIR spectra of THF solutions of dianions

The increase in donating abilities not only changes the energy of the transition but also its intensity. The extinction coefficient of $(Me_2N)_4\mathbf{2}$ is very high (ca. 70 000) making that compound an intense blue dye, while the absorptions of $(MeO)_4\mathbf{2}$ and $\mathbf{2}$ (purple and red) are weaker. The charge-transfer band of $(Me_2N)_4\mathbf{2}$ possesses two relatively close maxima at 602 and 674 nm. In $(MeO)_4\mathbf{2}$, this splitting is much less pronounced and in addition to one maximum (498 nm) there is only a shoulder at 580 nm. Compound $\mathbf{2}$ has only one maximum (354 nm) but a broad plateau which then tails over 500nm. Splitting of the absorption may be attributed to the near degeneracy of LUMO and LUMO+1.

Monoanions. The most distinctive absorption of monoanions is a broad band in the near-IR region. The energy of this transition decreases with increasing electron-donating power of the aryl substituents, indicating that the electron is excited from an orbital conjugated to them into another that is relatively less affected. This correlation and the low energy of the transition would be in a good agreement with a SOMO to LUMO transition.

8.4 Experimental

UV-vis spectra of the tetrones were recorded with UNICAM UV2 in acetonitrile as the solvent. The mono- and dianions of the tetrones were prepared in THF in the presence of the C(2.2.2) cryptand in the manner described in section 4.4. The progress of reduction was monitored within the optical cell attached to the sidearm with a Guided Wave Model 260 fiber-optic spectrophotometer.

BIBLIOGRAPHY

(1)   Deno, N. C.; Jaruzelski, J. J.; Schriesheim, A. *J. Am. Chem. Soc.* **1954,** 77, 3044.

Chapter 9

SUMARY AND CONCLUSIONS

The structures of mono and dianions of the terone **1** were proposed as discrete building blocks for assembly of molecular magnetic materials at the beginning of this work. Examination of their idealized and real behaviors composed the rest of it. Three major questions have been investigated in the course of this study:

- Can these anions and their neutral precursors be practically synthesized and handled?

- May derivatives of 1^{2-} have high-spin ground states?

- Will they tend to crystallize forming the hoped-for extended organometallic structures?

Chapter 3 has shown that synthesis of the neutral tetrone precursors can be achieved when aryl rings protect the reactive methylene groups (group of tetrones **2**). The synthetic route developed is relatively straightforward (two-steps), cost effective, and allows fast preparation of a broad variety of products from easily available synthons. Substantial progress toward extending the family of tetrones to alkyl substituted derivatives has also been achieved.

Electrochemical studies have shown that tetrone **2** and its derivatives can be reversibly reduced in two successive one electron processes to mono and dianions. These

results point to the stability of both mono and dianions of **2**, at least on the time-scale of the cyclic voltammetry experiment (seconds to minutes).

With the above facts established, the bulk of the work focused on the preparation and determination of the ground state of the dianions (with observation of the triplet state as a main goal). Those studies started with high quality *ab-initio* CASSCF calculations of the energies of the lowest singlet and triplet states of derivatives of 1^{2-} (chapter 2). The calculations confirmed what was predicted earlier by qualitative methods in chapter 1, that the singlet-triplet gap is small in those dianions. They also showed that control over the **S-T** gap could be achieved by structural modifications. For example, the strong (ca. 10 kcal/mol) calculated preference for the singlet in the noncoordinated, nonsubstituted dianion 1^{2-} is replaced by a 5 kcal/mol preference for the triplet state in the tightly coordinated one. Despite the relatively high level of these calculations the values of the absolute numbers obtained must be treated with skepticism. The most important outcome should be considered to be the understanding of the mechanism of the **S-T** tuning and the assessment of its approximate magnitude.

Experimental work was undertaken complementary to the calculations. Spectroscopic studies could not be performed with exactly the same species as those used for calculations. The available phenyl substituted derivatives **2** had to be used instead. In turn, high quality theoretical study could not be repeated on the tetraaryl substituted derivatives of **2**; the large number of atoms in those molecules placed such computations beyond the practical scope of available quantum chemistry software.

EPR study of the noncoordinated derivatives of 2^{-} prepared by reduction of tetrones with potassium in the presence of macrocyclic coligands confirmed their

expected structure. Unfortunately no triplet signal could be detected for dianions prepared in a similar manner. NMR studies could not however prove that they are closed shell singlets.

The failure to observe a triplet signal was not surprising, since the earlier calculations had already pointed to the necessity of tuning the electronic structure of the dianions by strong metal cation coordination in order to achieve triplet preference. The additional electronic perturbations introduced by the presence of the aryl groups may also contribute to the relative preference for the singlet state.

Solution studies of coordinated complexes $(M \cdot 2 \cdot M)^{x+}$ were considered and attempted but they turned out to be difficult to perform. In addition to solubility problems, the required stoichiometry and geometry of the complexes formed in solution could not be ensured. The anions and the cations might prefer unanticipated modes of association. This fact could not only prevent generation of the required complexes, but also lead to misleading 'positive' results. For example triplet EPR signals were generated by two monoradicals interacting with each other through Cs^+ in the complex $(2Cs2)^-$. The presence of such monoradical aggregates could not be excluded in solution even when great care was taken to control stoichiometry of the reduction since monoanions may be formed by decomposition of dianions.

An attempt to solve this problem by preparation of ion triples $2(SnBu_3)_2$ was undertaken (Figure 9.1). UV irradiation of a mixture of hexabutylditin (Sn_2Bu_6) and tetrone 2 was supposed to break weak Sn-Sn bond with formation of the trialkyltin radicals. Two equivalents of $Bu_3Sn \cdot$ radicals were then expected to add to one of the tetrones with formation of a tightly coordinated complex of 2. The bulky butyl groups of

the tin cations were supposed to prevent coordination of two of them to one side of the

anion or coordination of two anions to one cation, ensuring formation of only 2(SnBu$_3$)$_2$.
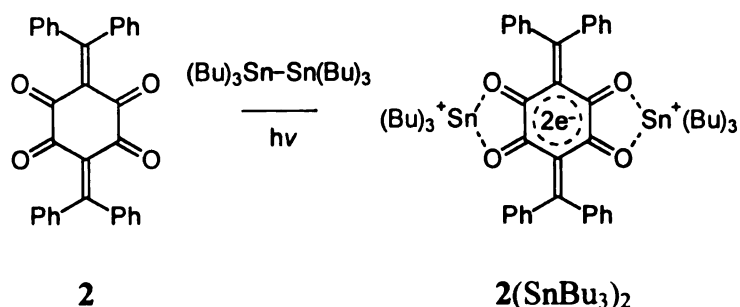
Figure 9.1. Photochemical generation of 2(SnBu$_3$)$_2$.

Photolysis of neat **2** and Sn$_2$Bu$_6$ indeed lead to the mixture of products which

besides strong EPR doublet, produced a triplet signal with a D value of ca. 200 G,

pointing to strong intramolecular interactions of the electrons. These results could not be

accepted as a proof that coordination of **2**$^{2-}$ leads to generation of triplet however,

because no information concerning the structure of the species responsible for the signal

could be obtained. Consequently these results have not been detailed in this thesis.

To conclude, EPR results alone, without good structural characterization, can not

unambiguously provide an answer to the question concerning the ground state of such

labile complexes. Definitely, an alternative approach must be chosen. Any spectroscopic

study must follow crystallization of the complex and its X-ray structure determination.

Only with such exact structural results in hand will interpretation of EPR or SQUID data

be meaningful.

An attempt to follow these principles has been undertaken in the latter part of

these studies. The problem of low solubility of the complexes has been solved by

synthesis of the *t*-Butyl substituted analog of the tetrone (MeO)₄2. The lipophilic butyl groups increased the solubility of both the tetrone and its complexes in the relatively non-polar but chemically inert and easy to dry ethereal solvents used in the reductions. Then anaerobic techniques of crystal growing were applied. Despite these efforts, all attempts to grow crystals of dianion were unsuccessful. The apparent reason was the slow decomposition of the dianion at room temperature. A temperature dependent kinetic study of the decomposition should be performed and, if a safe threshold of temperature can be found, temperature-controlled crystallization technique should be applied in order to achieve this goal. It is also likely that the stability of dianion salts will be increased by coordination to some metal cations.

In the meantime the crystallization effort of the air sensitive, but room temperature stable monoanion salt (*t*-Bu)₈(MeO)₄2K has been successfully accomplished. Analogously to dianions, the monoanions are viable building blocks for assembly of molecular magnets. The 1-D chain structures of their potassium and sodium salts have proved their tendency to form extended structures. The question, which remains to be answered, is whether the dimensionality of the net may be increased.

Only a small number of paramagnetic bridging ligands has been structurally characterized so far. Most of them are variations of neutral nitroxides or nitronyl-nitroxides, species of relatively high stability but with modest coordination abilities. The anions investigated in this work have properties that set them apart from this group and that may allow their application beyond the field of molecular magnets. Besides being anionic and having a robust chelating mode of coordination, they posses low and tunable reduction potentials. This tunability may allow assembly of systems with redox potentials

of the monoanions and the transition metal centers they are coordinated to being almost equal. An example where such equilibrium led to interesting phenomenon is valence tautomerism found in structurally related semiquinone complexes of transition metals. In certain temperatures phase transition may be observed where electrons cooperatively transfer from metal to semiquinone centers. It would be interesting to observe similar phenomenon in the extended rather then discrete systems and investigate its consequences.

APPENDICES

Table A1. Geometry of the unique atoms of $\mathbf{1}^{2-}$ and its complexes optimized at indicated level of geometry (6-31G* basis set)

TCSCF

$\mathbf{1}^{2-}$

C1	0.0000000000	1.4585402082	0.0000000000
C2	1.2998449695	0.7264314308	0.0000000000
C3	0.0000000000	2.7951931157	0.0000000000
O1	2.3581524018	1.3670568670	0.0000000000
H1	0.9271711617	3.3373483434	0.0000000000

$\mathbf{1}Li_2$

C1	0.0000000000	1.4862084218	0.0000000000
C2	1.2637584273	0.7181900799	0.0000000000
C7	0.0000000000	2.8126012595	0.0000000000
O1	2.3708573392	1.3129967865	0.0000000000
H1	0.9231996774	3.3580798268	0.0000000000
Li1	3.6294109899	0.0000000000	0.0000000000

$\mathbf{1}(BeF)_2$

C1	0.0000000000	1.5106324296	0.0000000000
C2	1.2318914718	0.7115756470	0.0000000000
C3	0.0000000000	2.8371442752	0.0000000000
O1	2.3924611694	1.2201339304	0.0000000000
H1	0.9229260360	3.3845033134	0.0000000000
Be1	3.4382197582	0.0000000000	0.0000000000
F1	4.8283738502	0.0000000000	0.0000000000

$\mathbf{1}(AlF_2)_2$

C1	0.0000000000	1.4962442533	0.0000000000
C2	1.2408255712	0.7108880983	0.0000000000
C3	0.0000000000	2.8239066235	0.0000000000
O1	2.3859764059	1.2604845714	0.0000000000
H1	0.9225973324	3.3714061945	0.0000000000
Al1	3.7343725931	0.0000000000	0.0000000000
F1	4.5714039244	0.0000000000	1.4043911054

Table A1. (con't)

$$F_41Li_2$$

C1	0.0000000000	1.4729477875	0.0000000000
C2	1.2735121843	0.7157051338	0.0000000000
C3	0.0000000000	2.8019780573	0.0000000000
O1	2.3866780569	1.3004466127	0.0000000000
F1	1.0503264806	3.5540764980	0.0000000000
Li1	3.6551654006	0.0000000000	0.0000000000

$$(OH)_41Li_2$$

C1	0.0000000000	1.4664843050	0.0000000000
C2	1.2709734910	0.7154595384	0.0000000000
C3	0.0000000000	2.8225747535	0.0000000000
O1	2.3981502585	1.2970816889	0.0000000000
O2	1.1204651797	3.5359119172	0.0000000000
H1	0.9584113899	4.4678444736	0.0000000000
Li1	3.6317863922	0.0000000000	0.0000000000

DMCB

C1	0.0000000000	1.0787892346	0.0000000000
C2	1.0092311570	0.0000000000	0.0000000000
C3	0.0000000000	2.4005871649	0.0000000000
H1	0.9186088459	2.9579997044	0.0000000000
H2	2.0827383088	0.0000000000	0.0000000000

ROHF

$$1^{2-}$$

C1	0.0000000000	1.4300354546	0.0000000000
C2	1.3290811444	0.7189049086	0.0000000000
C3	0.0000000000	2.7624645029	0.0000000000
O1	2.3774333686	1.3890045378	0.0000000000
H1	0.9283698910	3.3027945771	0.0000000000

$$1Li_2$$

C1	0.0000000000	1.4597239578	0.0000000000
C2	1.2742728843	0.7151761290	0.0000000000
C3	0.0000000000	2.7914967525	0.0000000000
O1	2.3807832515	1.3209204289	0.0000000000
H1	0.9238015580	3.3360806323	0.0000000000
LI1	3.6287246543	0.0000000000	0.0000000000

Table A1. (con't)

1(BeF)$_2$

C1	0.0000000000	1.4901642007	0.0000000000
C2	1.2336313938	0.7101789596	0.0000000000
C3	0.0000000000	2.8248970023	0.0000000000
O1	2.3964403160	1.2217418445	0.0000000000
H1	0.9234001510	3.3714283097	0.0000000000
Be1	3.4379926304	0.0000000000	0.0000000000
F1	4.8294428556	0.0000000000	0.0000000000

1(AlF$_2$)$_2$

C1	0.0000000000	1.4805812799	0.0000000000
C2	1.2388160420	0.7105045043	0.0000000000
C3	0.0000000000	2.8162899820	0.0000000000
O1	2.3860103334	1.2615779183	0.0000000000
H1	0.9230116297	3.3627576016	0.0000000000
Al1	3.7308259694	0.0000000000	0.0000000000
F1	4.5714154155	0.0000000000	1.4030614736

F$_4$1Li$_2$

C1	0.0000000000	1.4616977906	0.0000000000
C2	1.2718860074	0.7159750349	0.0000000000
C3	0.0000000000	2.7969827473	0.0000000000
O1	2.3863526663	1.3014250648	0.0000000000
F1	1.0493539348	3.5470741672	0.0000000000
Li1	3.6509184484	0.0000000000	0.0000000000

(OH)$_4$1Li$_2$

C1	0.0000000000	1.4758668281	0.0000000000
C2	1.2593115219	0.7186689653	0.0000000000
C3	0.0000000000	2.8323695130	0.0000000000
O1	2.3876038265	1.2919942984	0.0000000000
O2	1.1241263076	3.5474867515	0.0000000000
H1	0.9601131859	4.4788542793	0.0000000000
Li1	3.6261648579	0.0000000000	0.0000000000

DMCB

C1	0.0000000000	1.0417794666	0.0000000000
C2	1.0277765938	0.0000000000	0.0000000000
C3	0.0000000000	2.3757180133	0.0000000000
H1	0.9178218164	2.9346318045	0.0000000000
H2	2.0986331928	0.0000000000	0.0000000000

Table A1.(con't)

$$^1A_g \text{ CAS}(2,3)$$

$$1^{2-}$$

C1	0.0000000000	1.4643995291	0.0000000000
C2	1.2878403067	0.7341861650	0.0000000000
C7	0.0000000000	2.8089987094	0.0000000000
O1	2.3511309375	1.3584657248	0.0000000000
H1	0.9266028675	3.3518775913	0.0000000000

$$1Li_2$$

C1	0.0000000000	1.4889560523	0.0000000000
C2	1.2581525153	0.7209446130	0.0000000000
C7	0.0000000000	2.8175192391	0.0000000000
O1	2.3663778658	1.3106334147	0.0000000000
H1	0.9231942774	3.3627989200	0.0000000000
Li1	3.6270196004	0.0000000000	0.0000000000

$$1(BeF)_2$$

C1	0.0000000000	1.5135429884	0.0000000000
C2	1.2276350128	0.7135499215	0.0000000000
C3	0.0000000000	2.8411787046	0.0000000000
O1	2.3883018786	1.2191883246	0.0000000000
H1	0.9228164723	3.3884466798	0.0000000000
Be1	3.4350293267	0.0000000000	0.0000000000
F1	4.8248598191	0.0000000000	0.0000000000

$$1(AlF_2)_2$$

C1	0.0000000000	1.4991686030	0.0000000000
C2	1.2370605882	0.7124864545	0.0000000000
C3	0.0000000000	2.8275648418	0.0000000000
O1	2.3824318708	1.2593374055	0.0000000000
H1	0.9226590394	3.3746701952	0.0000000000
Al1	3.7320189079	0.0000000000	0.0000000000
F1	4.5692581898	0.0000000000	1.4039421416

$$F_41Li_2$$

C1	0.0000000000	1.4757968938	0.0000000000
C2	1.2700650861	0.7170669492	0.0000000000
C3	0.0000000000	2.8053083922	0.0000000000
O1	2.3838247558	1.2988504922	0.0000000000
F1	1.0511862047	3.5576903021	0.0000000000
Li1	3.6542153381	0.0000000000	0.0000000000

Table A1. (con't)

(OH)$_4$1Li$_2$

C1	0.0000000000	1.4687524044	0.0000000000
C2	1.2694409284	0.7161244466	0.0000000000
C3	0.0000000000	2.8243162664	0.0000000000
O1	2.3966448634	1.2961760235	0.0000000000
O2	1.1211724752	3.5382952889	0.0000000000
H1	0.9584481125	4.4700511956	0.0000000000
Li1	3.6316457257	0.0000000000	0.0000000000

^1A_g CAS(6,6)

DMCB

C1	0.0000000000	1.0786299819	0.0000000000
C2	1.0169682221	0.0000000000	0.0000000000
C3	0.0000000000	2.4161951606	0.0000000000
H1	0.9185037520	2.9739018425	0.0000000000
H2	2.0901298564	0.0000000000	0.0000000000

$^3B_{3u}$ CAS(6,6)

DMCB

C1	0.0000000000	1.0365581099	0.0000000000
C2	1.0249892104	0.0000000000	0.0000000000
C3	0.0000000000	2.4014242740	0.0000000000
H1	0.9186615356	2.9580096342	0.0000000000
H2	2.0962395269	0.0000000000	0.0000000000

^1A_g CAS(14,12)

1^{2-}

C1	0.0000000000	1.4649397806	0.0000000000
C2	1.2655812247	0.7432509967	0.0000000000
C3	0.0000000000	2.8483407587	0.0000000000
O1	2.3490236649	1.3461741037	0.0000000000
H1	0.9248032859	3.3946503398	0.0000000000

1Li$_2$

C1	0.0000000000	1.4943237524	0.0000000000
C2	1.2428262829	0.7256283108	0.0000000000
C3	0.0000000000	2.8508866342	0.0000000000
O1	2.3558276543	1.3097708136	0.0000000000
H1	0.9224347453	3.3964855867	0.0000000000
Li1	3.6258226865	0.0000000000	0.0000000000

Table A1. (con't)

1(BeF)₂

C1	0.0000000000	1.5239991145	0.0000000000
C2	1.2148486562	0.7184371267	0.0000000000
C3	0.0000000000	2.8750002228	0.0000000000
O1	2.3755365600	1.2193241104	0.0000000000
H1	0.9226354584	3.4210357464	0.0000000000
Be1	3.4293865176	0.0000000000	0.0000000000
F1	4.8160595613	0.0000000000	0.0000000000

1(AlF₂)₂

C1	0.0000000000	1.5042538191	0.0000000000
C2	1.2310267488	0.7131461393	0.0000000000
C3	0.0000000000	2.8513074834	0.0000000000
O1	2.3755593767	1.2590872679	0.0000000000
H1	0.9226181803	3.3970304957	0.0000000000
Al1	3.7304268525	0.0000000000	0.0000000000
F1	4.5593640311	0.0000000000	1.4072213033

F₄1Li₂

C1	0.0000000000	1.4899949986	0.0000000000
C2	1.2568926215	0.7203755377	0.0000000000
C3	0.0000000000	2.8347572722	0.0000000000
O1	2.3724017689	1.2971269441	0.0000000000
F1	1.0629503359	3.5915778088	0.0000000000
Li1	3.6585160270	0.0000000000	0.0000000000

(OH)₄1Li₂

C1	0.0000000000	1.4984561995	0.0000000000
C2	1.2567600102	0.7205389868	0.0000000000
C3	0.0000000000	2.8549084322	0.0000000000
O1	2.3817774451	1.2906088981	0.0000000000
O2	1.1380228764	3.5821861824	0.0000000000
H1	0.9603504400	4.5100369316	0.0000000000
Li1	3.6408808276	0.0000000000	0.0000000000

³B₂ᵤ CAS(14,12)

1²⁻

C1	0.0000000000	1.4746877122	0.0000000000
C2	1.2482405271	0.7691125605	0.0000000000
C3	0.0000000000	2.9087307647	0.0000000000
O1	2.3466013428	1.3325818677	0.0000000000
H1	0.9244125411	3.4548530733	0.0000000000

Table A1. (con't)

$^3B_{3u}$ CAS(14,12)

1^{2-}

C1	0.0000000000	1.4323836535	0.0000000000
C2	1.3195140226	0.7177758626	0.0000000000
C3	0.0000000000	2.7888564213	0.0000000000
O1	2.3779492532	1.3869955945	0.0000000000
H1	0.9268519725	3.3321464548	0.0000000000

$1Li_2$

C1	0.0000000000	1.4579442578	0.0000000000
C2	1.2718134185	0.7156580354	0.0000000000
C3	0.0000000000	2.8145907821	0.0000000000
O1	2.3789577155	1.3231370418	0.0000000000
H1	0.9231985572	3.3591716132	0.0000000000
Li1	3.6324437579	0.0000000000	0.0000000000

$1(BeF)_2$

C1	0.0000000000	1.4885560369	0.0000000000
C2	1.2324534653	0.7114097219	0.0000000000
C3	0.0000000000	2.8466127037	0.0000000000
O1	2.3940258576	1.2231498958	0.0000000000
H1	0.9230525819	3.3920404412	0.0000000000
Be1	3.4403335535	0.0000000000	0.0000000000
F1	4.8295731263	0.0000000000	0.0000000000

$1(AlF_2)_2$

C1	0.0000000000	1.4771337693	0.0000000000
C2	1.2372669101	0.7101475026	0.0000000000
C3	0.0000000000	2.8349531143	0.0000000000
O1	2.3832384265	1.2614441489	0.0000000000
H1	0.9234086492	3.3791837973	0.0000000000
Al1	3.7327178583	0.0000000000	0.0000000000
F1	4.5683921087	0.0000000000	1.4046532163

F_41Li_2

C1	0.0000000000	1.4620300807	0.0000000000
C2	1.2717836859	0.7164236700	0.0000000000
C3	0.0000000000	2.8125790464	0.0000000000
O1	2.3854408253	1.3034674015	0.0000000000
F1	1.0587872686	3.5663395965	0.0000000000
Li1	3.6606005600	0.0000000000	0.0000000000

Table A1. (con't)

$(OH)_4 1Li_2$

C1	0.0000000000	1.4772347650	0.0000000000
C2	1.2607441152	0.7194356555	0.0000000000
C3	0.0000000000	2.8430876436	0.0000000000
O1	2.3865308166	1.2926178509	0.0000000000
O2	1.1352676445	3.5661355725	0.0000000000
H1	0.9612206034	4.4949824284	0.0000000000
Li1	3.6380894530	0.0000000000	0.0000000000

Table A2. CAS(2,2) Frequencies (cm^{-1}) of vibrations of 1^{2-} and its complexes in singlet (TCSCF) and triplet (ROHF) state. Starred values are translations and rotations of molecules

	1^{2-}		1Li$_2$		1(BeF)$_2$	
	TCSCF	ROHF	TCSCF	ROHF	TCSCF	ROHF
1	6.43*	4.82*	2.51*	4.48*	3.09*	2.03*
2	0.82*	0.40*	2.19*	0.15*	0.26*	0.78*
3	0.16*	0.05*	0.21*	0.09*	0.20*	0.26*
4	0.02*	0.05*	0.08*	0.04*	0.06*	0.10*
5	2.78*	3.82*	0.05*	0.51*	1.57*	0.10*
6	6.28*	4.44*	2.79*	1.96*	1.59*	2.33*
7	42.26	52.25	52.40	67.07	41.96	46.25
8	46.87	78.26	104.53	112.39	88.98	89.59
9	55.68	85.07	108.62	119.71	94.72	100.54
10	277.71	278.37	158.81	158.86	138.59	145.45
11	362.90	369.43	191.13	194.08	143.09	145.87
12	367.88	378.78	299.06	304.77	151.50	152.13
13	380.98	395.85	322.40	327.53	188.47	189.99
14	421.44	411.10	340.76	339.02	233.82	237.94
15	439.69	440.82	340.81	345.31	298.38	300.11
16	446.83	444.67	400.21	422.39	310.46	321.22
17	460.30	452.35	433.49	441.15	335.40	336.66
18	461.80	461.34	441.40	444.37	389.96	391.31
19	500.96	468.80	458.45	456.58	409.93	407.35
20	593.36	580.91	466.58	466.53	439.90	442.79
21	618.56	681.42	470.19	468.66	459.08	460.04
22	697.58	697.32	582.24	588.47	463.25	491.47
23	700.50	710.34	599.95	600.83	488.42	497.75
24	708.59	761.96	636.17	640.58	508.95	512.07
25	798.05	790.64	666.75	667.72	530.71	533.51
26	829.01	835.65	669.62	675.27	647.94	652.83
27	830.42	855.99	688.78	684.19	650.45	664.90
28	925.81	917.37	693.48	705.15	661.30	665.37
29	928.43	1010.11	700.74	709.72	670.99	666.33
30	928.55	1011.57	723.74	763.16	685.27	685.45
31	1092.17	1093.31	823.71	807.63	698.43	699.54
32	1115.72	1100.17	827.27	825.78	703.22	722.70
33	1275.82	1288.75	848.28	853.62	723.77	729.37
34	1327.07	1357.09	935.39	940.36	743.06	739.89
35	1356.99	1360.62	1090.21	1119.28	816.97	790.93
36	1431.00	1413.10	1091.39	1120.17	849.17	845.02
37	1456.77	1459.64	1126.27	1128.75	850.85	859.78
38	1489.36	1481.25	1172.49	1168.96	938.38	947.90
39	1517.07	1518.50	1295.84	1297.80	1143.37	1148.43

Table A2. (con't)

40	1598.01	1573.98	1379.84	1378.47	1150.34	1158.28
41	1756.61	1778.78	1411.33	1412.72	1151.20	1158.84
42	1766.32	1796.80	1476.30	1507.50	1205.15	1204.24
43	1803.43	1807.69	1551.07	1534.84	1304.90	1307.13
44	1811.44	1828.64	1575.00	1562.27	1351.86	1358.22
45	3338.61	3339.82	1596.42	1574.86	1360.81	1362.69
46	3339.21	3340.36	1628.47	1608.87	1368.94	1367.59
47	3421.64	3425.86	1745.89	1745.54	1458.96	1459.97
48	3421.70	3425.94	1767.19	1753.59	1537.35	1554.60
49			1847.72	1806.03	1563.02	1575.24
50			1847.98	1820.53	1607.11	1583.51
51			3372.05	3372.90	1633.68	1597.39
52			3372.33	3373.16	1641.06	1655.93
53			3465.65	3469.52	1737.82	1723.36
54			3465.67	3469.55	1741.85	1731.45
55					1848.96	1795.17
56					1865.34	1818.99
57					3370.24	3370.95
58					3370.61	3371.32
59					3468.92	3472.52
60					3468.94	3472.54

Table A2. (con't)

	1(AlF$_2$)$_2$		F$_4$1Li$_2$		(OH)$_4$1Li$_2$	
	TCSCF	ROHF	TCSCF	ROHF	TCSCF	ROHF
1	1.07*	4.57*	16.54(I)	2.93	426.44 (I)	458.17 (I)
2	0.57*	0.27*	0.31*	2.67*	425.39 (I)	457.12 (I)
3	0.10*	0.03*	0.21*	1.66*	18.76 (I)	23.12 (I)
4	0.05*	0.02*	0.26*	0.24*	2.28*	3.85*
5	1.18*	0.68*	0.87*	0.06*	1.97*	3.03*
6	1.76*	1.60*	2.72*	0.05*	1.82*	1.69*
7	31.11	32.64	3.54*	11.17*	0.17*	0.18*
8	62.95	62.74	71.28	75.20	0.12*	0.07*
9	73.76	73.93	94.30	93.12	2.00*	0.08*
10	81.64	87.80	108.91	106.49	70.77	66.95
11	89.78	91.99	136.15	132.41	86.79	85.39
12	144.33	145.12	140.12	142.02	87.78	87.89
13	176.80	180.09	179.98	181.57	118.47	113.08
14	195.35	196.92	205.06	205.49	146.62	145.35
15	197.61	198.19	223.3	225.41	202.99	201.08
16	198.17	200.39	271.53	276.57	203.73	202.04
17	210.67	210.79	284.62	298.09	251.05	241.24
18	221.67	222.37	312.7	314.61	271.84	241.36
19	279.59	280.99	345.54	349.91	296.75	249.45
20	310.20	313.20	384.96	385.12	300.87	277.87
21	315.84	317.12	422.08	421.90	309.44	318.24
22	326.64	320.91	431.83	432.66	325.79	328.75
23	349.34	351.61	451.64	456.91	358.5	344.34
24	350.57	357.35	489.31	494.25	386.77	385.81
25	437.58	440.53	502.88	503.05	418.18	418.17
26	449.35	456.25	505.59	506.39	437.5	440.14
27	452.56	462.43	508.16	526.06	458.01	457.25
28	461.93	483.68	562.95	566.01	476.68	502.44
29	477.77	485.18	603.00	609.65	513.34	514.11
30	510.15	522.15	638.99	640.78	523.32	521.04
31	601.51	605.98	672.73	679.24	525.11	531.13
32	638.70	639.02	677.05	684.14	574.93	567.31
33	664.40	662.37	685.00	689.22	646.91	648.97
34	666.36	667.27	704.51	710.93	680.67	676.34
35	667.24	668.46	717.91	716.36	707.48	694.99
36	699.83	702.56	721.70	722.84	709.93	708.63
37	725.88	727.59	735.61	733.69	728.95	711.18
38	735.73	741.64	743.34	752.95	734.32	731.57
39	810.96	785.63	932.53	934.50	735.73	742.16
40	834.53	838.43	1018.21	1017.98	768.00	748.51
41	846.99	840.32	1110.47	1110.26	797.56	761.46

162

Table A2. (con't)

42	855.50	855.61	1164.59	1170.8	803.60	762.51
43	870.91	874.46	1309.66	1323.72	932.01	934.28
44	948.29	957.42	1338.43	1327.53	1005.23	995.38
45	992.70	990.26	1466.27	1474.49	1086.42	1077.35
46	993.62	991.18	1468.82	1480.92	1156.81	1163.72
47	1134.14	1140.90	1500.24	1515.58	1246.02	1240.94
48	1166.53	1166.18	1529.38	1522.13	1256.55	1250.40
49	1167.23	1166.77	1619.56	1590.14	1257.33	1255.55
50	1193.54	1195.40	1626.69	1643.96	1280.71	1306.04
51	1302.96	1305.49	1730.30	1737.38	1338.60	1376.41
52	1341.74	1356.46	1762.55	1756.83	1452.01	1454.03
53	1449.70	1449.57	1865.74	1832.65	1472.78	1478.12
54	1531.43	1554.92	1907.97	1873.65	1488.24	1485.29
55	1560.03	1565.95			1512.27	1524.64
56	1600.11	1570.07			1528.31	1536.21
57	1628.82	1589.29			1586.77	1575.44
58	1630.81	1654.63			1636.86	1649.01
59	1728.07	1718.30			1683.99	1715.31
60	1740.28	1729.86			1717.78	1721.63
61	1838.73	1789.61			1807.74	1816.76
62	1862.87	1819.13			1851.47	1857.21
63	3374.71	3376.09			4114.97	4118.13
64	3374.98	3376.50			4115.02	4118.27
65	3473.93	3478.43			4132.66	4135.12
66	3473.93	3478.48			4132.95	4137.31

APPENDIX B

Table B1.   Crystal data for **2**.

Identification code	**2**
Empirical formula	$C_{32} H_{20} O_4$
Formula weight	468.48
Temperature	173(2) K
Wavelength	0.71073 Å
Crystal system	Monoclinic
Space group	$P2_1/n$ (#14)
Unit cell dimensions	a = 13.8607(14) Å
	b = 4.6091(5) Å
	c = 19.121(2) Å
	alpha = 90 deg.
	beta = 109.922(2) deg.
	gamma = 90 deg.
Volume	1148.4(2) A^3
Z	2
Density (calculated)	1.355 Mg/m^3
Absorption coefficient	0.089 mm^{-1}
F(000)	488
Crystal size	0.315 x 0.180 x 0.075 mm
Theta range for data collection	1.59 to 25.00 deg.
Index ranges	$-16 \leq h \leq 18$, $-6 \leq k \leq 6$, $-24 \leq l \leq 16$
Reflections collected	5359
Independent reflections	2014 [R(int) = 0.0493]
Refinement method	Full-matrix least-squares on F^2
Data / restraints / parameters	2014 / 0 / 204
Goodness-of-fit on F^2	1.046
Final R indices [I>2sigma(I)]	R_1 = 0.0493, wR_2 = 0.0952
R indices (all data)	R_1 = 0.0858, wR_2 = 0.1077
Extinction coefficient	0.020(3)
Largest diff. peak and hole	0.184 and -0.146 $e.A^{-3}$

164

Table B2. Atomic coordinates (x 10^4) and equivalent isotropic displacement parameters (Å^2 x 10^3) for **2**. U(eq) is defined as one third of the trace of the orthogonalized Uij tensor.

	x	y	z	U(eq)
O(1)	824(1)	9390(3)	892(1)	36(1)
C(1)	550(2)	7129(5)	543(1)	26(1)
O(2)	-538(1)	5945(3)	1213(1)	40(1)
C(2)	-380(2)	5559(5)	635(1)	26(1)
C(3)	-1041(2)	3955(4)	-22(1)	24(1)
C(4)	-2090(2)	3670(4)	-177(1)	24(1)
C(5)	-2803(1)	3551(4)	-955(1)	24(1)
C(6)	-3691(2)	1844(5)	-1149(1)	28(1)
C(7)	-4372(2)	1820(5)	-1873(1)	37(1)
C(8)	-4198(2)	3546(5)	-2406(1)	35(1)
C(9)	-3334(2)	5268(5)	-2220(1)	32(1)
C(10)	-2637(2)	5272(5)	-1504(1)	27(1)
C(11)	-2553(2)	3676(5)	411(1)	28(1)
C(12)	-2143(2)	1959(5)	1044(1)	40(1)
C(13)	-2638(3)	1861(7)	1569(2)	58(1)
C(14)	-3505(2)	3487(8)	1476(2)	60(1)
C(15)	-3908(2)	5186(7)	861(2)	51(1)
C(16)	-3449(2)	5251(6)	331(1)	37(1)

Table B3. Bond lengths [Å] and angles [deg] for **2**.

O(1)-C(1)	1.226(2)
C(1)-C(3)#1	1.471(3)
C(1)-C(2)	1.540(3)
O(2)-C(2)	1.213(2)
C(2)-C(3)	1.476(3)
C(3)-C(4)	1.388(3)
C(3)-C(1)#1	1.471(3)
C(4)-C(11)	1.473(3)
C(4)-C(5)	1.480(3)
C(5)-C(10)	1.396(3)
C(5)-C(6)	1.400(3)
C(6)-C(7)	1.384(3)
C(6)-H(6)	1.00(2)
C(7)-C(8)	1.378(3)
C(7)-H(7)	0.98(2)
C(8)-C(9)	1.378(3)
C(8)-H(8)	1.00(2)
C(9)-C(10)	1.380(3)
C(9)-H(9)	1.01(2)
C(10)-H(10)	1.00(2)
C(11)-C(12)	1.395(3)
C(11)-C(16)	1.401(3)
C(12)-C(13)	1.397(4)
C(12)-H(12)	1.00(2)
C(13)-C(14)	1.375(4)
C(13)-H(13)	0.93(3)
C(14)-C(15)	1.365(4)
C(14)-H(14)	1.03(3)
C(15)-C(16)	1.368(3)
C(15)-H(15)	1.08(3)
C(16)-H(16)	0.96(2)
O(1)-C(1)-C(3)#1	121.9(2)
O(1)-C(1)-C(2)	116.9(2)
C(3)#1-C(1)-C(2)	121.0(2)
O(2)-C(2)-C(3)	126.7(2)
O(2)-C(2)-C(1)	117.0(2)
C(3)-C(2)-C(1)	116.1(2)
C(4)-C(3)-C(1)#1	121.0(2)
C(4)-C(3)-C(2)	122.0(2)
C(1)#1-C(3)-C(2)	116.7(2)
C(3)-C(4)-C(11)	122.3(2)
C(3)-C(4)-C(5)	120.7(2)

Table B3.(con't)

C(11)-C(4)-C(5)	116.9(2)
C(10)-C(5)-C(6)	118.4(2)
C(10)-C(5)-C(4)	120.7(2)
C(6)-C(5)-C(4)	120.9(2)
C(7)-C(6)-C(5)	120.5(2)
C(7)-C(6)-H(6)	119.2(13)
C(5)-C(6)-H(6)	120.3(13)
C(8)-C(7)-C(6)	120.3(2)
C(8)-C(7)-H(7)	120.0(14)
C(6)-C(7)-H(7)	119.7(14)
C(9)-C(8)-C(7)	119.8(2)
C(9)-C(8)-H(8)	120.8(12)
C(7)-C(8)-H(8)	119.5(12)
C(8)-C(9)-C(10)	120.7(2)
C(8)-C(9)-H(9)	121.4(13)
C(10)-C(9)-H(9)	117.9(13)
C(9)-C(10)-C(5)	120.4(2)
C(9)-C(10)-H(10)	119.7(12)
C(5)-C(10)-H(10)	119.9(12)
C(12)-C(11)-C(16)	118.2(2)
C(12)-C(11)-C(4)	120.4(2)
C(16)-C(11)-C(4)	121.2(2)
C(11)-C(12)-C(13)	119.2(3)
C(11)-C(12)-H(12)	117.3(13)
C(13)-C(12)-H(12)	123.5(13)
C(14)-C(13)-C(12)	120.7(3)
C(14)-C(13)-H(13)	128(2)
C(12)-C(13)-H(13)	112(2)
C(15)-C(14)-C(13)	120.5(3)
C(15)-C(14)-H(14)	118(2)
C(13)-C(14)-H(14)	122(2)
C(14)-C(15)-C(16)	119.6(3)
C(14)-C(15)-H(15)	117(2)
C(16)-C(15)-H(15)	123(2)
C(15)-C(16)-C(11)	121.8(3)
C(15)-C(16)-H(16)	123.5(13)
C(11)-C(16)-H(16)	114.7(13)

Symmetry transformations used to generate equivalent atoms: #1 −x,−y+1,−z.

Table B4. Anisotropic displacement parameters (Å^2 x 10^3) for **2**. The anisotropic displacement factor exponent takes the form:
$-2\pi^2[h^2a^{*2}U_{11}+...+2hka^*b^*U_{12}]$

	U_{11}	U_{22}	U_{33}	U_{23}	U_{13}	U_{12}
O(1)	33(1)	31(1)	38(1)	-13(1)	7(1)	-1(1)
C(1)	22(1)	27(1)	24(1)	-2(1)	-1(1)	4(1)
O(2)	36(1)	52(1)	33(1)	-15(1)	12(1)	-7(1)
C(2)	23(1)	26(1)	27(1)	-4(1)	4(1)	7(1)
C(3)	23(1)	22(1)	24(1)	0(1)	5(1)	3(1)
C(4)	27(1)	17(1)	27(1)	0(1)	7(1)	1(1)
C(5)	21(1)	22(1)	26(1)	-1(1)	5(1)	1(1)
C(6)	26(1)	27(1)	33(1)	1(1)	10(1)	-4(1)
C(7)	27(1)	39(2)	39(2)	-8(1)	4(1)	-9(1)
C(8)	31(1)	37(1)	29(1)	-3(1)	2(1)	2(1)
C(9)	33(1)	36(1)	26(1)	3(1)	9(1)	1(1)
C(10)	24(1)	28(1)	29(1)	0(1)	8(1)	-2(1)
C(11)	29(1)	28(1)	25(1)	-2(1)	6(1)	-7(1)
C(12)	45(2)	38(2)	30(1)	1(1)	4(1)	-11(1)
C(13)	80(2)	61(2)	26(2)	6(1)	9(2)	-29(2)
C(14)	56(2)	86(2)	45(2)	-24(2)	28(2)	-37(2)
C(15)	46(2)	68(2)	44(2)	-20(2)	22(2)	-17(2)
C(16)	32(1)	43(2)	38(2)	-5(1)	14(1)	-4(1)

Table B5. Hydrogen coordinates (x 10^4) and isotropic displacement parameters (Å^2 x 10^3) for **2**.

	X	y	z	U(eq)
H(6)	-3836(16)	598(49)	-766(12)	40(6)
H(7)	-4980(18)	580(51)	-2004(13)	48(7)
H(8)	-4701(15)	3539(45)	-2923(12)	35(6)
H(9)	-3178(17)	6506(52)	-2602(13)	52(7)
H(10)	-2016(15)	6553(45)	-1376(11)	32(6)
H(12)	-1520(16)	798(50)	1084(12)	41(7)
H(13)	-2326(20)	558(60)	1948(15)	60(8)
H(14)	-3883(20)	3428(61)	1856(15)	73(9)
H(15)	-4589(22)	6417(64)	817(15)	88(10)
H(16)	-3715(16)	6330(49)	-125(13)	44(7)

Table B6.   Crystal data for $(NMe_2)_42 \cdot ((CH_3)_2SO)_3$.

Identification code	$(NMe_2)_42$
Empirical formula	$C_{46}H_{58}N_4O_7S_3$
Formula weight	875.16
Temperature	293(2) K
Wavelength	0.71073 A
Crystal system	Monoclinic
Space group	$P2_1/n$ (#14)
Unit cell dimensions	a = 21.092(4) Å
	b = 8.0588(16) Å
	c = 26.781(5) Å
	alpha = 90 deg.
	Beta = 101.31(3) deg.
	Gamma = 90 deg.
Volume	4463.7(15) Å^3
Z	4
Density (calculated)	1.302 Mg/m^3
Absorption coefficient	0.176 mm^{-1}
F(000)	1840
Crystal size	
Theta range for data collection	1.37 to 28.30 deg.
Limiting indices	$-26 \leq h \leq 27$, $-9 \leq k \leq 10$, $-34 \leq l \leq 35$
Reflections collected	37199
Independent reflections	10489 [R(int) = 0.1328]
Refinement method	Full-matrix least-squares on F^2
Data / restraints / parameters	10489 / 0 / 541
Goodness-of-fit on F^2	0.856
Final R indices [I>2sigma(I)]	R_1 = 0.0690, wR_2 = 0.1743
R indices (all data)	R_1 = 0.1556, wR_2 = 0.1968
Extinction coefficient	0.020(3)
Largest diff. Peak and hole	1.468 and –0.627 e.A^{-3}

Table B7. Atomic coordinates (x 10^4) and equivalent isotropic displacement parameter ($Å^2$ x 10^3) for (NMe$_2$)$_4$2·((CH$_3$)$_2$SO)$_3$. U(eq) is defined as one third of the trace of the orthogonalized Uij tensor.

	X	y	z	U(eq)
C(1)	5350(1)	3157(4)	2109(1)	21(1)
C(2)	4824(1)	1962(4)	2056(1)	20(1)
C(3)	4304(2)	2133(4)	2394(1)	22(1)
C(4)	4484(1)	2954(4)	2890(1)	20(1)
C(5)	5085(2)	3944(4)	2985(1)	24(1)
C(6)	5424(2)	4313(4)	2536(1)	22(1)
O(7)	4753(1)	772(3)	1757(1)	30(1)
O(8)	3787(1)	1406(3)	2236(1)	35(1)
O(9)	5315(1)	4632(4)	3390(1)	44(1)
O(10)	5753(1)	5590(3)	2571(1)	37(1)
C(11)	5781(1)	3216(4)	1754(1)	21(1)
C(12)	5541(1)	2915(4)	1210(1)	22(1)
C(13)	4912(1)	3410(4)	967(1)	24(1)
C(14)	4691(2)	3236(4)	456(1)	27(1)
C(15)	5083(2)	2486(4)	136(1)	24(1)
C(16)	5705(2)	1905(4)	380(1)	24(1)
C(17)	5921(2)	2119(4)	897(1)	24(1)
N(18)	4869(1)	2305(4)	-373(1)	31(1)
C(19)	4218(2)	2851(5)	-617(1)	39(1)
C(20)	5285(2)	1619(6)	-699(1)	44(1)
C(21)	6465(1)	3566(4)	1924(1)	22(1)
C(22)	6798(2)	3140(4)	2422(1)	26(1)
C(23)	7454(2)	3330(4)	2574(1)	26(1)
C(24)	7838(2)	3992(4)	2243(1)	26(1)
C(25)	7507(2)	4514(4)	1748(1)	25(1)
C(26)	6854(2)	4304(4)	1606(1)	24(1)
N(27)	8493(1)	4118(4)	2390(1)	29(1)
C(28)	8809(2)	3777(5)	2922(1)	35(1)
C(29)	8930(2)	4434(5)	2028(1)	38(1)
C(30)	4098(2)	2796(4)	3270(1)	22(1)
C(31)	3395(2)	2708(4)	3145(1)	22(1)
C(32)	3031(2)	1809(4)	3448(1)	23(1)
C(33)	2364(2)	1701(4)	3334(1)	24(1)
C(34)	2007(2)	2542(4)	2899(1)	26(1)
C(35)	2363(2)	3483(4)	2602(1)	28(1)
C(36)	3029(2)	3543(4)	2721(1)	24(1)
N(37)	1348(1)	2383(4)	2772(1)	34(1)
C(38)	975(2)	1690(5)	3121(2)	45(1)
C(39)	993(2)	2874(5)	2261(2)	51(1)

170

Table B7. (con't)

C(40)	4406(1)	2694(4)	3814(1)	22(1)
C(41)	5002(2)	1840(4)	3981(1)	24(1)
C(42)	5279(2)	1686(4)	4485(1)	25(1)
C(43)	4988(2)	2408(4)	4875(1)	25(1)
C(44)	4397(2)	3295(4)	4707(1)	28(1)
C(45)	4120(2)	3399(4)	4196(1)	25(1)
N(46)	5251(1)	2259(4)	5376(1)	29(1)
C(47)	5892(2)	1509(5)	5541(1)	38(1)
C(48)	4911(2)	2850(5)	5770(1)	37(1)
S(49)	2730(1)	2157(2)	811(1)	54(1)
O(50)	3080(2)	3827(4)	865(1)	73(1)
C(51)	2462(2)	1793(6)	1387(2)	57(1)
C(52)	3348(2)	628(6)	892(2)	60(1)
S(53)	2099(1)	5416(1)	-153(1)	47(1)
O(54)	1654(1)	6036(4)	-625(1)	66(1)
C(55)	2379(2)	7159(6)	234(2)	59(1)
C(56)	2853(2)	4991(6)	-328(2)	47(1)
S(57)	2273(1)	871(2)	-965(1)	55(1)
O(58)	2863(1)	246(5)	-590(1)	78(1)
C(59)	2006(2)	-773(5)	-1401(2)	50(1)
C(60)	1620(2)	770(6)	-639(2)	56(1)

Table B8.   Bond lengths [Å] and angles [deg] for (NMe₂)₄2·((CH₃)₂SO)₃.

C(1)-C(11)	1.440(4)
C(1)-C(2)	1.455(4)
C(1)-C(6)	1.459(4)
C(2)-O(7)	1.240(4)
C(2)-C(3)	1.559(4)
C(3)-O(8)	1.237(4)
C(3)-C(4)	1.464(4)
C(4)-C(30)	1.429(4)
C(4)-C(5)	1.477(4)
C(5)-O(9)	1.231(4)
C(5)-C(6)	1.545(5)
C(6)-O(10)	1.234(4)
C(11)-C(21)	1.453(4)
C(11)-C(12)	1.464(4)
C(12)-C(13)	1.415(4)
C(12)-C(17)	1.422(4)
C(13)-C(14)	1.363(4)
C(14)-C(15)	1.437(5)
C(15)-N(18)	1.357(4)
C(15)-C(16)	1.426(4)
C(16)-C(17)	1.383(4)
N(18)-C(20)	1.462(4)
N(18)-C(19)	1.466(4)
C(21)-C(22)	1.421(4)
C(21)-C(26)	1.422(4)
C(22)-C(23)	1.373(4)
C(23)-C(24)	1.416(5)
C(24)-N(27)	1.364(4)
C(24)-C(25)	1.436(4)
C(25)-C(26)	1.364(4)
N(27)-C(28)	1.476(4)
N(27)-C(29)	1.484(4)
C(30)-C(31)	1.458(4)
C(30)-C(40)	1.475(4)
C(31)-C(36)	1.412(4)
C(31)-C(32)	1.419(4)
C(32)-C(33)	1.382(4)
C(33)-C(34)	1.428(4)
C(34)-N(37)	1.371(4)
C(34)-C(35)	1.416(5)
C(35)-C(36)	1.378(4)
N(37)-C(38)	1.447(5)
N(37)-C(39)	1.479(5)

Table B8. (con't)

C(40)-C(45)	1.404(4)
C(40)-C(41)	1.427(4)
C(41)-C(42)	1.367(4)
C(42)-C(43)	1.434(5)
C(43)-N(46)	1.353(4)
C(43)-C(44)	1.431(4)
C(44)-C(45)	1.383(4)
N(46)-C(48)	1.466(4)
N(46)-C(47)	1.468(4)
S(49)-O(50)	1.527(3)
S(49)-C(51)	1.769(4)
S(49)-C(52)	1.774(4)
S(53)-O(54)	1.505(3)
S(53)-C(56)	1.776(4)
S(53)-C(55)	1.776(5)
S(57)-O(58)	1.524(3)
S(57)-C(60)	1.773(4)
S(57)-C(59)	1.781(4)
C(11)-C(1)-C(2)	121.7(3)
C(11)-C(1)-C(6)	120.8(3)
C(2)-C(1)-C(6)	117.4(3)
O(7)-C(2)-C(1)	124.6(3)
O(7)-C(2)-C(3)	115.8(3)
C(1)-C(2)-C(3)	119.7(3)
O(8)-C(3)-C(4)	125.4(3)
O(8)-C(3)-C(2)	115.6(3)
C(4)-C(3)-C(2)	118.6(3)
C(30)-C(4)-C(3)	121.6(3)
C(30)-C(4)-C(5)	120.9(3)
C(3)-C(4)-C(5)	117.5(3)
O(9)-C(5)-C(4)	125.0(3)
O(9)-C(5)-C(6)	115.9(3)
C(4)-C(5)-C(6)	118.9(3)
O(10)-C(6)-C(1)	124.4(3)
O(10)-C(6)-C(5)	116.1(3)
C(1)-C(6)-C(5)	119.5(3)
C(1)-C(11)-C(21)	121.1(3)
C(1)-C(11)-C(12)	120.7(3)
C(21)-C(11)-C(12)	118.2(3)
C(13)-C(12)-C(17)	116.3(3)
C(13)-C(12)-C(11)	121.4(3)
C(17)-C(12)-C(11)	122.3(3)
C(14)-C(13)-C(12)	122.5(3)

Table B8. (con't)

C(13)-C(14)-C(15)	121.3(3)
N(18)-C(15)-C(16)	121.3(3)
N(18)-C(15)-C(14)	121.9(3)
C(16)-C(15)-C(14)	116.8(3)
C(17)-C(16)-C(15)	120.8(3)
C(16)-C(17)-C(12)	122.3(3)
C(15)-N(18)-C(20)	121.3(3)
C(15)-N(18)-C(19)	120.8(3)
C(20)-N(18)-C(19)	117.8(3)
C(22)-C(21)-C(26)	115.2(3)
C(22)-C(21)-C(11)	121.6(3)
C(26)-C(21)-C(11)	123.2(3)
C(23)-C(22)-C(21)	122.3(3)
C(22)-C(23)-C(24)	121.5(3)
N(27)-C(24)-C(23)	121.3(3)
N(27)-C(24)-C(25)	121.7(3)
C(23)-C(24)-C(25)	117.1(3)
C(26)-C(25)-C(24)	120.1(3)
C(25)-C(26)-C(21)	123.7(3)
C(24)-N(27)-C(28)	120.3(3)
C(24)-N(27)-C(29)	123.3(3)
C(28)-N(27)-C(29)	116.1(3)
C(4)-C(30)-C(31)	122.4(3)
C(4)-C(30)-C(40)	120.5(3)
C(31)-C(30)-C(40)	117.0(3)
C(36)-C(31)-C(32)	115.5(3)
C(36)-C(31)-C(30)	122.2(3)
C(32)-C(31)-C(30)	122.3(3)
C(33)-C(32)-C(31)	123.1(3)
C(32)-C(33)-C(34)	120.1(3)
N(37)-C(34)-C(35)	122.3(3)
N(37)-C(34)-C(33)	120.3(3)
C(35)-C(34)-C(33)	117.3(3)
C(36)-C(35)-C(34)	121.1(3)
C(35)-C(36)-C(31)	122.7(3)
C(34)-N(37)-C(38)	121.9(3)
C(34)-N(37)-C(39)	120.6(3)
C(38)-N(37)-C(39)	117.5(3)
C(45)-C(40)-C(41)	116.4(3)
C(45)-C(40)-C(30)	121.9(3)
C(41)-C(40)-C(30)	121.7(3)
C(42)-C(41)-C(40)	122.1(3)
C(41)-C(42)-C(43)	121.5(3)
N(46)-C(43)-C(44)	121.2(3)

Table B8. (con't)

N(46)-C(43)-C(42)	122.4(3)
C(44)-C(43)-C(42)	116.4(3)
C(45)-C(44)-C(43)	120.9(3)
C(44)-C(45)-C(40)	122.6(3)
C(43)-N(46)-C(48)	121.4(3)
C(43)-N(46)-C(47)	120.6(3)
C(48)-N(46)-C(47)	118.0(3)
O(50)-S(49)-C(51)	107.1(2)
O(50)-S(49)-C(52)	105.8(2)
C(51)-S(49)-C(52)	97.5(2)
O(54)-S(53)-C(56)	106.66(19)
O(54)-S(53)-C(55)	108.0(2)
C(56)-S(53)-C(55)	95.4(2)
O(58)-S(57)-C(60)	105.8(2)
O(58)-S(57)-C(59)	107.4(2)
C(60)-S(57)-C(59)	96.4(2)

Symmetry transformations used to generate equivalent atoms: #1 -x,-y+1,-z.

175

Table B9. Anisotropic displacement parameters ($\text{Å}^2 \times 10^3$) for $(NMe_2)_42 \cdot ((CH_3)_2SO)_3$. The anisotropic displacement factor exponent takes the form: $-2\pi^2[h^2a^{*2}U_{11}+\ldots+2hka^*b^*U_{12}]$

	U_{11}	U_{22}	U_{33}	U_{23}	U_{13}	U_{12}
C(1)	19(2)	17(2)	26(2)	2(1)	3(1)	1(1)
C(2)	16(2)	19(2)	23(2)	2(1)	3(1)	3(1)
C(3)	21(2)	15(2)	30(2)	4(1)	4(1)	3(1)
C(4)	18(2)	19(2)	24(2)	1(1)	6(1)	1(1)
C(5)	23(2)	23(2)	27(2)	-2(2)	6(1)	0(2)
C(6)	21(2)	18(2)	26(2)	3(1)	2(1)	1(2)
O(7)	25(1)	27(2)	38(1)	-12(1)	7(1)	-4(1)
O(8)	24(1)	42(2)	40(1)	-12(1)	8(1)	-10(1)
O(9)	45(2)	56(2)	33(2)	-19(1)	14(1)	-27(1)
O(10)	50(2)	24(2)	42(2)	-10(1)	18(1)	-19(1)
C(11)	26(2)	12(2)	26(2)	2(1)	5(1)	1(1)
C(12)	24(2)	18(2)	24(2)	2(1)	7(1)	2(1)
C(13)	23(2)	25(2)	25(2)	1(2)	7(1)	5(2)
C(14)	24(2)	29(2)	30(2)	3(2)	5(1)	7(2)
C(15)	27(2)	18(2)	28(2)	-1(2)	6(1)	-3(2)
C(16)	27(2)	20(2)	29(2)	-4(2)	12(1)	1(2)
C(17)	21(2)	23(2)	27(2)	2(2)	5(1)	2(1)
N(18)	34(2)	32(2)	27(2)	-5(1)	5(1)	2(1)
C(19)	40(2)	45(3)	30(2)	-3(2)	1(2)	6(2)
C(20)	49(2)	55(3)	29(2)	-9(2)	10(2)	2(2)
C(21)	23(2)	17(2)	26(2)	2(1)	7(1)	-2(1)
C(22)	31(2)	19(2)	28(2)	3(2)	8(1)	-3(2)
C(23)	30(2)	21(2)	25(2)	2(2)	2(1)	1(2)
C(24)	28(2)	12(2)	37(2)	-6(2)	7(2)	-3(1)
C(25)	28(2)	21(2)	29(2)	-1(2)	11(1)	-4(2)
C(26)	29(2)	19(2)	24(2)	-1(2)	6(1)	1(2)
N(27)	21(2)	23(2)	42(2)	0(1)	4(1)	-4(1)
C(28)	28(2)	33(2)	41(2)	-6(2)	2(2)	-4(2)
C(29)	25(2)	32(2)	57(2)	-4(2)	8(2)	-4(2)
C(30)	27(2)	10(2)	29(2)	-2(1)	6(1)	1(1)
C(31)	26(2)	14(2)	25(2)	-2(1)	6(1)	-1(1)
C(32)	26(2)	20(2)	23(2)	2(2)	4(1)	-1(2)
C(33)	28(2)	19(2)	27(2)	-2(2)	9(1)	-4(2)
C(34)	22(2)	14(2)	43(2)	-6(2)	10(2)	0(1)
C(35)	26(2)	23(2)	33(2)	5(2)	3(1)	3(2)
C(36)	28(2)	15(2)	32(2)	7(2)	10(1)	-3(2)
N(37)	24(2)	32(2)	45(2)	1(2)	5(1)	-1(1)
C(38)	26(2)	51(3)	60(3)	-16(2)	17(2)	-12(2)
C(39)	31(2)	43(3)	70(3)	1(2)	-10(2)	2(2)

Table B9. (con't)

C(40)	23(2)	18(2)	26(2)	-2(1)	7(1)	-6(1)
C(41)	24(2)	23(2)	26(2)	-2(2)	7(1)	-1(2)
C(42)	19(2)	20(2)	37(2)	0(2)	6(1)	1(1)
C(43)	27(2)	19(2)	28(2)	-1(2)	5(1)	-7(2)
C(44)	30(2)	28(2)	28(2)	-5(2)	9(1)	-2(2)
C(45)	22(2)	19(2)	34(2)	-1(2)	8(1)	0(1)
N(46)	30(2)	30(2)	26(2)	-2(1)	2(1)	1(1)
C(47)	32(2)	46(3)	33(2)	-1(2)	0(2)	-3(2)
C(48)	40(2)	39(3)	31(2)	-6(2)	5(2)	-1(2)
S(49)	60(1)	52(1)	49(1)	2(1)	6(1)	17(1)
O(50)	113(3)	29(2)	82(2)	4(2)	34(2)	1(2)
C(51)	45(3)	74(4)	48(3)	9(2)	1(2)	3(2)
C(52)	40(2)	44(3)	95(4)	-9(3)	8(2)	10(2)
S(53)	35(1)	45(1)	64(1)	16(1)	18(1)	1(1)
O(54)	42(2)	68(2)	82(2)	14(2)	-4(2)	-2(2)
C(55)	70(3)	71(4)	37(2)	-3(2)	12(2)	27(3)
C(56)	45(2)	50(3)	49(3)	-4(2)	14(2)	1(2)
S(57)	58(1)	33(1)	80(1)	-11(1)	26(1)	-8(1)
O(58)	29(2)	92(3)	108(3)	-27(2)	1(2)	-1(2)
C(59)	67(3)	34(3)	47(2)	0(2)	8(2)	8(2)
C(60)	37(2)	62(3)	69(3)	-8(3)	10(2)	13(2)

Table B10. Hydrogen coordinates (x 10^4) and isotropic displacement parameters (Å^2 x 10^3) for $(NMe_2)_4\mathbf{2}\cdot((CH_3)_2SO)_3$.

	x	y	z	U(eq)
H(13)	4639	3871	1164	29
H(14)	4278	3610	313	33
H(16)	5969	1375	189	29
H(17)	6330	1729	1046	29
H(19A)	4150	2629	-976	59
H(19B)	4176	4020	-563	59
H(19C)	3903	2261	-472	59
H(20A)	5053	1588	-1045	66
H(20B)	5414	515	-589	66
H(20C)	5662	2304	-677	66
H(22)	6562	2718	2652	31
H(23)	7651	3017	2902	31
H(25)	7737	4996	1523	30
H(26)	6652	4663	1284	28
H(28A)	9267	3941	2960	53
H(28B)	8725	2650	3006	53
H(28C)	8641	4516	3145	53
H(29A)	9368	4496	2213	57
H(29B)	8813	5464	1854	57
H(29C)	8891	3547	1785	57
H(32)	3252	1268	3737	28
H(33)	2148	1080	3540	29
H(35)	2144	4070	2322	33
H(36)	3246	4160	2514	29
H(38A)	525	1682	2964	67
H(38B)	1037	2352	3425	67
H(38C)	1117	575	3207	67
H(39A)	539	2682	2238	76
H(39B)	1144	2227	2007	76
H(39C)	1065	4030	2206	76
H(41)	5210	1374	3739	29
H(42)	5664	1100	4577	30
H(44)	4196	3807	4946	33
H(45)	3730	3960	4100	30
H(47A)	6001	1500	5906	57
H(47B)	6207	2144	5409	57
H(47C)	5886	392	5416	57
H(48A)	5170	2634	6100	55
H(48B)	4505	2282	5737	55
H(48C)	4835	4022	5730	55

Table B10. (con't)

H(51A)	2114	2538	1411	85
H(51B)	2813	1976	1670	85
H(51C)	2314	669	1394	85
H(52A)	3559	650	605	90
H(52B)	3160	-447	917	90
H(52C)	3658	855	1198	90
H(55A)	2030	7606	375	88
H(55B)	2534	7990	31	88
H(55C)	2723	6822	505	88
H(56A)	2809	4043	-549	71
H(56B)	3172	4766	-27	71
H(56C)	2984	5934	-501	71
H(59A)	2308	-918	-1623	75
H(59B)	1588	-506	-1599	75
H(59C)	1979	-1780	-1215	75
H(60A)	1675	1600	-377	84
H(60B)	1609	-308	-489	84
H(60C)	1221	962	-875	84

Table B11. Crystal data for $(t\text{-Bu})_8(MeO)_42K\cdot(C_4H_8O)_4$.

Identification code	$(t\text{-Bu})_8(MeO)_42K$
Empirical formula	$C_{84}H_{124}O_{12}K$
Formula weight	1364.99
Temperature	293(2) K
Wavelength	0.71073 Å
Crystal system	triclinic
Space group	*P1*
Unit cell dimensions	a = 9.5055(2) Å
	b = 13.0026(2) Å
	c = 17.1668(2) Å
	alpha = 77.2809(11)
	beta = 85.5001(12)
	gamma = 77.6417(10)
Volume	2020.64(7) Å^3
Z	1
Density (calculated)	1.384 Mg/m^3
Absorption coefficient	0.182 mm^{-1}
F(000)	890
Crystal size	
Theta range for data collection	1.64 to 28.33 deg.
Index ranges	$-12 \leq h \leq 12$, $-17 \leq k \leq 17$, $-22 \leq l \leq 22$
Reflections collected	22327
Independent reflections	17415 [R(int) = 0.0182]
Refinement method	Full-matrix least-squares on F^2
Data / restraints / parameters	17415 / 3 / 874
Goodness-of-fit on F^2	0.91
Final R indices [I>2sigma(I)]	R1 = 0.0844, wR2 = 0.2430
R indices (all data)	R1 = 0.1437, wR2 = 0.3117
Extinction coefficient	
Largest diff. peak and hole	0.619 and -0.458 e.Å^{-3}

Table B12. Atomic coordinates (x 10^4) and equivalent isotropic displacement parameters (Å^2 x 10^3). U(eq) is defined as one third of the trace of the orthogonalized Uij tensor.

	x	y	z	U(eq)
K	5254(3)	6177(2)	1615(2)	90(1)
C(1)	10216(6)	6702(5)	754(3)	35(1)
C(2)	11564(6)	6144(5)	1102(4)	36(1)
C(3)	11601(6)	5616(5)	2003(4)	34(1)
C(4)	10281(6)	5637(4)	2486(3)	30(1)
C(5)	8924(7)	6213(5)	2111(3)	38(2)
C(6)	8876(6)	6729(4)	1244(3)	30(1)
C(7)	10347(6)	5098(5)	3287(3)	28(1)
C(8)	9434(6)	5561(4)	3913(3)	30(1)
C(9)	8922(7)	4898(5)	4593(3)	35(1)
C(10)	8153(7)	5320(5)	5202(4)	40(2)
C(11)	7954(7)	6432(6)	5162(4)	42(2)
C(12)	8256(7)	7131(5)	4442(4)	47(2)
C(13)	9067(7)	6655(5)	3850(4)	43(2)
C(14)	7503(10)	4557(7)	5918(4)	63(2)
C(15)	8125(16)	4616(10)	6699(5)	127(5)
C(16)	7576(14)	3474(7)	5695(6)	113(5)
C(17)	6103(15)	4926(8)	6190(9)	167(8)
O(18)	7305(5)	6861(4)	5799(3)	54(1)
C(19)	8277(13)	6963(12)	6330(7)	123(5)
C(20)	7810(10)	8365(6)	4296(6)	78(3)
C(21)	8090(12)	8914(6)	3481(7)	96(3)
C(22)	6336(14)	8709(8)	4587(9)	152(7)
C(23)	8830(30)	8797(9)	4833(11)	253(13)
O(24)	7753(4)	6251(5)	2474(3)	71(2)
O(25)	12752(5)	6133(4)	751(3)	62(2)
O(26)	7682(5)	7124(4)	958(3)	56(1)
O(27)	12816(4)	5298(4)	2269(2)	48(1)
C(28)	11262(6)	4030(4)	3531(3)	30(1)
C(29)	11494(6)	3306(4)	3012(3)	32(1)
C(30)	12181(7)	2218(5)	3245(4)	40(2)
C(31)	12421(10)	1502(6)	2614(4)	60(2)
C(32)	13919(11)	780(8)	2671(5)	100(4)
C(33)	12353(12)	2196(7)	1752(4)	92(3)
C(34)	11242(15)	831(9)	2700(6)	113(4)
C(35)	12630(7)	1890(5)	4025(4)	43(2)
O(36)	13178(8)	780(4)	4303(3)	81(2)
C(37)	11814(19)	233(8)	4658(7)	163(7)
C(38)	12550(7)	2573(4)	4560(4)	37(1)

Table B12. (con't)

C(39)	13198(9)	2246(5)	5372(4)	56(2)
C(40)	12193(19)	1863(17)	6004(5)	198(9)
C(41)	13305(13)	3217(7)	5717(5)	91(3)
C(42)	14858(15)	1566(12)	5323(8)	157(6)
C(43)	11857(6)	3657(5)	4286(3)	31(1)
C(44)	10181(6)	7270(4)	-68(3)	34(1)
C(45)	9270(6)	8360(4)	-299(3)	29(1)
C(46)	8675(7)	8724(5)	-1050(3)	36(1)
C(47)	7985(7)	9778(5)	-1312(4)	40(2)
C(48)	7960(8)	10510(4)	-812(4)	42(2)
C(49)	8357(7)	10127(5)	3(3)	36(1)
C(50)	9043(6)	9063(5)	207(3)	33(1)
C(51)	8096(8)	10844(5)	624(4)	50(2)
C(52)	8218(17)	10181(8)	1444(5)	108(4)
C(53)	6642(11)	11635(7)	537(6)	84(3)
C(54)	9308(12)	11524(10)	527(8)	119(5)
O(55)	7421(9)	11564(4)	-1090(3)	85(2)
C(56)	8304(15)	12198(9)	-1367(6)	109(4)
C(57)	7275(9)	10127(6)	-2158(4)	54(2)
C(58)	7031(15)	9186(7)	-2416(6)	120(5)
C(59)	5956(16)	10852(13)	-2153(7)	213(11)
C(60)	8098(16)	10865(7)	-2741(5)	120(4)
C(61)	11091(6)	6820(5)	-684(3)	36(1)
C(62)	11604(6)	7464(5)	-1352(3)	38(2)
C(63)	12349(6)	7052(5)	-1997(4)	36(1)
C(64)	12589(6)	5949(5)	-1924(4)	37(2)
C(65)	12197(7)	5238(5)	-1236(4)	42(2)
C(66)	11457(6)	5697(5)	-632(3)	38(2)
C(67)	12837(8)	7866(7)	-2700(4)	57(2)
C(68)	13012(11)	8858(7)	-2471(6)	89(3)
C(69)	14588(15)	7336(12)	-2810(11)	170(8)
C(70)	11657(14)	8301(12)	-3311(6)	172(8)
O(71)	13179(5)	5532(4)	-2589(3)	48(1)
C(72)	12198(12)	5410(10)	-3137(6)	99(4)
C(73)	12693(11)	4017(6)	-1095(6)	73(3)
C(74)	12840(20)	3576(8)	-186(7)	247(13)
C(75)	14291(14)	3660(11)	-1356(8)	146(6)
C(76)	11650(20)	3491(9)	-1300(19)	321(19)
O(101)	6346(7)	4093(6)	2396(7)	146(4)
C(102)	5680(13)	3330(9)	2507(11)	136(6)
C(103)	6535(14)	2380(9)	3084(8)	127(4)
C(104)	7692(14)	2666(14)	3347(12)	183(8)
C(105)	7570(20)	3769(13)	2848(18)	350(20)
O(201)	4078(11)	8310(9)	907(8)	166(5)

Table B12. (con't)

C(202)	5010(11)	9025(10)	514(14)	181(9)
C(203)	4330(20)	9490(30)	-98(15)	295(18)
C(204)	3014(18)	9432(13)	-175(7)	137(5)
C(205)	2756(9)	8765(11)	651(12)	174(8)
O(301)	4168(9)	6945(10)	3073(7)	151(4)
C(302)	2846(12)	7451(12)	3195(10)	144(6)
C(303)	2692(14)	7380(20)	4110(12)	223(12)
C(304)	3510(40)	6390(30)	4210(20)	380(20)
C(305)	4831(12)	6179(13)	3746(8)	131(5)
O(401)	6165(11)	5379(9)	65(7)	173(5)
C(402)	7779(19)	4930(20)	-300(16)	292(19)
C(403)	7720(19)	5557(15)	-1145(9)	164(6)
C(404)	6460(20)	6136(16)	-1232(12)	202(8)
C(405)	6020(60)	6120(20)	-519(15)	540(40)

Table B13. Bond lengths [Å] and angles [deg] for (t-Bu)$_8$(MeO)$_4$2K·(C$_4$H$_8$O)$_4$.

K-O(101)	2.763(8)
K-O(201)	2.796(10)
K-O(27)#1	2.845(5)
K-O(26)	2.884(5)
K-O(301)	2.929(10)
K-O(25)#1	2.917(6)
K-O(24)	2.922(6)
K-O(401)	3.061(12)
C(1)-C(2)	1.434(8)
C(1)-C(44)	1.440(8)
C(1)-C(6)	1.470(7)
C(2)-O(25)	1.236(7)
C(2)-C(3)	1.547(8)
C(3)-O(27)	1.228(7)
C(3)-C(4)	1.449(7)
C(4)-C(7)	1.398(8)
C(4)-C(5)	1.464(9)
C(5)-O(24)	1.229(7)
C(5)-C(6)	1.492(8)
C(6)-O(26)	1.233(7)
C(7)-C(28)	1.465(8)
C(7)-C(8)	1.477(7)
C(8)-C(13)	1.372(8)
C(8)-C(9)	1.411(8)
C(9)-C(10)	1.374(8)
C(10)-C(11)	1.405(9)
C(10)-C(14)	1.575(9)
C(11)-O(18)	1.380(7)
C(11)-C(12)	1.412(9)
C(12)-C(13)	1.401(9)
C(12)-C(20)	1.538(10)
C(14)-C(17)	1.396(13)
C(14)-C(15)	1.530(13)
C(14)-C(16)	1.525(11)
O(18)-C(19)	1.393(12)
C(20)-C(22)	1.461(13)
C(20)-C(21)	1.455(13)
C(20)-C(23)	1.645(18)
O(25)-K#2	2.917(6)
O(27)-K#2	2.845(5)
C(28)-C(43)	1.399(7)
C(28)-C(29)	1.407(8)
C(29)-C(30)	1.409(8)

Table B13. (con't)

C(30)-C(35)	1.384(9)
C(30)-C(31)	1.552(8)
C(31)-C(34)	1.541(13)
C(31)-C(33)	1.553(11)
C(31)-C(32)	1.526(11)
C(35)-C(38)	1.400(8)
C(35)-O(36)	1.412(8)
O(36)-C(37)	1.624(15)
C(38)-C(43)	1.414(8)
C(38)-C(39)	1.505(9)
C(39)-C(40)	1.463(14)
C(39)-C(41)	1.532(10)
C(39)-C(42)	1.641(14)
C(44)-C(61)	1.457(8)
C(44)-C(45)	1.482(7)
C(45)-C(50)	1.369(8)
C(45)-C(46)	1.391(8)
C(46)-C(47)	1.379(8)
C(47)-C(48)	1.410(9)
C(47)-C(57)	1.583(9)
C(48)-O(55)	1.348(7)
C(48)-C(49)	1.431(8)
C(49)-C(50)	1.378(8)
C(49)-C(51)	1.538(9)
C(51)-C(53)	1.532(12)
C(51)-C(52)	1.479(12)
C(51)-C(54)	1.574(12)
O(55)-C(56)	1.292(13)
C(57)-C(59)	1.399(12)
C(57)-C(58)	1.457(11)
C(57)-C(60)	1.520(13)
C(61)-C(62)	1.385(8)
C(61)-C(66)	1.410(8)
C(62)-C(63)	1.410(8)
C(63)-C(64)	1.382(8)
C(63)-C(67)	1.534(9)
C(64)-O(71)	1.400(7)
C(64)-C(65)	1.409(9)
C(65)-C(66)	1.380(8)
C(65)-C(73)	1.526(10)
C(67)-C(68)	1.472(12)
C(67)-C(70)	1.526(13)
C(67)-C(69)	1.673(15)
O(71)-C(72)	1.430(10)

Table B13. (con't)

C(73)-C(76)	1.426(18)
C(73)-C(75)	1.551(14)
C(73)-C(74)	1.546(16)
O(101)-C(102)	1.261(13)
O(101)-C(105)	1.383(14)
C(102)-C(103)	1.525(18)
C(103)-C(104)	1.370(17)
C(104)-C(105)	1.485(19)
O(201)-C(205)	1.333(14)
O(201)-C(202)	1.444(16)
C(202)-C(203)	1.24(3)
C(203)-C(204)	1.29(2)
C(204)-C(205)	1.523(19)
O(301)-C(302)	1.312(13)
O(301)-C(305)	1.436(15)
C(302)-C(303)	1.55(2)
C(302)-C(304)	2.02(4)
C(303)-C(304)	1.33(4)
C(304)-C(305)	1.44(3)
O(401)-C(405)	1.22(3)
O(401)-C(402)	1.65(2)
C(402)-C(403)	1.50(2)
C(403)-C(404)	1.27(2)
C(404)-C(405)	1.26(3)
O(101)-K-O(201)	176.7(5)
O(101)-K-O(27)#1	74.31(19)
O(201)-K-O(27)#1	104.1(3)
O(101)-K-O(26)	107.01(19)
O(201)-K-O(26)	74.6(2)
O(27)#1-K-O(26)	178.4(2)
O(101)-K-O(301)	95.0(4)
O(201)-K-O(301)	81.8(4)
O(27)#1-K-O(301)	69.71(18)
O(26)-K-O(301)	109.2(2)
O(101)-K-O(25)#1	107.6(2)
O(201)-K-O(25)#1	73.1(3)
O(27)#1-K-O(25)#1	53.45(13)
O(26)-K-O(25)#1	126.39(15)
O(301)-K-O(25)#1	107.1(2)
O(101)-K-O(24)	73.1(2)
O(201)-K-O(24)	106.1(3)
O(27)#1-K-O(24)	126.93(16)
O(26)-K-O(24)	53.21(14)

186

Table B13. (con't)

O(301)-K-O(24)	72.7(2)
O(25)#1-K-O(24)	179.3(2)
O(101)-K-O(401)	86.2(4)
O(201)-K-O(401)	97.0(4)
O(27)#1-K-O(401)	106.9(3)
O(26)-K-O(401)	74.1(3)
O(301)-K-O(401)	175.9(3)
O(25)#1-K-O(401)	68.8(2)
O(24)-K-O(401)	111.4(2)
C(2)-C(1)-C(44)	120.1(5)
C(2)-C(1)-C(6)	120.0(5)
C(44)-C(1)-C(6)	119.9(5)
O(25)-C(2)-C(1)	124.5(5)
O(25)-C(2)-C(3)	115.6(5)
C(1)-C(2)-C(3)	119.5(5)
O(27)-C(3)-C(4)	124.4(6)
O(27)-C(3)-C(2)	114.6(5)
C(4)-C(3)-C(2)	120.6(5)
C(7)-C(4)-C(3)	119.0(5)
C(7)-C(4)-C(5)	122.6(5)
C(3)-C(4)-C(5)	118.4(5)
O(24)-C(5)-C(4)	122.5(5)
O(24)-C(5)-C(6)	115.8(6)
C(4)-C(5)-C(6)	121.5(5)
O(26)-C(6)-C(1)	122.2(5)
O(26)-C(6)-C(5)	117.7(5)
C(1)-C(6)-C(5)	120.0(5)
C(4)-C(7)-C(28)	121.3(5)
C(4)-C(7)-C(8)	121.1(5)
C(28)-C(7)-C(8)	117.5(5)
C(13)-C(8)-C(9)	118.0(5)
C(13)-C(8)-C(7)	120.7(5)
C(9)-C(8)-C(7)	121.4(5)
C(10)-C(9)-C(8)	121.6(5)
C(9)-C(10)-C(11)	118.6(6)
C(9)-C(10)-C(14)	119.7(6)
C(11)-C(10)-C(14)	121.7(6)
C(10)-C(11)-O(18)	119.7(6)
C(10)-C(11)-C(12)	120.5(6)
O(18)-C(11)-C(12)	119.3(6)
C(13)-C(12)-C(11)	116.9(6)
C(13)-C(12)-C(20)	119.1(6)
C(11)-C(12)-C(20)	123.9(6)
C(8)-C(13)-C(12)	122.8(6)

Table B13. (con't)

C(17)-C(14)-C(15)	91.5(10)
C(17)-C(14)-C(16)	108.7(8)
C(15)-C(14)-C(16)	120.6(9)
C(17)-C(14)-C(10)	117.5(8)
C(15)-C(14)-C(10)	109.2(7)
C(16)-C(14)-C(10)	109.0(6)
C(11)-O(18)-C(19)	113.7(6)
C(22)-C(20)-C(21)	113.2(8)
C(22)-C(20)-C(12)	111.6(8)
C(21)-C(20)-C(12)	114.2(7)
C(22)-C(20)-C(23)	105.3(13)
C(21)-C(20)-C(23)	103.7(11)
C(12)-C(20)-C(23)	108.1(8)
C(5)-O(24)-K	118.3(5)
C(2)-O(25)-K#2	120.0(4)
C(6)-O(26)-K	119.0(4)
C(3)-O(27)-K#2	124.2(4)
C(43)-C(28)-C(29)	117.2(5)
C(43)-C(28)-C(7)	123.1(5)
C(29)-C(28)-C(7)	119.6(5)
C(28)-C(29)-C(30)	122.9(5)
C(35)-C(30)-C(29)	116.1(5)
C(35)-C(30)-C(31)	125.4(6)
C(29)-C(30)-C(31)	118.4(6)
C(34)-C(31)-C(33)	106.9(8)
C(34)-C(31)-C(30)	110.9(7)
C(33)-C(31)-C(30)	111.2(6)
C(34)-C(31)-C(32)	111.1(8)
C(33)-C(31)-C(32)	105.6(8)
C(30)-C(31)-C(32)	111.0(6)
C(30)-C(35)-C(38)	124.8(5)
C(30)-C(35)-O(36)	117.3(6)
C(38)-C(35)-O(36)	117.9(6)
C(35)-O(36)-C(37)	107.0(7)
C(35)-C(38)-C(43)	116.1(5)
C(35)-C(38)-C(39)	124.8(5)
C(43)-C(38)-C(39)	119.1(5)
C(40)-C(39)-C(38)	112.7(8)
C(40)-C(39)-C(41)	93.8(9)
C(38)-C(39)-C(41)	112.4(6)
C(40)-C(39)-C(42)	120.2(11)
C(38)-C(39)-C(42)	110.7(7)
C(41)-C(39)-C(42)	105.4(8)
C(28)-C(43)-C(38)	122.5(5)

Table B13. (con't)

C(1)-C(44)-C(61)	121.2(5)
C(1)-C(44)-C(45)	120.5(5)
C(61)-C(44)-C(45)	118.2(5)
C(50)-C(45)-C(46)	117.6(5)
C(50)-C(45)-C(44)	120.8(5)
C(46)-C(45)-C(44)	121.4(5)
C(47)-C(46)-C(45)	122.1(5)
C(46)-C(47)-C(48)	118.1(5)
C(46)-C(47)-C(57)	119.4(6)
C(48)-C(47)-C(57)	122.5(5)
O(55)-C(48)-C(47)	119.0(5)
O(55)-C(48)-C(49)	120.3(5)
C(47)-C(48)-C(49)	120.4(5)
C(50)-C(49)-C(48)	115.9(5)
C(50)-C(49)-C(51)	120.7(5)
C(48)-C(49)-C(51)	123.4(5)
C(45)-C(50)-C(49)	124.4(5)
C(53)-C(51)-C(52)	110.2(8)
C(53)-C(51)-C(49)	112.7(6)
C(52)-C(51)-C(49)	110.7(6)
C(53)-C(51)-C(54)	107.6(7)
C(52)-C(51)-C(54)	105.6(9)
C(49)-C(51)-C(54)	109.7(6)
C(56)-O(55)-C(48)	118.9(9)
C(59)-C(57)-C(58)	108.1(10)
C(59)-C(57)-C(60)	97.9(11)
C(58)-C(57)-C(60)	116.8(8)
C(59)-C(57)-C(47)	112.4(6)
C(58)-C(57)-C(47)	110.2(5)
C(60)-C(57)-C(47)	110.8(7)
C(62)-C(61)-C(66)	117.1(5)
C(62)-C(61)-C(44)	122.1(5)
C(66)-C(61)-C(44)	120.8(5)
C(61)-C(62)-C(63)	123.0(6)
C(64)-C(63)-C(62)	116.4(5)
C(64)-C(63)-C(67)	126.5(6)
C(62)-C(63)-C(67)	117.0(6)
O(71)-C(64)-C(63)	117.6(5)
O(71)-C(64)-C(65)	118.7(5)
C(63)-C(64)-C(65)	123.6(5)
C(66)-C(65)-C(64)	116.7(5)
C(66)-C(65)-C(73)	119.4(6)
C(64)-C(65)-C(73)	123.5(6)
C(65)-C(66)-C(61)	122.9(5)

189

Table B13. (con't)

C(68)-C(67)-C(63)	113.0(6)
C(68)-C(67)-C(70)	101.7(9)
C(63)-C(67)-C(70)	110.5(6)
C(68)-C(67)-C(69)	97.4(8)
C(63)-C(67)-C(69)	102.5(7)
C(70)-C(67)-C(69)	131.0(10)
C(64)-O(71)-C(72)	117.4(5)
C(65)-C(73)-C(76)	113.1(9)
C(65)-C(73)-C(75)	113.0(8)
C(76)-C(73)-C(75)	118.7(14)
C(65)-C(73)-C(74)	108.1(8)
C(76)-C(73)-C(74)	103.4(15)
C(75)-C(73)-C(74)	98.2(10)
C(102)-O(101)-C(105)	108.9(11)
C(102)-O(101)-K	124.6(7)
C(105)-O(101)-K	125.5(7)
O(101)-C(102)-C(103)	107.8(10)
C(104)-C(103)-C(102)	110.4(10)
C(103)-C(104)-C(105)	99.6(12)
O(101)-C(105)-C(104)	113.0(11)
C(205)-O(201)-C(202)	106.5(10)
C(205)-O(201)-K	130.6(9)
C(202)-O(201)-K	120.1(7)
O(201)-C(202)-C(203)	101.1(13)
C(204)-C(203)-C(202)	122(2)
C(203)-C(204)-C(205)	98.4(15)
O(201)-C(205)-C(204)	104.0(11)
C(302)-O(301)-C(305)	116.2(11)
C(302)-O(301)-K	125.1(9)
C(305)-O(301)-K	108.6(7)
O(301)-C(302)-C(303)	104.8(13)
O(301)-C(302)-C(304)	71.4(13)
C(303)-C(302)-C(304)	41.2(13)
C(304)-C(303)-C(302)	88.6(18)
C(303)-C(304)-C(305)	121(2)
C(303)-C(304)-C(302)	50.2(15)
C(305)-C(304)-C(302)	83.0(14)
O(301)-C(305)-C(304)	89.4(17)
C(405)-O(401)-C(402)	88(2)
C(405)-O(401)-K	111.8(13)
C(402)-O(401)-K	130.5(14)
C(403)-C(402)-O(401)	102.2(13)
C(404)-C(403)-C(402)	106.7(17)
C(403)-C(404)-C(405)	102(3)
O(401)-C(405)-C(404)	130(3)

Table B14. Anisotropic displacement parameters ($\mathring{A}^2$ x 10^3) for (t-Bu)$_8$(MeO)$_4$2K·(C$_4$H$_8$O)$_4$. The anisotropic displacement factor exponent takes the form: $-2\pi^2[h^2a^{*2}U_{11}+...+2hka^*b^*U_{12}]$

	U_{11}	U_{22}	U_{33}	U_{23}	U_{13}	U_{12}
K	29(1)	103(1)	109(1)	38(1)	-3(1)	-12(1)
C(1)	24(3)	34(3)	34(3)	11(2)	2(2)	5(2)
C(2)	21(3)	43(3)	33(3)	5(3)	6(2)	0(3)
C(3)	21(3)	35(3)	36(3)	5(2)	4(2)	2(2)
C(4)	28(3)	32(3)	27(3)	-3(2)	10(2)	-4(2)
C(5)	35(3)	44(4)	25(3)	7(2)	6(3)	0(3)
C(6)	27(3)	33(3)	22(3)	1(2)	5(2)	-1(2)
C(7)	21(3)	38(3)	22(3)	-4(2)	3(2)	-1(2)
C(8)	27(3)	26(3)	29(3)	-1(2)	7(2)	8(2)
C(9)	51(4)	28(3)	22(3)	2(2)	-1(3)	-8(3)
C(10)	42(4)	49(4)	25(3)	1(3)	0(3)	-12(3)
C(11)	38(3)	56(4)	29(3)	-9(3)	4(3)	-4(3)
C(12)	34(3)	40(4)	55(4)	-3(3)	14(3)	5(3)
C(13)	40(4)	33(3)	48(4)	0(3)	9(3)	-8(3)
C(14)	82(5)	81(5)	36(4)	-14(3)	27(3)	-45(4)
C(15)	198(13)	140(9)	38(4)	9(5)	-2(5)	-52(9)
C(16)	200(12)	68(6)	79(6)	-19(5)	90(7)	-74(7)
C(17)	165(11)	77(6)	260(15)	-68(8)	181(12)	-62(7)
O (18)	51(3)	62(3)	48(3)	-27(2)	9(2)	1(3)
C(19)	82(7)	203(15)	111(9)	-106(10)	0(7)	-17(8)
C(20)	86(7)	38(4)	85(6)	-4(4)	26(5)	20(4)
C(21)	118(6)	34(3)	121(7)	-12(4)	31(5)	-1(4)
C(22)	125(9)	68(6)	172(12)	54(7)	83(9)	66(6)
C(23)	490(30)	45(5)	238(16)	-32(7)	-240(20)	-10(10)
O(24)	20(2)	124(5)	39(3)	16(3)	10(2)	15(3)
O(25)	31(3)	92(4)	38(3)	24(2)	8(2)	1(2)
O(26)	25(2)	73(3)	49(3)	17(2)	0(2)	2(2)
O(27)	25(2)	72(3)	30(2)	12(2)	4(2)	2(2)
C(28)	31(3)	34(3)	21(3)	-1(2)	5(2)	-7(3)
C(29)	36(3)	31(3)	28(3)	-7(2)	-6(2)	-1(3)
C(30)	44(4)	31(3)	46(4)	-16(3)	-6(3)	-1(3)
C(31)	91(6)	47(4)	40(4)	-23(3)	-19(4)	9(4)
C(32)	110(7)	111(7)	67(5)	-63(5)	-23(5)	58(6)
C(33)	142(8)	74(5)	36(4)	-9(4)	-2(4)	31(5)
C(34)	186(13)	99(7)	84(7)	-25(5)	-19(7)	-86(8)
C(35)	49(4)	34(3)	39(4)	-3(3)	-12(3)	5(3)
O(36)	141(6)	36(3)	52(3)	-8(2)	-24(3)	23(3)
C(37)	340(20)	61(5)	108(8)	45(5)	-89(10)	-123(9)
C(38)	53(4)	28(3)	28(3)	-7(2)	-6(3)	-3(3)

191

Table B14. (con't)

C(39)	82(6)	37(4)	44(4)	-9(3)	-25(4)	11(4)
C(40)	231(15)	350(20)	26(4)	55(7)	-30(6)	-178(16)
C(41)	149(9)	61(5)	70(5)	-26(4)	-51(5)	-5(5)
C(42)	128(9)	172(12)	151(11)	-77(10)	-102(9)	91(9)
C(43)	30(3)	30(3)	25(3)	3(2)	-7(2)	4(2)
C(44)	32(3)	28(3)	32(3)	7(2)	7(3)	0(2)
C(45)	23(3)	25(3)	32(3)	3(2)	-1(2)	2(2)
C(46)	48(4)	29(3)	30(3)	-11(2)	2(3)	-6(3)
C(47)	43(4)	40(3)	30(3)	4(3)	-16(3)	4(3)
C(48)	69(4)	20(3)	35(3)	-1(2)	-17(3)	-2(3)
C(49)	45(4)	38(3)	23(3)	2(2)	-6(3)	-8(3)
C(50)	31(3)	43(3)	20(3)	6(2)	-1(2)	-9(3)
C(51)	64(5)	44(4)	44(4)	-10(3)	-11(3)	-8(3)
C(52)	219(14)	73(6)	43(5)	-37(4)	-2(6)	-30(7)
C(53)	91(7)	78(6)	84(6)	-29(5)	-9(5)	-7(5)
C(54)	98(7)	138(9)	166(11)	-115(9)	-6(7)	-37(7)
O(55)	172(7)	22(2)	50(3)	4(2)	-33(4)	2(3)
C(56)	185(11)	76(6)	69(6)	-2(5)	-21(6)	-39(7)
C(57)	83(6)	45(4)	28(3)	0(3)	-28(4)	3(4)
C(58)	206(12)	55(5)	104(7)	20(4)	-133(8)	-29(6)
C(59)	217(15)	269(16)	109(8)	-139(10)	-142(10)	199(14)
C(60)	242(13)	72(5)	56(5)	19(4)	-57(6)	-65(6)
C(61)	30(3)	43(3)	26(3)	8(3)	0(3)	-5(3)
C(62)	27(3)	45(4)	34(3)	-2(3)	13(3)	-1(3)
C(63)	29(3)	43(3)	33(3)	-4(3)	10(3)	-5(3)
C(64)	21(3)	46(4)	39(4)	-11(3)	9(3)	4(3)
C(65)	40(4)	36(3)	40(3)	-5(3)	3(3)	7(3)
C(66)	34(3)	35(3)	27(3)	10(2)	8(3)	8(3)
C(67)	56(4)	86(5)	26(3)	-2(3)	14(3)	-26(4)
C(68)	108(7)	50(5)	91(7)	1(5)	60(6)	-18(5)
C(69)	154(11)	131(11)	244(17)	-88(11)	158(12)	-79(9)
C(70)	172(11)	255(16)	71(6)	112(8)	-56(7)	-134(12)
O(71)	36(2)	62(3)	42(3)	-16(2)	12(2)	-1(2)
C(72)	77(7)	155(11)	83(7)	-81(7)	-11(6)	-4(7)
C(73)	77(6)	38(4)	87(7)	-4(4)	21(5)	8(4)
C(74)	420(30)	71(6)	107(8)	63(6)	146(12)	130(11)
C(75)	109(8)	144(10)	105(8)	21(7)	38(7)	86(8)
C(76)	232(18)	41(6)	700(50)	-44(14)	-230(30)	-14(8)
O(101)	52(4)	88(5)	286(12)	8(6)	-69(5)	-14(4)
C(102)	81(7)	79(7)	271(18)	-85(10)	-31(9)	-4(6)
C(103)	128(9)	103(7)	146(9)	7(6)	-52(7)	-33(6)
C(104)	79(7)	174(14)	270(20)	58(13)	-22(10)	-63(8)
C(105)	250(20)	129(11)	650(50)	160(20)	-350(30)	-108(13)
O(201)	94(7)	128(8)	241(13)	24(8)	-47(7)	5(6)

Table B14. (con't)

C(202)	44(5)	88(7)	390(30)	27(11)	-49(9)	-21(5)
C(203)	130(15)	560(60)	220(20)	-60(30)	55(15)	-180(30)
C(204)	165(13)	157(12)	105(8)	-57(9)	-40(8)	-20(10)
C(205)	37(4)	124(9)	310(20)	66(11)	-15(8)	-18(5)
O(301)	81(5)	230(11)	184(9)	-109(9)	42(6)	-75(7)
C(302)	69(6)	177(12)	214(14)	-123(12)	3(7)	-2(7)
C(303)	87(8)	410(30)	258(19)	-280(20)	21(10)	-34(12)
C(304)	320(40)	380(40)	400(50)	30(30)	220(40)	-160(40)
C(305)	91(7)	169(14)	96(8)	-16(8)	5(6)	38(8)
O(401)	118(7)	184(9)	156(8)	-6(7)	38(6)	57(6)
C(402)	92(10)	310(30)	340(30)	180(30)	-12(14)	1(14)
C(403)	123(13)	213(16)	128(11)	34(11)	7(9)	-51(12)
C(404)	168(15)	188(16)	205(16)	-13(12)	-83(13)	61(13)
C(405)	1220(110)	220(20)	140(20)	-56(18)	200(40)	-120(40)

Table B15. Hydrogen coordinates (x 10^4) and isotropic displacement parameters (Å^2 x 10^3) for (t-Bu)$_8$(MeO)$_4$2K·(C$_4$H$_8$O)$_4$.

	x	y	z	U(eq)
H(9)	9110	4157	4630	42
H(13)	9370	7099	3394	51
H(15A)	9154	4386	6674	191
H(15B)	7729	4154	7137	191
H(15C)	7883	5343	6774	191
H(16A)	8536	3209	5510	170
H(16B)	6914	3561	5279	170
H(16C)	7322	2970	6156	170
H(17A)	5439	4982	5782	250
H(17B)	6034	5621	6313	250
H(17C)	5873	4430	6661	250
H(19A)	7758	7271	6754	184
H(19B)	8905	7422	6053	184
H(19C)	8838	6266	6549	184
H(21A)	9066	8649	3320	144
H(21B)	7947	9674	3457	144
H(21C)	7442	8782	3130	144
H(22A)	6212	8318	5123	227
H(22B)	5673	8570	4248	227
H(22C)	6154	9466	4581	227
H(23A)	9824	8583	4677	380
H(23B)	8688	8492	5388	380
H(23C)	8575	9568	4747	380
H(29)	11180	3557	2492	39
H(32A)	14634	1216	2606	150
H(32B)	14060	370	2260	150
H(32C)	14006	298	3185	150
H(33A)	13091	2614	1670	139
H(33B)	11426	2669	1679	139
H(33C)	12499	1734	1375	139
H(34A)	11243	393	3230	169
H(34B)	11428	378	2317	169
H(34C)	10319	1305	2609	169
H(37A)	12146	-524	4857	245
H(37B)	11146	340	4242	245
H(37C)	11344	561	5085	245
H(40A)	12658	1661	6508	297
H(40B)	11898	1251	5892	297
H(40C)	11363	2427	6029	297
H(41A)	13957	3612	5388	137

Table B15. (con't)

H(41B)	13654	2972	6250	137
H(41C)	12369	3675	5730	137
H(42A)	15367	1923	4875	235
H(42B)	14846	852	5259	235
H(42C)	15333	1524	5806	235
H(43)	11795	4139	4621	37
H(46)	8745	8242	-1386	43
H(50)	9373	8804	724	39
H(52A)	9130	9686	1491	162
H(52B)	7453	9786	1555	162
H(52C)	8148	10639	1820	162
H(53A)	6574	12059	3	126
H(53B)	6564	12100	909	126
H(53C)	5877	11241	646	126
H(54A)	10234	11049	582	178
H(54B)	9166	11946	931	178
H(54C)	9261	11994	9	178
H(56A)	7770	12920	-1536	163
H(56B)	8853	11966	-1813	163
H(56C)	8945	12180	-956	163
H(58A)	7918	8666	-2405	180
H(58B)	6686	9397	-2951	180
H(58C)	6328	8875	-2064	180
H(59A)	6086	11467	-1966	319
H(59B)	5275	10507	-1806	319
H(59C)	5600	11078	-2685	319
H(60A)	9058	10481	-2829	181
H(60B)	8139	11478	-2524	181
H(60C)	7616	11102	-3240	181
H(62)	11449	8201	-1377	46
H(66)	11188	5247	-170	45
H(68A)	13329	9333	-2930	133
H(68B)	13716	8680	-2065	133
H(68C)	12107	9206	-2269	133
H(69A)	14692	6656	-2964	255
H(69B)	15053	7231	-2314	255
H(69C)	15025	7816	-3217	255
H(70A)	11446	7716	-3508	259
H(70B)	11979	8807	-3747	259
H(70C)	10804	8652	-3062	259
H(72A)	12730	5122	-3566	149
H(72B)	11609	6099	-3349	149
H(72C)	11596	4928	-2864	149
H(74A)	13162	2808	-85	370

Table B15. (con't)

H(74B)	11924	3753	81	370
H(74C)	13530	3892	10	370
H(75A)	14553	2889	-1240	219
H(75B)	14896	3944	-1070	219
H(75C)	14415	3928	-1919	219
H(76A)	12008	2727	-1189	481
H(76B)	11455	3738	-1858	481
H(76C)	10773	3653	-990	481
H(10A)	5591	3129	2004	164
H(10B)	4721	3547	2730	164
H(10C)	5918	2148	3537	152
H(10D)	6870	1783	2818	152
H(10E)	8593	2198	3238	220
H(10F)	7595	2672	3913	220
H(10G)	7548	4271	3193	423
H(10H)	8411	3793	2494	423
H(20A)	5953	8629	384	217
H(20B)	5117	9526	838	217
H(20C)	4346	10252	-171	354
H(20D)	4883	9243	-544	354
H(20E)	2924	9063	-597	165
H(20F)	2377	10134	-269	165
H(20G)	2236	9219	1002	209
H(20H)	2214	8223	620	209
H(30A)	2154	7108	3018	173
H(30B)	2699	8196	2911	173
H(30C)	3125	7889	4293	268
H(30D)	1713	7394	4323	268
H(30E)	2908	5917	4114	461
H(30F)	3750	6170	4768	461
H(30G)	5635	6385	3944	157
H(30H)	5091	5447	3662	157
H(40D)	8529	5076	-14	351
H(40E)	7940	4161	-280	351
H(40F)	8435	6007	-1245	197
H(40G)	7908	5074	-1516	197
H(40H)	5858	5828	-1511	242
H(40I)	6484	6864	-1519	242
H(40J)	6400	6677	-365	646
H(40K)	4987	6384	-551	646